USING METABOLIC AND GENETIC ENGINEERING TO DEVELOP NOVEL CELL PLATFORMS FOR THE PRODUCTION OF RECOMBINANT GLYCOPROTEINS WITH ENHANCED PHARMACOKINETIC PROPERTIES

By
Matthew Joseph Buettner

A thesis submitted to Johns Hopkins University in conformity with the requirements for the degree of Master of Science

Baltimore, Maryland
May 2019

Abstract

Biopharmaceuticals are a burgeoning class of therapeutics that are revolutionizing the way disease is treated. Despite their considerable success, the ability to control glycosylation—a key design parameter that ensures safety, optimizes biological response, and influences the pharmacokinetic properties of biopharmaceuticals—has been elusive, which has slowed the development of this class of drugs. One specific glycan, sialic acid, has received considerable attention due to its role in the efficacy, pharmacodynamic, and pharmacokinetic properties of biopharmaceuticals. The first part of this project used a combined genetic and metabolic engineering strategy to gain enhanced exogenous control over the magnitude and type of sialyation produced by Chinese hamster ovary (CHO) cells. In order to significantly reduce endogenous flux of ManNAc into the sialic acid biosynthetic pathway (SABP) two key enzymes in this pathway, UDP-GlcNAc 2-epimerase/ManNAc kinase (Gne) and renin binding protein (Renbp), were knocked out. This was followed by exogenous supplementation with high-flux tri-butyrated mannosamine analogs (1,3,4-O-Bu_3ManNAc and 1,3,4-O-Bu_3ManNAz) in order to modulate CHO sialylation and install non-natural chemical moieties. Elimination of Gne and Renbp resulted in lower sialylation relative to wild type cells, however analog supplementation could still improve sialylation in a concentration dependent manner. Despite lower basal levels of sialic acid the Gne and Renbp knockout CHO cells showed a higher percent incorporation of the azide modified analog. Overall, these results provide evidence that this strategy could be used to develop biopharmaceuticals with a more homogenous glycoprofile and with increased incorporation of functional groups for bioconjugation. The second portion of this project aimed to develop a CHO cell line producing the coagulation factor IX (FIX) with “humanized” sialylation and an augmented serum half-life. A CHO cell line expressing ST6GAL1, a sialyltransferase found in humans but naturally silent in CHO cells, and producing FIX was successfully created. FIX will provide an excellent test protein to demonstrate that the Yarema Lab’s metabolic analogs can be used to increase sialylation to ultimately improve FIX serum half-life.

Thesis committee

Dr. Kevin J. Yarema (Primary Advisor)
Associate Professor
Department of Biomedical Engineering
Department of Chemical & Biomolecular Engineering
Johns Hopkins University

Dr. Jordan J. Green
Professor
Department of Biomedical Engineering
Department of Chemical & Biomolecular Engineering
Department of Ophthalmology
Department of Oncology
Department of Neurosurgery
Department of Materials Science & Engineering
Johns Hopkins University

Dr. Jamie B. Spangler
Assistant Professor
Department of Biomedical Engineering
Department of Chemical & Biomolecular Engineering
Johns Hopkins University

Acknowledgements

My past two years at Johns Hopkins University have been amazing and given me the opportunity to learn more than I could have ever imagined. My completion of this thesis project would not have been possible without a number of people who helped teach, guide, mentor, and encourage me throughout the process. First, I want to give a special thanks to Dr. Kevin Yarema for giving me the opportunity to conduct research in his lab and for mentoring me throughout my time at JHU. I would also like to thank my committee members Dr. Jamie Spangler and Dr. Jordan Green for graciously giving their time to review my thesis. I would especially like to thank Dr. Christopher Saeui and Dr. Sagar Shah for teaching me numerous experimental techniques and providing mentorship throughout my entire thesis project. Finally, I would like to thank all lab members and collaborators who aided me with experiments including Dr. Christian Agatemor, Vrinda Dharmarha, Ryan Ariss, Edward Cai, Marian Park, Prateek Gowda, Amelia Clarke, Melissa Austin, Keerthana Muthiah, PJ Krohl, Dallas Auer, Bahar Zarrabi, and Dr. Hao Zhang. Without their help this thesis project would not have been possible.

Table of Contents

List of Tables

List of Figures

Abbreviations

ADC, antibody-drug conjugate; ADCC, antibody-dependent cellular cytotoxicity; BCA, bicinchoninic acid; BSA, bovine serum albumin; Cas, CRISPR associated protein; CHO, Chinese hamster ovary; $CHO^{+FIX/+ST6GAL1}$, CHO cells expression FIX and ST6GAL1; $CHO^{+ST6GAL1}$, CHO cells expressing ST6GAL1; CHO^{-Gne}, CHO cells with Gne knocked out; $CHO^{-Gne/-Renbp}$, CHO cells with Gne and Renbp knocked out; CHO^{-Renbp}, CHO cells with Renbp knocked out; CHO^{WT}, wild type CHO cells; CRISPR, clustered regularly interspaced short palindromic repeats; DBCO-Cy5, dibenzocyclooctyne-Cy5; DMSO, dimethyl sulfoxide; EGF, epidermal growth factor; EMA, European Medicines Agency; EPO, erythropoietin; ER, endoplasmic reticulum; FACS, fluorescent activated cell sorting; FPLC, fast protein liquid chromatography; FBS, fetal bovine serum; Fc, fragment crystallizable; FDA, Food and Drug Administration; FIX, factor IX; gDNA, genomic DNA; GFP, green fluorescent protein; GNE/Gne, UDP-GlcNAc 2-epimerase/ManNAc kinase; GPI, glycosylphosphatidylinositol; gRNA, guide RNA; GSL, glycosphingolipid; HBP, hexosamine biosynthetic pathway; HBSS, Hanks buffered salt solution; HDR, homology directed repair; HEK293, human embryonic kidney 293; HRP, horse radish peroxidase; IFN-γ, interferon γ; IgG, immunoglobin; IVIG, intravenous immunoglobin; LB, lysogeny broth; LLO, lipid-linked oligosaccharide; mAb, monoclonal antibody; ManNPe, *N*-pentanoylmannosamine; ManNPr, *N*-propanoylmannosamine; MGE, metabolic glycoengineering; MOI, multiplicity of infection; MUSCLE, multiple sequence alignment tool; Neu5Ac, *N*-acetylneuraminic acid; Neu5Gc, *N*-glycolylneuraminic acid; NHEJ, non-homologous end joining; OGA, nucleocytoplasmic β-*N*-acetylglucosamineidase; OGT, O-GlcNAc transferase; PAM, protospacer adjacent motif; PBS, phosphate buffered saline; PBST, PBS with 0.1% (v/v) Tween 20; PI, propidium iodide; PTM, post-translational modification; RENBP/Renbp, renin binding protein; RIPA, radioimmunoprecipitation assay buffer; SABP, sialic acid biosynthetic pathway; SNA, *Sambucus nigra*; ST6GAL1, α(2,6)-sialyltransferse; SOC, super optimal broth with catabolite repression; TBST, tris buffered saline with tween 20; TU, transducing units; FSC, forward-scattered light; SSC, side-scattered light; SDS, sodium dodecyl sulfate;

Chapter 1: Introduction

1.1 Overview

The goal of this first chapter is to introduce the reader to key concepts and ideas that are relevant to understanding this thesis project. This section begins with an overview of glycosylation including the three main types: N-linked, O-linked, and glycolipids. This is followed by a discussion on how glycoengineering is being used to augment biopharmaceutical products with a special emphasis on metabolic glycoengineering (MGE). Each subsequent chapter also includes brief introductory information that is specifically pertinent to that chapter. Portions of this chapter have been published as Improving Immunotherapy through Glycodesign in Frontiers in Immunology *(1)*.

1.2 Glycosylation

All of life is composed of four primary classes of macromolecules: proteins, nucleic acid, lipids, and carbohydrates. Carbohydrates are biomolecules made of carbon, hydrogen and oxygen atoms although other elements may be present in some variants. The simplest forms of carbohydrates are referred to as monosaccharides, which cannot be further hydrolyzed and take on the general chemical formula $C_nH_{2n}O_n$ *(2, 3)*. Monosaccharides are commonly combined together through glyosidic linkages between the anomeric carbon of a sugar donor and a hydroxyl oxygen of an acceptor sugar resulting in the formation of carbohydrate chains called oligosaccharides and polysaccharides. The formation of polysaccharides and their attachment to other organic biomolecules, particularly proteins, is broadly referred to as glycosylation. Glycosylation is unique compared to other types of macromolecules in that its synthesis is not template driven and its potential structural diversity is orders of magnitude larger. These inherent properties of glycosylation lead to enormous complexity making it both difficult to study and challenging to predict *(2, 4)*. Yet, the enormous complexity is critical for many specific biological functions and provides endless potential for modifying molecules to perform new functions. The next three sections discuss

the three main types of glycosylation (N-linked, O-linked, and glycolipids) including their general chemical composition, biosynthesis, and some critical biological roles.

1.2.1 N-Linked Glycans

N-Glycans are oligosaccharides covalently linked to the amide nitrogen of asparagine; they constitute one of the most common and almost certainly the most complex types of post-translational modification (PTM) *(5, 6)*. This section provides an overview of the general process by which mammalian N-glycans are synthesized and covalently attached to proteins.

1.2.1.1 Early Stages in N-Glycan Biosynthesis

N-Glycan biosynthesis occurs in two distinct stages in the endoplasmic reticulum (ER) and the Golgi apparatus, respectively *(6, 7)*. The first stage of N-glycan biosynthesis is highly conserved and begins in the ER with the synthesis of the lipid-linked oligosaccharide (LLO) structure. This process begins with the transmembrane insertion of dolichol into the ER membrane. Dolichol is an isoprenoid lipid made of five carbon isoprene units that functions as an oligosaccharide carrier during early LLO synthesis *(6, 8, 9)*. Once dolichol has been phosphorylated (dolichol-P) a family of glycosyltransferases encoded by the *ALG* (asparagine linked glycosylation) genes act sequentially to synthesize the complete LLO. In mammals, Dpagt1, a GlcNAc-1-phosphotransferase, initiates this process by catalyzing the transfer of GlcNAc-1-P from UDP-GlcNAc to dolichol-P forming dolichol-P-P-GlcNAc *(10)*. The second GlcNAc residue is then added through the catalysis of a bipartite protein complex comprised of Alg13 and Alg14 *(7, 11)*. Subsequently, five mannose residues are transferred from GDP-mannose by a series of three mannosyltransferases (Alg1, Alg2, Alg11) forming $Man_5GlcNAc_2$-P-P-dolichol, the final product on the cytoplasmic side of the ER membrane. This glycolipid is translocated into the ER lumen by a flippase *(12, 13)* where it is further elaborated to the final 14-mer LLO structure ($Glc_3Man_9GlcNAc_2$-P-P-dolichol). The LLO is then transferred by an

oligosaccharyltransferase to an asparagine residue in the consensus motif Asn-X-Ser/Thr (X cannot be proline) of a nascent polypeptide chain during its translation across the ER membrane *(14, 15)*.

1.2.1.2 N-Glycan Processing and Structural Diversification

The second phase of N-glycan biosynthesis encompasses the processing of LLOs into three general categories (high mannose, hybrid, and complex) which can be decorated with thousands of potential structural motifs *(16-18)* after transport of the host protein from the ER to the Golgi. This diversification of N-glycans – being a non-template based process – results in numerous and difficult to predict glycoforms. As described below, the sequential modification with mannose, GlcNAc, galactose, fucose, and sialic acid modulates many aspects of biology *(5)*.

N-Glycan processing begins in the ER with the sequential cleavage of the three glucose moieties of the LLO glycan structure via α-glucosidase I (Mogs) and II (Ganab) *(19)*. The removal and re-addition of up to one glucose group is critical for calnexin and calreticulin mediated regulation of the glycoprotein folding process *(20-22)*. Removal of the innermost glucose residue signals the glycoprotein is correctly folded, enabling ER α-mannosidase I (Man1b1) to remove the outermost α(1,2)-Man from the central arm resulting in $Man_8GlcNAc_2$, thereby signaling the glycoprotein is ready for further processing in the *cis*-Golgi.

In the *cis*-Golgi after removal of the innermost glucose residue a proportion of the $Man_{8/9}GlcNAc_2$ structures avoid further modification (beyond the cleavage of mannose residues to form $Man_{5-9}GlcNAc_2$) resulting in high mannose type N-glycans *(6)* that affect glycoprotein secretion, folding, and stability *(23)*. In most cases, high mannose type N-glycans are further processed in the Golgi resulting in hybrid- and complex-type N-glycans. The process of N-glycan branching and elongation begins in the *medial*-Golgi with the transfer of GlcNAc to the $Man_5GlcNAc_2$ structure by N-acetylglucosaminyltransferase, Mgat1 *(24)*. For hybrid N-glycans, the high mannose branch remains unaltered while the branch ending in GlcNAc is usually further elongated with galactose and GlcNAc

or capped with sialic acid, or fucose. Complex type N-glycans have two additional mannose residues cleaved by α-mannosidases (Man2a1 or Man2a2) to produce $GlcNAcMan_3GlcNAc_2$ *(25)*, which is elaborated with bi- (and sometimes tri-, and tetra-) antennary branches by the sequential addition of GlcNAc residues via Mgat2, Mgat4, and Mgat5. The GlcNAc transferases have decreasing affinity (higher K_m values) for the substrate UDP-GlcNAc creating an ultrasensitive cascade that usually limits branching to bi-antennary structures (**Fig. 1.1**) *(24, 26)*.

The discerning reader may have noted the curious omission of Mgat3 from the previous paragraph; the reason is that this enzyme is an outlier that counteracts several aspects of N-glycan diversification and elongation. Specifically, Mgat3-catalyzed addition of GlcNAc to the β-mannose of an N-glycan in a bisecting orientation *(27, 28)* inhibits the activity of Mgat4 and Mgat5 negating tri- and tetra-antennary branching (and subsequent elongation of the resultant antennary branches) and also reduces core fucosylation (**Fig. 1.1**) *(24, 29, 30)*. Although only a single monosaccharide, the ability of bisecting GlcNAc to block subsequent branching and core fucosylation has a disproportional impact on overall N-glycan structure and bioactivity (e.g., in cancer metastasis *(31-34)*, apolipoprotein B function *(35)* and the epithelial-mesenchymal transition *(36, 37)*).

After GlcNAc has been added to a nascent N-glycan to form hybrid or complex structures, this moiety is commonly elongated with galactose by a β(1,4)-galactosyltransferase, which creates the Gal-β(1-4)-GlcNAc unit known as "LacNAc" *(38, 39)*. Additional galactose residues may be added by β(1,4)- or α(1,3)-galactosyltransferases, either consecutively or interspersed with other monosaccharides (e.g., GlcNAc) to create a variety of N-glycan structures.

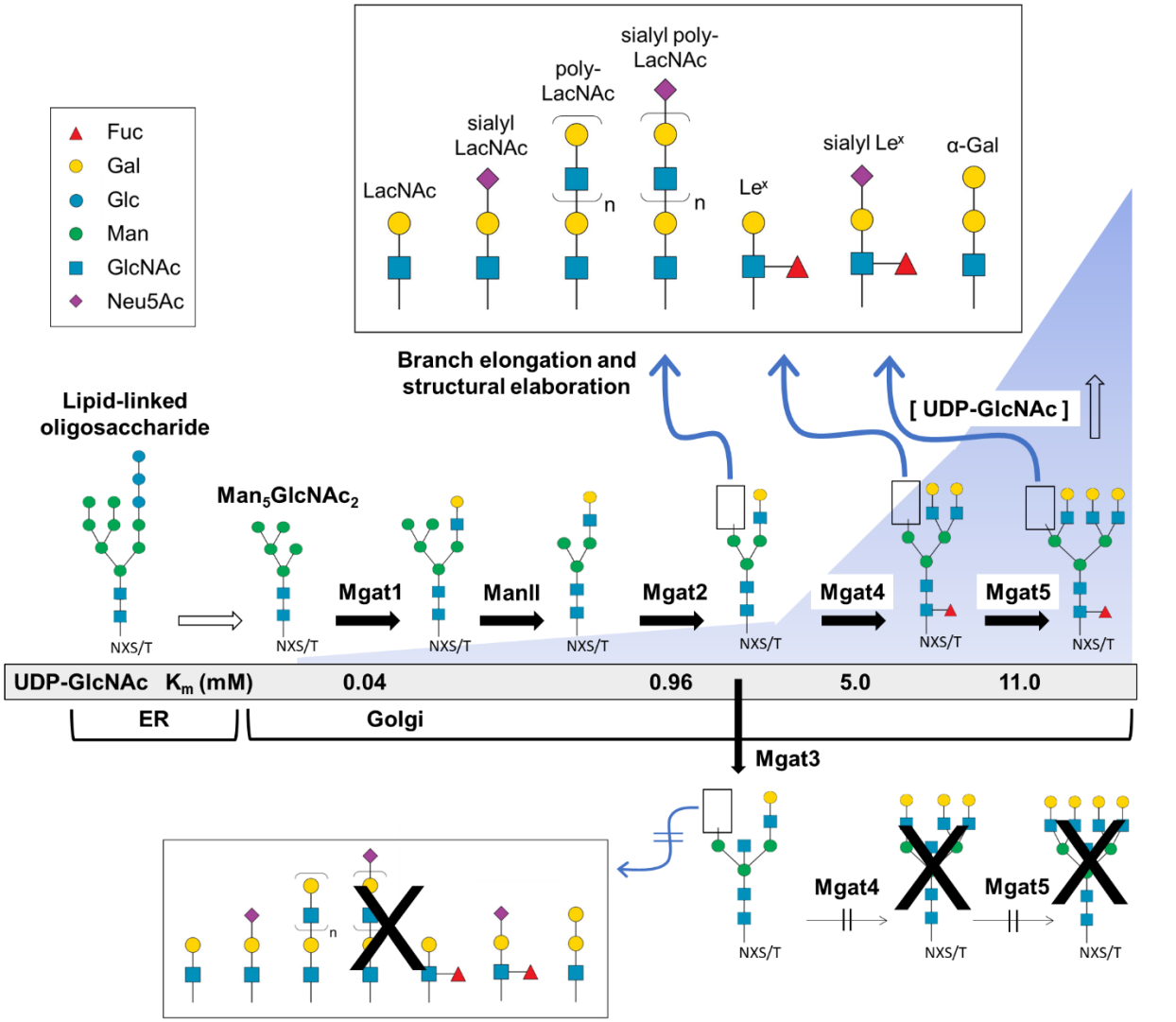

Figure 1.1 Branch elongation and structural diversity of N-glycans *(1)*. The $Glc_3Man_9GlcNAc_2$-P-P-dolichol LLO structure is synthesized in the ER where it is further processed and transferred to the Golgi resulting in high mannose (e.g., $Man_5GlcNAc_2$), hybrid, and complex type N-glycans that undergo branching via Mgat1, 2, 4, and 5 GlcNAc transferase activity that respectively creates di-, tri-, or tetra-antennary structures. Following the initial branching step, the glycan structure may be fucosylated or undergo additional elongation and capping modifications (top panel). Alternatively, Mgat3 may add a bisecting GlcNAc residue which blocks Mgat4 and 5 activity thereby preventing tri- and tetra-antennary branching and further terminal diversification (bottom panel). The presence of a bisecting GlcNAc also hinders core fucosylation (red triangle) and reduces the capacity for downstream elongation and capping. [All glycan symbol structures in this figure and throughout this document were made using software from Cheng and coauthors *(40)*]

Hybrid and complex type N-glycan branches often end with GlcNAc or galactose but can also be decorated with fucose or terminally capped with sialic acids, meaning that typically once these sugars are added, the oligosaccharide chain cannot be further elongated. Fucose is a prevalent modification of the complex type N-glycans; in humans fucosyltransferases add this sugar in an α(1,2) (FUT1,2), α(1,3/4) (FUT3-7,9), or α(1,6) (FUT8) orientation; in all mammals, Fut8 adds a fucose residue exclusively to the innermost Asn-linked GlcNAc group (*a.k.a.*, "core" fucosylation). Fucose can also be added as a capping moiety to an outermost galactose by Fut1,2 forming Lewis and blood group antigens *(41, 42)*.

Sialic acids – a family of α-keto acids comprised of a nine carbon backbone with over 50 different variants – ubiquitously cap glycans *(5, 6, 43)*. N-Acetylneuraminic acid (Neu5Ac), modified with an N-acetyl group at the C-5 position, is the predominant sialic acid in humans and is typically found at the termini of N-glycan branches where it is added to the penultimate galactose via α(2,3)-, α(2,6)-, or less commonly, α(2,8)-sialyltransferases (throughout the remainder of this thesis mention of sialic acid refers to Neu5Ac unless otherwise stated) *(44, 45)*. Depending on its linkage (e.g., α(2,3)- *vs.* α(2,6)-) Neu5Ac exhibits numerous biological functions in nervous system embryogenesis, cancer metastasis, immune responses, and protein bioactivity and stability *(45, 46)*.

1.2.2 O-Linked Glycans

O-Glycans are monosaccharides or oligosaccharides covalently linked to a serine or threonine residue. Similar to N-glycans, O-glycan synthesis is not template based and is defined by a vast array of possible structural permutations that have many important biological and pathological functions including: protein stability, structure, folding, activity, metabolism, cell signaling, cell-cell interactions, and oncogenesis *(47-50)*. This section focuses on synthesis and structural diversity of O-glycans particularly mucin type O-glycans.

1.2.2.1 O-GalNAc Glycans

Mucin-type O-glycans, so named because of their abundance in mucins (and their initial isolation and characterization from mucus), are defined by having a GalNAc at the reducing terminus *(47)*. Biosynthesis of mucin-type O-glycans begins in the Golgi with the transfer of GalNAc to a serine or threonine residue by one of ~22 GalNAc transferases *(51-53)*. While possible, a single unextended GalNAc (Tn antigen) is uncommon, instead various glycosyltransferases generate one of eight core structures (**Fig. 1.2**) *(49, 50)*. These core structures can be further elongated and capped (generally with GlcNAc, galactose, sialic acid, or fucose) to create numerous motifs such as the Lewis antigens (e.g., Le^y, Le^x, sLe^x, Le^a, sLe^a, Le^b), thereby substantially increasing structural diversity *(47, 50, 54)*. Mucin-type O-glycans are involved in many biological functions including fertilization, signal transduction, cell structure, adhesion, cell homing, glycoprotein clearance, stability, and immunity *(47, 50)*.

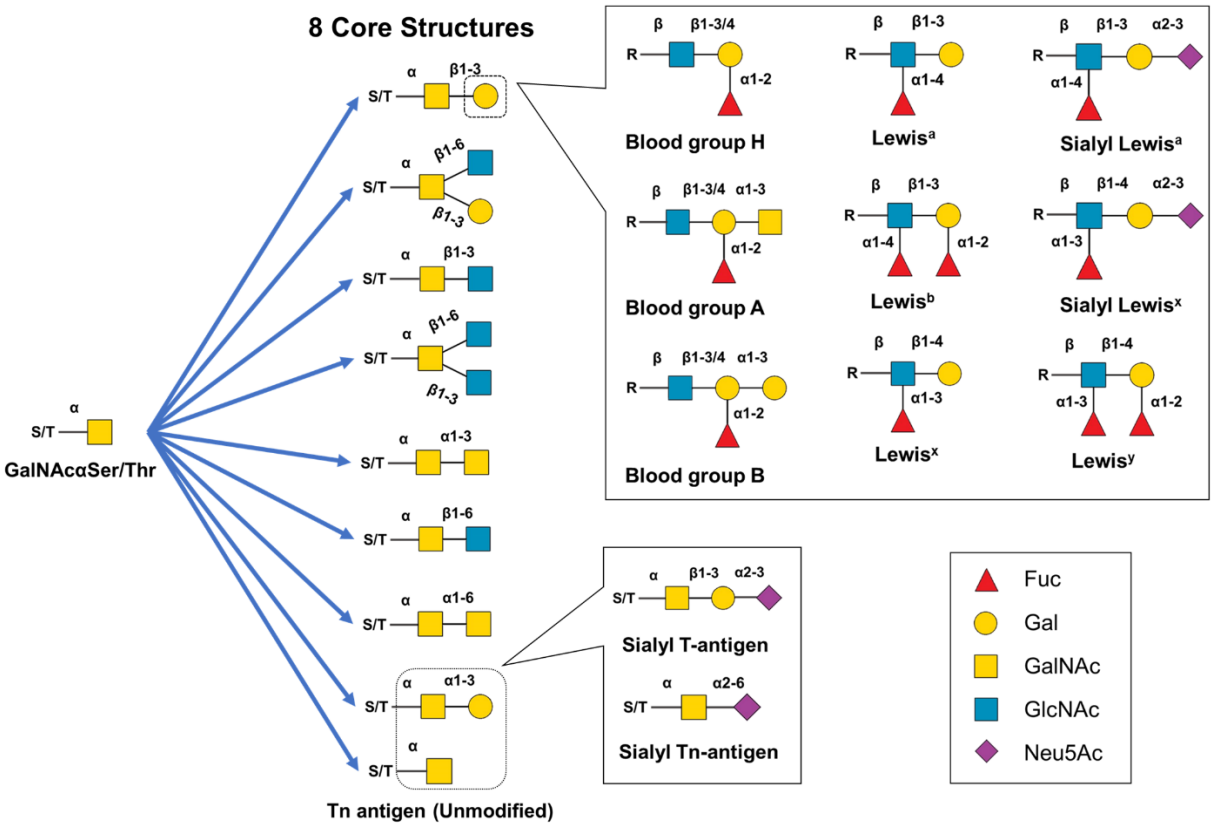

Figure 1.2 Structural diversity of mucin-type O-glycans *(1)***.** Mucin type O-glycan biosynthesis begins with the transfer of GalNAc to serine or threonine. The GalNAc monosaccharaide can be left unmodified, but is typically extended to create eight different core structures that can be further modified with single monosaccharides, Lewis structural epitopes, blood group antigen groups, or other glycan epitopes (e.g., the cancer-related sT or sTn antigens).

1.2.2.2 O-GlcNAc Glycans

O-GlcNAc is an uncharged acetylated hexosamine sugar that modifies serine or threonine residues on nuclear, mitochondrial, and cytoplasmic proteins. The O-GlcNAc modification is unique in that it is rarely elongated and is often times added and removed numerous times during a protein's lifetime. O-GlcNAc has been implicated in many biological roles especially those relating to cellular signaling pathways and disease progression *(55, 56)*.

O-GlcNAc is synthesized via the hexosamine biosynthetic pathway (HBP) which is an offshoot of glycolysis that diverts glucose to the production of UDP-GlcNAc, the nucleotide precursor sugar of O-

GlcNAcylation. In humans the pathway begins with its rate limiting step, the conversion of fructose 6-phosphate and glutamine to glucosamine 6-phosphate and glutamate catalyzed by glutamine: fructose 6-phosphate transaminase (GFAT). Glucosamine 6-phosphate combines with acetyl-coenzyme A to form GlcNAc 6-phosphate and coenzyme A which is catalyzed by glucosamine-phosphate N-acetyltransferase (GNPNAT). Next, GlcNAc phosphomutase (PGM3) isomerizes GlcNAc 6-phosphate to GlcNAc 1-phophate. The HBP ends with the conversion of UTP and GlcNAc 1-phosphate to UDP-GlcNAc catalyzed by UDP-*N*-acetylglucosamine pyrophosphorylase (UAP1). HBP production of UDP-GlcNAc is considered a nutrient sensing pathway as the levels of UDP-GlcNAc can be directly correlated with the relative abundance or lack of various critical macromolecules. The transfer of O-GlcNAc on and off proteins is controlled by two enzymes O-GlcNAc transferase (OGT) and nucleocytoplasmic β-N-acetylglucosamineidase (OGA). OGT catalyzes the transfer of GlcNAc from UDP-GlcNAc to a serine or threonine residue of a protein, while OGA catalyzes the reverse reaction. O-GlcNAc cycling is both rapid and dynamic, however regulation of OGT is convoluted and poorly understood *(55-57)*.

1.2.2.3 Other Types of O-Glycans

O-Fucose and O-glucose are a highly specific form of glycosylation that strictly modifies the hydroxyl groups of serine and threonine residues within epidermal growth factor (EGF) repeats of a limited number of proteins (~100 and ~50 in humans, respectively). Fucose is transferred from GDP-fucose to the serine or threonine residue of EGF repeats containing the consensus sequence $C^2X_4(S/T)C^3$ (where C^2 and C^3 are the second and third conserved cysteines of the EGF-like repeat) by protein O-fucosyltransferase 1. The fucose residue can then be further elongated by a series of GlcNAc, galactose, and sialic acid transferases *(48)*. O-Fucose has been heavily implicated as an important player in the Notch signal transduction pathway which is vital for numerous biological functions including neuronal development, angiogenesis, and cell differentiation *(48, 58)*. O-Glucose glycan structures occur at the consensus motif $C^1XSX(P/A)C^2$ between the first and second conserved

cysteines (i.e. C^1 and C^2) of EGF repeats. The O-glucose modification has also been shown to impact the Notch signal transduction pathway to some degree and the inability to produce this specific PTM is associated with various congenital diseases *(48)*.

O-Mannose glycans are a more common PTM that have a diverse set of potential chemical structures, but can be generally divided into three core classes: M1, M2, and M3. In the ER, mannose is added to a serine or threonine residue from a dolichol-P-mannose donor by a heterodimer made of protein O-mannosyltransferase 1 and 2. Core M1 O-mannose glycans are generated by the addition of a β(1,2)-GlcNAc to the base O-mannose residue catalyzed by an N-acetylglucosaminyltransferase. From here, core M1 O-mannose glycans may be converted to core M2 type O-mannose glycans by the addition of a β(1,6)-GlcNAc to the core O-mannose. M1 and M2 O-mannose glycans may be further elaborated by various galactose, fucose, glucuronic and sialic acid transferases leading to significant structural diversity. Core M3 type O-mannose glycans are generated by the addition of a GlcNAc residue in a β(1,4) orientation. This disaccharide is specifically elongated with a GalNAc residue followed by the addition of two ribitol-5-phosphate groups and finally the addition of a repeating disaccharide called matriglycan. Broadly, O-mannose is vital for normal development and growth and has been identified as a key player in multiple diseases including congenital muscular dystrophy, viral entry, and cancer metastasis *(48, 59)*.

1.2.3 Glycolipids

Glycolipids are the third class of glycosylation, broadly defined as amphiphilic macromolecules composed of a hydrophilic polar carbohydrate group connected to a hydrophobic apolar lipid group through a glyosidic bond. The sugar portion of glycolipids can be highly variable with a range of sizes and complexities. Due to the lipid moiety, glycolipids are most often anchored in a molecular membrane, but can still perform a variety of biological functions including recognition, adhesion, and cell signaling *(60)*.

1.2.3.1 Glycosphingolipids

Mammalian glycosphingolipids (GSLs) are one subclass of glycolipids and are comprised of a sphingolipid, fatty acid, and carbohydrate (**Fig. 1.3A**). GSLs are the predominant form of glycolipid found in vertebrates and are vital for numerous biological functions including cellular adhesion, cell-cell interactions, signal transduction, oncogenesis, ontogenesis, and immunogenicity *(61-63)*. The biosynthesis of GSLs is a stepwise process beginning with the synthesis of ceramide in the cytosol and subsequent transfer to the luminal ER. From here, typically glucose or galactose is the first glycan added to ceramide. Glucose is added to ceramide (GlcCer) on the cytoplasmic face of the ER and early Golgi where it can be further elaborated by a series of glycosyltransferases forming one of seven base tetrasaccharide neutral sugar core structures (**Fig. 1.3B**). Conversely, galactose can be added to ceramide (GalCer) on the luminal face of the ER and transported to the Golgi where a sulfate is added to form sulfatide which may be sialylated, but is otherwise rarely elongated with other monosaccharide units (**Fig. 1.3C**) *(61)*.

1.2.3.2 Glycosylphosphatidylinositol Anchors

The second major form of glycolipids is glycosylphosphatidylinositol (GPI), a PTM attached to the C-terminus of proteins to anchor cell surface proteins in a lipid membrane. GPI-anchored proteins usually face the extracellular surface and at least 150 GPI-anchored proteins are found in humans. The only known biological role of GPI itself is to provide a stable membrane anchor for proteins, however GPI-anchored proteins are critical for a variety of biological purposes including: signal transduction, immune response, adhesion, protease inhibition, and disease progression. Nearly all GPI anchors share the ubiquitous base structure ethanolamine-PO_4-6Manα(1,2)Manα(1,6)-Manα(1,4)GlcNα(1,6)*myo*-inositol-1-PO_4-lipid which can be modified at various locations to generate considerable chemical diversity. A GPI precursor is synthesized on a phosphatidylinositol lipid anchored in the ER membrane and subsequently attached to the C-terminus end of a nascent

protein in the lumen of the ER. From here, the GPI-protein is chemically modified in the ER and Golgi leading to vast heterogeneity in the final GPI-protein structure *(64-66)*.

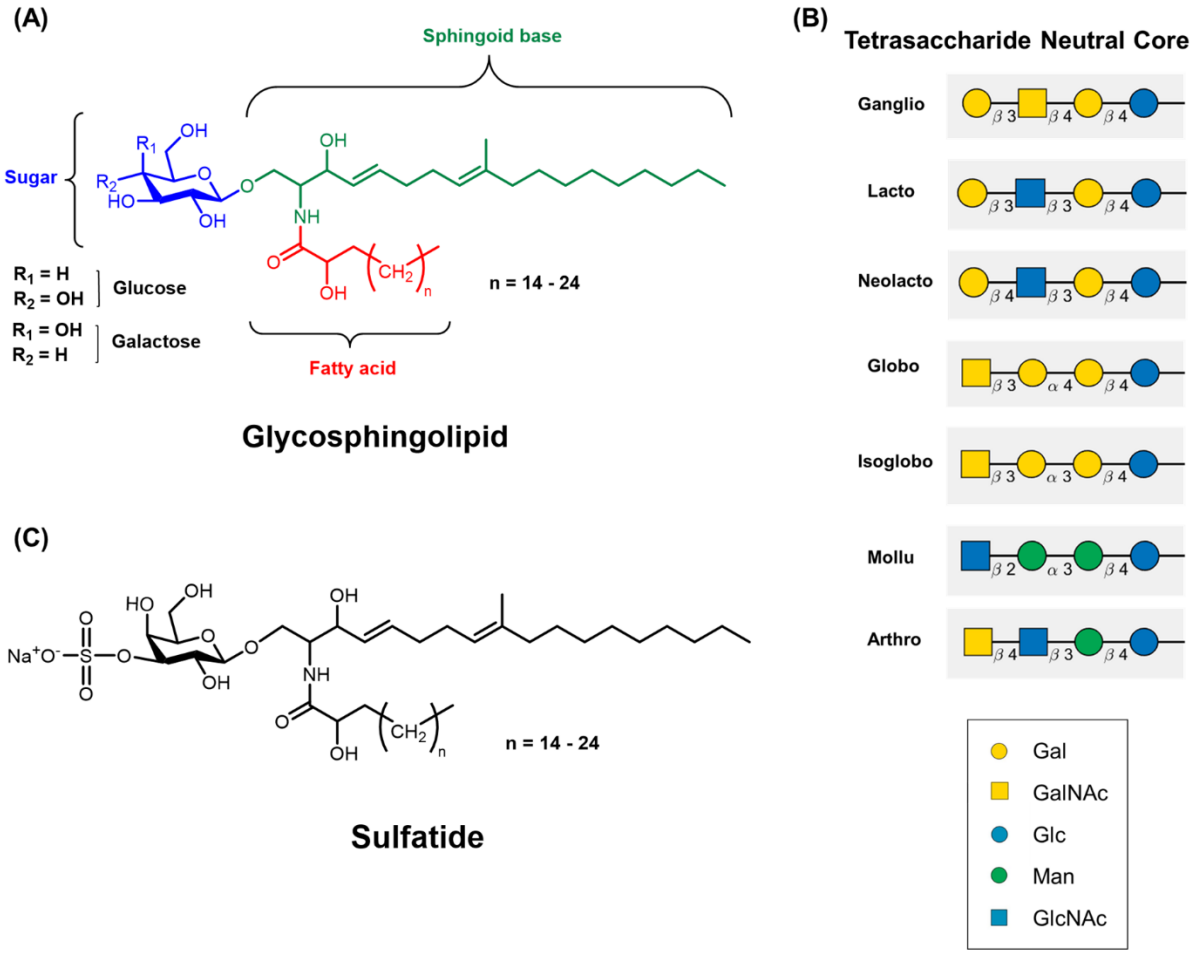

Figure 1.3 Structures and classes of glycosphingolipids. (A) Glycosphingolipids are comprised of a sphingoid base and fatty acid (forming ceramide) conjugated to a carbohydrate via a glyosidic bond. (B) Most commonly, ceramide is linked to a glucose residue which can be further elaborated into one of seven tetrasaccharide neutral core structures. (C) Ceramide may also be conjugated to galactose which is subsequently sulfated to form sulfatide which is rarely further elaborated.

1.3 Glycoengineering for Biopharmaceutical Applications

Biopharmaceuticals, defined as any biologically derived therapeutic product, continue to be one of the predominant therapies for a wide range of disease. Biopharmaceuticals encompass a variety of different products including monoclonal antibodies (mAbs), clotting factors, growth factors, hormones, stem cells, vaccines, and interleukins (**Fig. 1.4**). From 2010 – 2014 the Food and Drug Administration (FDA) and European Medicines Agency (EMA) approved 54 new biopharmaceutical products *(67)*. Furthermore, in 2016 the biopharmaceutical industry totaled approximately 228 billion USD in global sales *(68)* and current market projects expect a compound annual growth rate of 8.59% between 2018 – 2023 *(69)*. In order to maintain this robust growth and to develop the next generation of biopharmaceuticals the industry is starting to focus considerable effort on glycosylation, which plays a pivotal role in both the efficacy and safety of biopharmaceuticals *(70)*. This section begins by discussing considerations for selecting a cell system with an emphasis on how glycosylation impacts this decision. This is followed by a section highlighting various genetic glycoengineering strategies that have been used to manipulate the glycoprofile of biopharmaceuticals. Lastly, this section discusses MGE technology with a focus on how it can be used to ameliorate biopharmaceuticals.

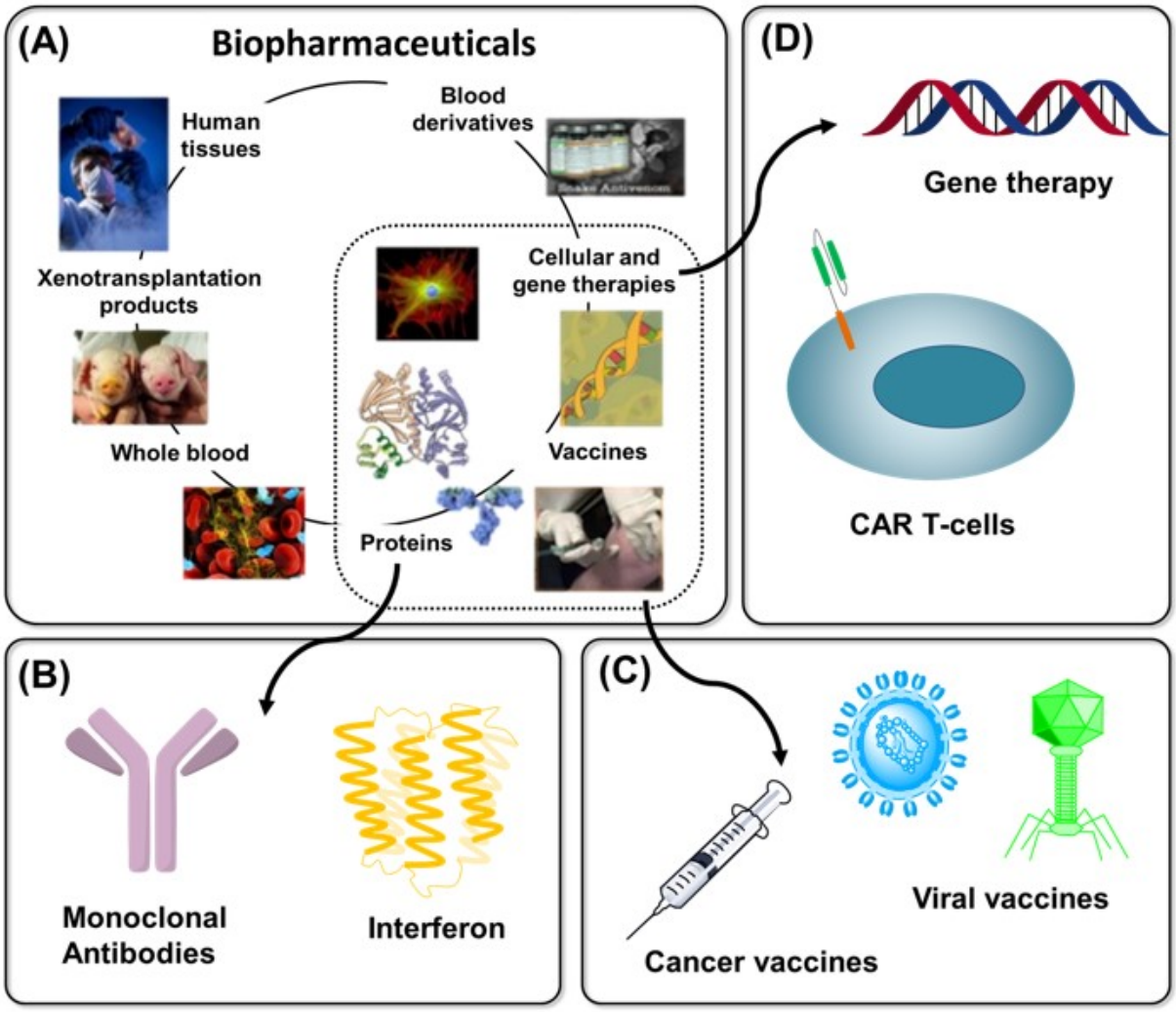

Figure 1.4 Overview of common biopharmaceuticals *(1)***.** (A) Biopharmaceuticals is a broad term that refers to any therapy created using material derived from a living system, several examples are shown. (B) Protein-based biologics dominate today's commercial products including mAbs and interferon. (C) Until a few decades ago, vaccines dominated the biopharmaceutical landscape, a 200-year old endeavor, with cancer vaccines representing one example of this trend today. (D) The extraordinarily diverse nature of biopharmaceuticals is illustrated by emerging cell-based and gene therapies.

1.3.1 Cell Host Selection

Early generations of biopharmaceuticals, such as vaccines, largely were produced in embryonated eggs or collected from animal products and human blood donations *(71, 72)*. Most of today's biopharmaceuticals, however, exploit recombinant DNA technology to produce proteins in cell-based manufacturing platforms (whereas certain biopharmaceuticals consist of the cells

themselves). Cell-based biomanufacturing efforts have explored a wide range of expression systems including non-mammalian (bacteria, yeast, plant, and insect) and mammalian (human, hamster, and mouse) cells *(73)* to optimize product yield and install appropriate PTMs. From 2004 to 2013 biopharmaceuticals approved by the FDA and EMA were obtained from mammalian cells (56%), *Escherichia coli* (24%), *Saccharomyces cerevisiae* (13%), insect cells (4%) and transgenic animals and plants (3%) *(74)*. The majority of products, obtained from mammalian cells, includes virtually all recent therapeutic proteins where PTMs, especially glycosylation, can be optimized for safety, biological activity, function, stability, physicochemical properties, and pharmacokinetics *(46, 75, 76)*. For this reason – after providing a brief synopsis of non-mammalian options – this section will focus on the selection of mammalian expression systems used in biomanufacturing beginning with the use of human and murine cell lines used in the early production of modern biopharmaceuticals. As discussed below, each of these cell lines has substantial pitfalls, leading to today's consolidation of production in CHO cells.

1.3.1.1 Non-Mammalian Cell lines

Insulin, the earliest recombinant human protein, was produced in *E. coli*, which benefits from low cost and high productivity *(74, 77)*. Although a few biologics are still produced in *E. coli*, the lack of N-glycans (that ensure quality control during folding) *(78)* makes prokaryotic production untenable for most glycoproteins including mAbs. Yeast (*S. cerevisiae* and *Pichia pastoris*) provide another high productivity, low cost production platform *(79, 80)* and – being eukaryotic cells – do have N-glycans; yeast glycans, however, tend to be highly mannosylated which reduces serum longevity thus compromising pharmacokinetics and also impacting downstream effector functions *(81)*. Even though efforts have been made to "humanize" yeast glycosylation, these cells have not become a widely-accepted biomanufacturing platform *(81)*. Finally, insect (e.g., *Trichoplusia and Drosophila*) cells have been investigated for recombinant glycoprotein production, but despite efforts to

humanize glycosylation *(82, 83)*, these cells also have substantial pitfalls for biomanufacturing including minimal sialylation ability *(82, 84)*.

1.3.1.2 Human Cell Lines

The inability of the initial bacterial, yeast, and insect production platforms to produce properly glycosylated human proteins led to production efforts in human cells. The first immortalized human cell line, HeLa, was derived from cervical cancer in 1951 *(85)* and paved the way for the development of other immortalized human cell lines, notably human embryonic kidney 293 (HEK293) and fibrosarcoma HT-1080 cells used to produce viral vaccines *(86-88)*. However, it wasn't until ~2001 that the first therapeutic glycoprotein produced in human cells (HEK293), Drotecogin alfa, was approved by the FDA and EMA; since then several glycoprotein biopharmaceuticals have been produced in human cells primarily in the HEK293 and HT-1080 lines *(73)*.

Human cells offer important advantages over other production platforms including the ability to closely mimic PTMs, particularly glycosylation, naturally found in people. For example, human cell lines express MGAT3, α(1,3/4)-fucosyl transferase, and α(2,6)-sialyltransferse (ST6GAL1) which are silent or missing in CHO cells. Furthermore, human cell lines do not produce immunogenic structures, such as α-Gal and N-glycolylneuraminic acid (Neu5Gc), thus minimizing safety and compatibility concerns. These factors reduce the need to genetically engineer cells and limit the cost of downstream processing *(86, 87, 89)*. Although human cells have these attractive features as a production platform, they also have substantial limitations and drawbacks. For example, human lines suffer from low growth rates, production capacities, and protein yields making them impractical for the production of many therapeutic proteins including most mAbs. Furthermore, the absence of a species barrier makes human cell lines a significant safety risk due to the potential for contamination and transmission of human pathogens. In theory, these disadvantages can be overcome with

advances in technology and adherence to stringent good manufacturing practices *(86, 87, 89)*; in practice, most biopharmaceuticals are now produced in rodent cells, as described next.

1.3.1.3 Murine Cell Lines

Murine myeloma cells, predominantly NS0 and Sp2/0, are another cell platform that is periodically used for the production of recombinant glycoproteins. Both the NS0 and Sp2/0 cell lines were developed from tumors and subsequently genetically engineered to stop producing their native immunoglobins yet retain the cellular machinery to secrete recombinant proteins at high levels *(90, 91)*. Accordingly, these lines have been used to produce the commercial mAbs Cetuximab, Palivizumab, Dinutuximab, Necitumumab, and Elotuzumab *(73, 87, 92)*. A downside of murine cells is their ability to incorporate α-Gal and Neu5Gc into glycans, thereby presenting a considerable risk of immunogenicity *(93-95)*. Thus, murine cells used for therapeutic protein production must be thoroughly screened for clones lacking these immunogenic epitopes while producing desirable glycan profiles.

1.3.1.4 Chinese Hamster Ovary Cells

In 1986 tissue plasminogen became the first FDA-approved recombinant biopharmaceutical to be produced in CHO cells *(87, 89, 96)*; since then these cells have become the predominant manufacturing platform for biologics producing an estimated 70% of recombinant biopharmaceutical proteins *(76, 97, 98)*. Furthermore, over 90% of commercial antibodies are now produced in CHO cells *(67, 73, 87)*. The success of CHO cells in commercial biomanufacturing stems from several key advantages. First, CHO cells can be grown in large bioreactors as a cell suspension in serum-free, chemically-defined media while maintaining high production rates. From a safety perspective, many viral entry genes are not expressed in CHO cells and there is a species barrier that minimizes risk of transferring infectious agents to humans *(99, 100)*. Furthermore, over the past three decades the extensive documentation that CHO cells are safe hosts aids in facilitating regulatory

approval to bring biopharmaceutical products to the market *(89, 96)*. Perhaps most importantly, CHO cells produce recombinant glycoproteins with compatible glycoforms that are bioactive in humans *(73, 87, 96, 101)*.

Despite the advantages of CHO cell production platforms, shortcomings exist. CHO cells (as with most mammalian cell lines) retain the ability to produce glycans not found in humans including α-Gal and Neu5Gc *(94, 102)*. Humans inherently express antibodies against these immunogenic epitopes that can lead to severe, potentially fatal immunogenic responses and/or negate the effects of biotherapeutics *(93-95)*. However, the levels of α-Gal and Neu5Gc are relatively low (<2% Neu5Gc and <0.2% α-Gal) in CHO cells, meaning this issue can be circumvented by selecting clones lacking these non-human epitopes *(73, 94)*. CHO cells also lack certain types of glycosylation found in humans, such as α(2,6)-sialylation, α(1,3/4)-fucosylation, and bisecting GlcNAc *(103-106)*. Overcoming these differences by "humanizing" CHO cell glycosylation is, at least in theory, possible through genetic engineering and MGE approaches.

1.3.2 Genetic Glycoengineering

Various approaches to modulate glycans in living cells – i.e., glycoengineering methods – have been developed over the past three decades concurrent with the unraveling of the importance of glycosylation in immunity. Today, these parallel developments have set the stage to employ the various glycoengineering strategies now available to generate recombinant proteins (or even entire cells) with desirable glycan profiles *(104, 105, 107)* during biopharmaceutical design and manufacturing. Glycoengineering falls into two main approaches: genetic and metabolic; this section discusses specific examples of both approaches while describing general strengths and drawbacks to each approach. Although glycoengineering strategies are being developed for many production platforms (bacteria *(106)*, yeast *(108)*, plants *(109)*, insects *(110)*), this section will focus on mammalian cells as they are used to produce the vast majority of today's biopharmaceuticals.

Many genetic approaches have been used to target glycosylation pathways and enzymes via gene knockdown, knockout, overexpression, knock-in, and selective nucleotide mutation. These genetic engineering strategies have been used to reduce or silence undesirable glycosyltransferase activities, enhance glycosyltransferase activities, activate endogenously silent genes, introduce new glycosites, mimic hypomorphic disease mutations, and insert foreign genes *(109)*. In recent years, genetic glycoengineering has been galvanized by the discovery and development of zinc-finger nucleases, transcription activator-like effector nucleases (TALENs), and clustered regularly interspaced short palindromic repeats (CRISPR)-CRISPR-associated protein (Cas) technology *(109, 111, 112)*. A strength of genetic approaches is their versatility and ability to make permanent cellular modifications; however, genetic approaches have limitations such as off-target effects, inefficient *in vivo* delivery systems, confounding epigenetic regulation of glycosylation pathways, and unpredictable alterations to cellular physiology *(109, 113)*.

Sialic acid is one of the most frequently targeted monosaccharides for glycoengineering due to its manifold impact on the pharmacokinetics of recombinant glycoproteins and its specific impact on bioactivity in antibody-dependent cellular cytotoxicity (ADCC), intravenous immunoglobin (IVIG) therapy, and antibody-drug conjugates (ADCs). Of particular interest, sialic acid masks the penultimate galactose and GlcNAc residues from the hepatocyte asialoglycoprotein receptor inhibiting protein endocytosis and clearance from circulation *(114, 115)*. This effect is bolstered by the net negative charge of sialic acid which reduces proteolytic degradation and subsequent clearance of the protein by the kidneys due to the cationic and anionic elements within the renal glomerular basement membrane and epithelium *(70, 116, 117)*.

Genetic manipulation of sialyltransferases constitutes a common approach to glycoengineer sialic acid; in particular expression of β-galactoside α(2,6)-sialyltransferases (usually ST6GAL1) in CHO cells enables the production of glycoproteins with both α(2,3)-sialic acids (from the cells' endogenous sialyltransferases) and α(2,6)-linked sialic acids (from the newly-expressed ST6GAL1),

similar to glycoproteins produced in humans *(112, 118-120)*. In addition, overexpression of ST6GAL1 (or other sialyltransferases) increases the overall sialylation of therapeutic glycoproteins including erythropoietin (EPO) *(120-122)*, tissue plasminogen activator *(119, 123)*, interferon γ (IFN-γ) *(124, 125)*, and immunoglobin G (IgG) *(123, 126, 127)*. Other studies have targeted the preceding step, the addition of galactose, to enhance terminal sialylation levels. Multiple studies have demonstrated that concomitant over-expression of β(1,4)-galactosyltransferase and α(2,3)-sialyltransferase in CHO cells yields increased sialylation and galactosylation in EPO, IgG, and tissue plasminogen activator *(121, 123)*. Another strategy is to overexpress Mgat4 and 5 to increase tri- and tetra-antennary branched N-glycans, thereby creating more sites for terminal sialylation; this strategy has been employed in EPO *(122)*, albumin EPO *(128)*, and IFN-γ *(129, 130)*.

Another strategy for improving sialylation targets enzymes and transporters in the SABP to increase CMP-Neu5Ac levels. One approach recapitulated point mutations in the bifunctional enzyme GNE associated with sialuria *(131, 132)*, a congenital disease that leads to excessive synthesis of sialic acid due to the absence of feedback regulation *(133)*, which led to increases in intracellular CMP-sialic acid levels and EPO sialylation *(134, 135)*. Although increasing intracellular CMP-Neu5Ac levels can increase glycoprotein sialylation there may be a saturation point due to the inefficiency of the CMP-sialic acid transporter responsible for transporting CMP-Neu5Ac to the Golgi. To overcome this barrier one study overexpressed CMP-sialic acid transporter in CHO cells, but only saw modest increases (4% - 16%) in IFN-γ sialylation *(136)*. Inhibiting or eliminating sialidases (or neuraminidases) is a complementary strategy for enhancing glycoprotein sialylation levels and retention times; these enzymes are glycosidases that catalyze the hydrolytic removal of sialic acid from glycoproteins, glycolipids, and polysaccharides *(137)*. One study utilized short interfering RNA and short-hairpin RNA to lower expression of the Neu1 and Neu3 sialidase in CHO cells, which increased recombinant IFN-γ sialylation by up to 33% *(138)*.

In a different approach, genetic glycoengineering can be utilized to introduce new glycosites into glycoproteins through creation of the Asn-X-Ser/Thr consensus sequence for N-glycosylation. This approach is illustrated by darbepoetin alfa, a genetically modified form of EPO that has five (instead of three) N-glycan sites *(139)*; this enhanced level of glycosylation improved serum longevity ~3-fold *(139)*, but was accompanied by adverse effects such as increased risk of stroke *(140)*. (As a caveat, there is no evidence that increased risk is a general feature of over-glycosylated therapeutic proteins beyond darbepoeitin alfa or a direct consequence of the newly-installed glycans). Another interesting example of building in N-glycosites is provided by Ibalizumab, where the strategic addition of an N-glycan to this mAb improves its HIV-neutralizing activity *(141)*.

1.3.3 Metabolic Glycoengineering

The second major strategy to control glycosylation is MGE, where living cells or entire organisms are supplemented with monosaccharide precursors that either increase natural flux through a biosynthetic pathway or increasingly, substitute natural metabolites with their non-natural counterparts. The exogenously-supplied synthetic monosaccharides are processed by the biosynthetic pathway, ultimately yielding glycans with enhanced glycoforms (e.g., improved sialylation) or non-natural chemical groups *(142-144)*. One advantage of MGE is its simplicity, where an analog can be directly added to cell culture medium to exploit the intrinsic cellular machinery without any need to genetically manipulate the host cell, thus averting off-target complications. However, MGE can be non-trivial due to the need for custom synthesis of the required monosaccharides and expensive to implement on an industrial scale because their concentration in culture media must be maintained to obtain a desired glycan profile *(142, 143)*.

One of the most common uses of MGE has been to increase the sialylation of recombinant proteins to improve their serum half-life. Numerous MGE strategies have aimed to take advantage of sialic acid's role in these protein metabolic degradation pathways by increasing flux through the SABP. One

of the most common and effective strategies has been to supplement cells with ManNAc or chemically modified ManNAc analogs *(145)*. The permissiveness of the SABP was discovered accidently by the Sartorelli group when trying to use a fluorinated ManNAc analog to block sialylation in cancer cells *(146, 147)*. Instead of blocking sialic acid production the fluorinated ManNAc analog was incorporated into the pathway and subsequently displayed in cell surface glycosylation. The Reutter group built on this initial discovery by developing hexosamine analogs capable of installing non-natural monosaccharides on cell surface glycans *(144, 148)*. Since these breakthroughs ManNAc has become the prevailing base unit for MGE analogs because of (i) cost, (ii) synthetic amenability, (iii) and high tolerability for incorporation into the SABP *(1, 142, 143)*. In some cases, even unmodified ManNAc has been shown to increase free intracellular and protein sialic acid levels. In one study supplementing CHO cells with 20 mM ManNAc increased the intracellular CMP-sialic acid pool by 30-fold and recombinantly produced IFN-γ sialylation increased by at least 15% *(30)*. This result was later corroborated by a study which found that addition of 20 mM ManNAc to CHO cells led to a 30-fold increase in CMP-sialic acid levels and a 32% increase in recombinant IFN-γ sialylation *(149)*. In contrast, a different study found that tissue inhibitor of metalloproteinase 1 recombinantly produced in CHO and NS0 cells supplemented with 20 mM ManNAc did not lead to any change in sialylation levels despite increases in intracellular CMP-sialic acid *(150)*. Additionally, experiments by Hills *et al.* found that adding 20 mM ManNAc to NS0 cells did not increase recombinantly produced IgG 1 sialylation despite a 44-fold increase in intracellular CMP-sialic acid levels *(151)*. These seemingly conflicting results may be attributed to the accessibility of the protein glycosites to sialyltransferases exemplified by the sterically hindered location of IgG fragment crystallizable (Fc) N-glycans *(151, 152)*. One major pitfall of using unmodified ManNAc is the requisite high concentrations (≥20 mM) rendering this strategy economically infeasible for production of recombinant proteins at an industrial scale *(153)*.

The shortcomings of unmodified ManNAc has led to the development of chemically modified versions of ManNAc with augmented uptake efficiency. To this end, our group peracetylated ManNAc creating Ac_4ManNAc which is metabolized and incorporated into the SABP 900-fold more efficiently than natural ManNAc. This allows Ac_4ManNAc to be used at more reasonable concentrations between 100 – 500 μM, yet at these concentrations Ac_4ManNAc is cytotoxic leading to reduced protein yields making this analog impractical for recombinant protein production (**Fig. 1.5**) *(154, 155)*. To circumvent this issue our group butyrated ManNAc creating a new array of analogs including 1,3,4-O-Bu_3ManNAc which is 2100-fold more efficient than its ManNAc precursor and critically has no cytotoxic effects at concentrations less than or equal to 500 μM (**Fig. 1.5**) *(156-158)*. Multiple studies have demonstrated that treating CHO cells with 300 μM of 1,3,4-O-Bu_3ManNAc increased erythropoietin (EPO) sialylation by at least 40% while supplementation with natural ManNAc at 20 mM resulted in only a 20% increase in EPO sialylation *(159, 160)*. Another added benefit of this compound is it leads to higher protein expression in CHO cells, specifically for IgG and EPO *(161)*. In theory supplementation of cell culture with 1,3,4-O-Bu_3ManNAc could be extended to any recombinant protein to ameliorate pharmacokinetic properties and increase protein yield.

In an alternative approach chemically modified ManNAc was used to create the analogs *N*-propanoylmannosamine (ManNPr) and *N*-pentanoylmannosamine (ManNPe) capable of causing cells to produce non-natural N-propanoyl or N-pentanoyl sialic acid *(144, 162, 163)*. When CHO cells producing EPO were supplemented with ManNPr or ManNPe the corresponding non-natural versions of sialic acid were installed in significant proportions on EPO. Critically, the glycoengineered EPO with N-propanoyl or N-pentanoyl sialic acid was more resistant to sialidases prolonging the residence time of sialic acids on EPO *(163)*.

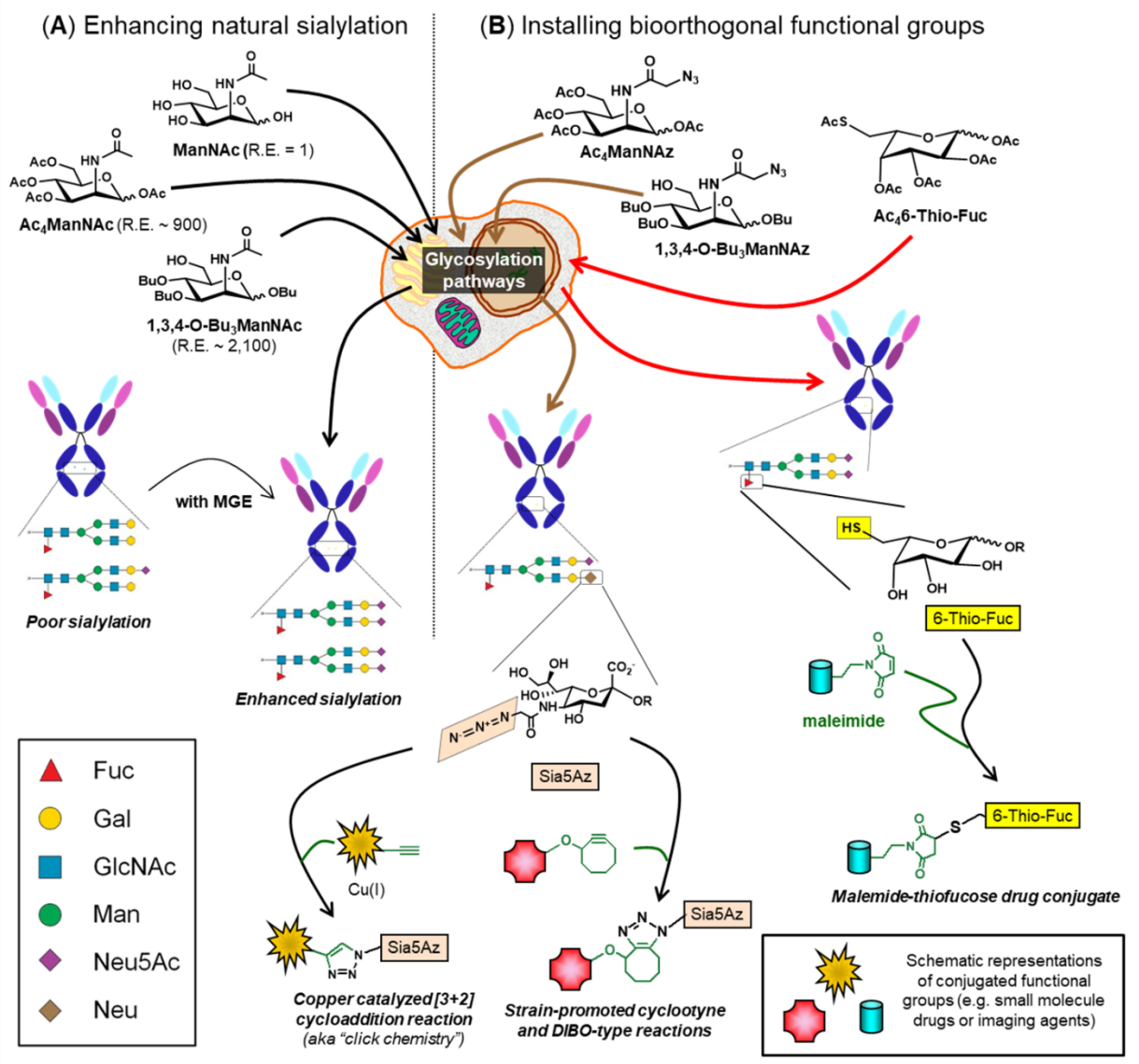

Figure 1.5 Glycoengineering mAbs for enhanced sialylation and glycan-targeted ADC production *(1)*. (A) Cells can be supplemented with ManNAc or analogs (e.g., Ac_4ManNAc or 1,3,4-O-Bu_3ManNAc), which intercept and increase flux through the SABP with the indicated relative efficiencies ("R.E." values) increasing sialylation of recombinant glycoproteins, such as mAbs. (B) Alternatively, cells can be supplemented with analogs containing non-natural chemical moieties (e.g., Ac_4ManNAz or 1,3,4-O-Bu_3ManNAz to install azide groups or $Ac_4$6-Thio-Fuc to install thiols). These functional groups, which do not naturally occur in glycans, constitute chemical handles for conjugation to small molecules including drugs, toxins, or imaging agents.

In a second MGE-based approach, ManNAc analogs can be used to install non-natural chemical moieties into glycans, in essence creating a chemical handle for bioorthogonal conjugation of small molecules including toxins, drugs, genes, imaging agents and polymers *(143)*. This strategy has been used to incorporate numerous non-natural functional groups such as ketones *(164-166)*, azides *(157, 167)*, alkynes *(168)*, diazirines *(169)*, aryl azides *(170)*, and thiols *(171)* into glycans for subsequent conjugation via click chemistry. A sialic acid-based MGE approach can be used to introduce conjugation sites restricted to the Fc region of mAbs for developing ADCs *(155, 172, 173)*; similarly, the fucose-replacing analog 6-thiofucose can introduce thiol moieties into 70% of IgG heavy chains with 90% conjugation efficiency to small molecule drugs via maleimide chemistry *(174)*. As superior metabolic analogs (e.g. 1,3,4-O-Bu_3ManNAz *(157)*) and conjugation chemistries (e.g., strain-promoted alkyne-azide cycloaddition *(156, 157)*) are developed MGE will continue to grow as an effective method for developing new biopharmaceuticals.

On a final note, the field of MGE has often been regarded as a genetically silent method to label glycans based on the assumption that the glycosylation machinery of a cell is not substantially perturbed while processing the exogenously-supplied sugars required for this methodology. While this premise is basically accurate, our group (and others) have described how metabolic flux engendered by MGE monosaccharide analogs (and even natural sugars) can on occasion affect the expression of glycogenes with this effect most well studied for the SABP *(175-177)*. The ability of MGE analogs to affect gene expression and cell physiology extends beyond glycogenes *per se* and can have a profound impact on cellular processes such as cell differentiation *(178-180)*. These effects are mentioned both to caution researchers to the complex interplay between metabolism, genetics, and cell fate that can occur during MGE interventions, but also to highlight the opportunities to use this technology to tune biological activity, which will facilitate future generations of biopharmaceuticals.

Chapter 2: Engineering CHO Cells for Improved Control Over Sialylation

2.1 Overview

The second chapter gives an in-depth description of the primary project for this thesis. The goal of this project was to use a combination of genetic engineering and MGE techniques to gain enhanced control over the quantity and type of sialylation produced by CHO cells. This chapter starts with a brief introduction to concepts important for this project that were not thoroughly discussed in Chapter 1. This is followed by (in order) a description of the specific aims of this project, methods, results, and a discussion of the current state of the project.

2.2 Background

This section briefly covers background information relevant to this chapter that was not extensively covered in the introduction. This section begins by explaining the discovery and mechanism of CRISPR-Cas technology. This is followed by an overview of sialic acid synthesis with an emphasis on the SABP.

2.2.1 Clustered Regularly Interspaced Short Palindromic Repeats

CRISPR-Cas technology has revolutionized genome engineering by enabling fast and precise modifications to be made to the genomes of a variety of organisms. The CRISPR-Cas system was originally discovered as part of an adaptive immune mechanism in bacteria and archaea to protect against phage infection and foreign plasmid transfer, but has since been repurposed as a technology for editing genomes *(181, 182)*. Generally, the CRISPR-Cas system utilizes a non-specific endonuclease (in most cases Cas9) to cut the genome at a location specified by a guide RNA (gRNA). The gRNA is comprised of two components (i) a crRNA which is a ~20 nucleotide RNA strand that has unique homology with one site in the target genome and (ii) a tracrRNA which acts as a scaffold

connecting the crRNA to the Cas endonuclease. The target genome site must contain an upstream (5') protospacer adjacent motif (PAM) sequence to initiate Cas recognition of the target site; the most common PAM motif is 5'-NGG-3' where N is any base pair. Once the Cas endonuclease recognizes the target genome site it creates a double stranded break in the DNA three to four nucleotides upstream of the PAM motif. The resulting double stranded break is then repaired by either non-homologous end joining (NHEJ) or homology directed repair (HDR). NHEJ is more common as it is the more efficient of the two pathways, however NHEJ tends to be error prone leading to random indel generation. Conversely, HDR has lower efficiency, but has higher fidelity enabling it to be used for precise genome edits *(183-185)*. A generalized workflow for implementing CRISPR-Cas technology is outlined in **Figure 2.1**. In this way any given region of the genome may be edited with both speed and specificity.

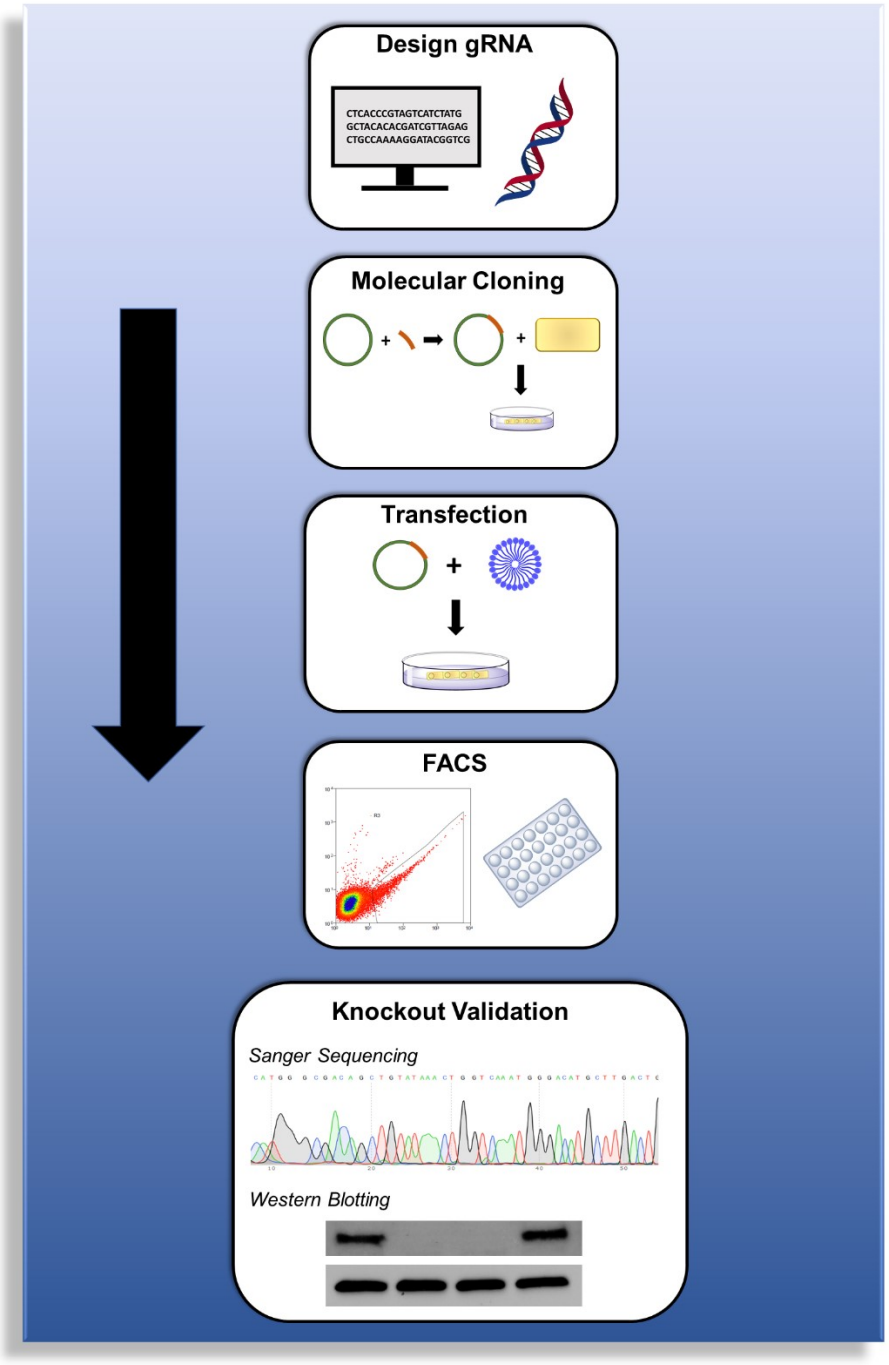

Figure 2.1 Overview of workflow for using CRIPSR-Cas technology to knockout a protein.

2.2.2 Sialic Acid Biosynthetic Pathway

Sialic acids are nine-carbon α-keto acids with over 50 different variants found throughout nature. Neu5Ac is modified with an N-acetyl group at the C-5 position of the carbon backbone and critically is the most prevalent form of sialic acid in humans. Sialic acids are primarily found as the penultimate glycan on various glycoconjugates and have numerous critical biological functions *(45)*. Crucial to this project sialic acid is known to protect proteins from metabolic degradation thereby extending their serum half-life (**1.3.2 Genetic Glycoengineering**). Sialic acids have different anabolic pathways in bacteria and mammals, however this section will focus on the mammalian pathway for the synthesis of Neu5Ac as it is most relevant to this work.

In mammals the *de novo* synthesis of sialic acid occurs in the cytosol beginning with the epimerization of UDP-GlcNAc to ManNAc which is subsequently phosphorylated to ManNAc 6-phosphate catalyzed by the bifunctional enzyme Gne. Gne is the rate limiting enzyme of the SABP and its epimerase activity is feedback inhibited by the final product of the pathway, CMP-sialic acid. Critically, the only other sources of ManNAc for the SABP is (i) from the epimerization of GlcNAc to ManNAc catalyzed by Renbp (also known as GlcNAc 2-epimerase [G2E]), (ii) the conversion of sialic acid to ManNAc and pyruvate catalyzed by sialic acid lyase, (iii) and nutritional sources (which contain only trace amounts of ManNAc) *(133)*. In the next step Neu5Ac 9-phosphate is formed via a condensation reaction between ManNAc 6-phosphate and phosphoenolpyruvate catalyzed by Neu5Ac 9-phophate synthase (Nans). This reaction is followed by the Neu5Ac 9-phosphate phosphatase (Nanp) catalyzed dephosphorylation of Neu5Ac 9-phophate yielding Neu5Ac. Neu5Ac is then transferred to the nucleus where it is converted to CMP-Neu5Ac by the CMP-Neu5Ac synthetase. From here CMP-Neu5Ac is transported to the Golgi apparatus via the CMP-sialic acid transporter where it can finally be transferred to glycan chains via one of approximately 20 different sialyltransferases (**Fig. 2.2**) *(45, 133)*.

2.3 Specific Aims

MGE is a technique that uses synthetic monosaccharides similar in structure to natural precursors in a biosynthetic pathway to manipulate cellular glycosylation processes (**1.3.3 Metabolic Glycoengineering**). Our lab has previously developed *(156, 157)* and characterized *(158)* novel butyrated ManNAc analogs (1,3,4-O-Bu_3ManNAc and 1,3,4-O-Bu_3ManNAz) capable of increasing metabolic flux through the SABP thereby increasing glycoprotein sialylation and installing non-natural chemical groups on protein sialylation *(159, 160)*. The butyl groups enable efficient transport across the cellular membrane and are subsequently cleaved by nonspecific esterases to yield a ManNAc molecule which intercepts the SABP. In addition to increasing sialic acid levels the analog, 1,3,4-O-Bu_3ManNAz, can be used to incorporate sialic acid with an azide moiety onto glycoproteins. Incorporation of non-natural chemical groups enables conjugation of various chemical compounds to recombinant glycoproteins. However, these analogs do not give complete control over quantity and type of sialic acid produced due to endogenous ManNAc flux through the SABP. ManNAc, which is the feedstock for the SABP, is produced endogenously in mammals by three enzymes Gne *(133, 186)*, Renbp *(187)*, and sialic acid lyase *(45)*.

In mammals, Gne is regarded as the primary enzyme that supplies ManNAc for incorporation into the SABP *(133, 188)*. Gne is a bifunctional enzyme that catalyzes the isomerization of UDP-GlcNAc to ManNAc and subsequent phosphorylation to ManNAc 6-phosphate. Critically, CMP sialic acid, a downstream SABP intermediate, feedback inhibits the epimerase activity of Gne, thus facilitating MGE. Two sets of experiments illustrate the important role of Gne activity in tuning the metabolic incorporation of ManNAc analogs into the SABP. First, in cells with a mutant form of Gne that lacked feedback inhibition, the resulting very high levels of ManNAc endogenously produced in these cells almost completely obliterated the incorporation of non-natural ManNAc analogs into the SABP *(132, 154)*. Conversely, diminished ManNAc production in cells lacking Gne reduced competition for non-

natural ManNAc analog uptake from endogenously-produced ManNAc into the SABP and facilitated cell surface presentation of the resulting non-natural sialic acids *(189)*.

These experiments suggested that MGE will achieve optimal efficiency in cells lacking the ability to produce ManNAc endogenously. Consequently, one goal of the project was to knockout Gne, which is the primary endogenous source of ManNAc in mammalian cells including CHO-K1 cells commonly used in biomanufacturing. There are, however, secondary routes by which ManNAc can enter the SABP. One mechanism is by conversion from GlcNAc through an epimerization reaction catalyzed by Renbp, where GlcNAc is the thermodynamically favored product under normal conditions (equilibrium ratio of 3.9:1) *(190)*. Renbp can produce ManNAc if the GlcNAc to ManNAc ratio is high. Such an excess of GlcNAc, leading to conversion of ManNAc, is expected in Gne knockout cells *(133, 191)*. Accordingly, a second goal of this project was to knockout Renbp in CHO-K1 cells in order to eliminate another route by which ManNAc is endogenously incorporated into the SABP (**Fig. 2.2**). A final route for ManNAc production in mammalian cells is through sialic acid lyase, which coverts sialic acid back to ManNAc and pyruvate. This enzyme is primarily involved in sialoside recycling and has been shown to be able to salvage sialic acids present on glycoproteins in fetal bovine serum (FBS) used in cell culture *(192)*. In this project we focus on CHO cells that can be grown in reduced serum media, which minimizes this salvage mechanism and lessens the impact of metabolic flux competition on ManNAc analogs used in MGE (However, the additional knockout of sialic acid lyase is discussed in the context of Future Work (**2.7.4 Knockout Sialic Acid Lyase**). In theory, for the first time, these strategies will allow for enhanced control of sialic acid levels and composition via supplementation with our butyrated ManNAx analogues. This project was pursued with a focus on the following specific aims:

Aim 1: Eliminate competing endogenous routes for ManNAc to enter the SABP. CRISPR-Cas technology was used to knockout Gne and Renbp in CHO-K1 cells thereby preventing the primary and secondary routes by which ManNAc can enter the SABP.

Aim 2: Determine how knocking out the *Gne* and *Renbp* genes impacts cellular uptake and incorporation of 1,3,4-O-Bu$_3$ManNAc. The genetically engineered cell lines were supplemented with varying concentrations of 1,3,4-O-Bu$_3$ManNAc and levels of free intracellular sialic acid were analyzed through multiple assays.

Aim 3: Determine how knocking out the *Gne* and *Renbp* genes impacts cellular uptake and incorporation of 1,3,4-O-Bu$_3$ManNAz. The genetically engineered cell lines were supplemented with varying concentrations of 1,3,4-O-Bu$_3$ManNAz and azide incorporation levels were analyzed through click chemistry-based assays.

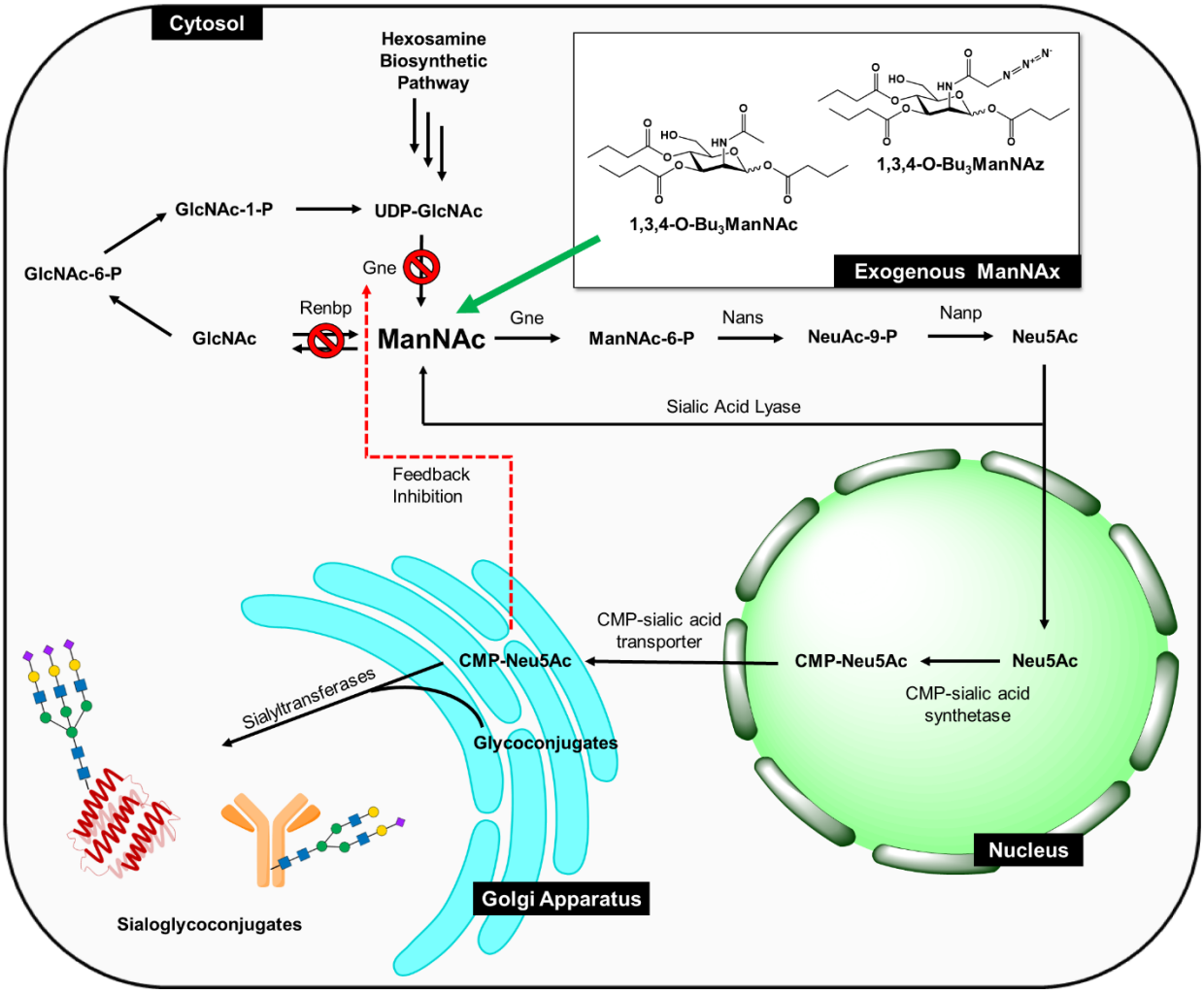

Figure 2.2 Overview of the strategy to gain enhanced control over glycoprotein sialylation levels and composition. To achieve this aim, a combination of genetic engineering and MGE was employed. CRISPR-Cas technology was used to knockout Gne and Renbp in CHO-K1 cells to cut off the primary endogenous routes by which ManNAc can flux into the SABP. After cell engineering, ManNAc analogs (1,3,4-O-Bu_3ManNAc and 1,3,4-O-Bu_3ManNAz) were added to the cell culture media to precisely modulate sialylation levels and improve the percent incorporation levels of non-natural forms of sialic acid.

2.4 Materials & Methods

2.4.1 Cell Culture

The CHO-K1 cell line (ATCC, CCL-61) was used for all cell engineering and experiments performed in this chapter. The CHO-K1 cell line is a subclone of the parental CHO cell line derived by Puck *et al.* from a biopsy of an ovary of an adult *Cricetulus griseus* (Chinese hamster) *(193)*. Unless

stated otherwise CHO-K1 cells were cultured in an adherent monolayer in F-12K nutrient mixture (Kaighn's modification) (Corning, 10-025-CV) supplemented with 10% (v/v) heat inactivated, sterile filtered FBS, 1% (v/v) antibiotic-antimycotic solution (100x) (Sigma Aldrich, A5955-100ML), and 5% CO_2 in a humidified environment at 37 °C. CHO-K1 cells were kept at or below 1 x 10^5 cells cm^{-2} to prevent them from reaching a confluent and quiescent growth stage. The cells were passaged every three to four days by aspirating the spent media, washing once with phosphate buffered saline (PBS) (pH = 7.4), detached using 0.25% trypsin-EDTA (Gibco, 25200-056), and incubated in a 5% CO_2, humidified 37 °C environment for 5 – 10 minutes. After incubation, cell detachment was verified using a microscope and fresh complete F-12K media was used to transfer cells to a conical tube. Cells were pelleted via centrifugation for 5 minutes at 1057 x g, resuspended in 5 mL of complete F-12K media and seeded at a density of 1 x 10^4 cells cm^{-2}. Cell density was determined using a Beck Z2™ Coulter Particle Count and Size Analyzer (Beckman-Coulter) with a 100 μm aperture, dilution factor of 1:101, and boundaries set between 7 and 25 μm. Two measurements were made per sample and averaged to determine cell density.

2.4.2 Mammalian Cell Cryopreservation

CHO-K1 cells were detached, pelleted, resuspended, and counted as described above (**2.4.1 Cell Culture**). Cells were preserved by combining 10% (v/v) dimethyl sulfoxide (DMSO) with 1 x 10^6 cells suspended in fresh, complete F-12K media in a screw top cryopreservation tube. The cells were placed in a "Mr. Frosty" freezing container with 2-propanol and frozen in a -80 °C freezer at a controlled rate of 1 °C per minute. After 24 hours the cells were transferred from the "Mr. Frosty" freezing container to a liquid nitrogen cryopreservation vessel (final temperature -196 °C) for long term storage.

2.4.3 Thawing Cryopreserved Cells

Cryopreserved cells were removed from liquid nitrogen storage and thawed quickly (< 1 minute) in a 37 °C water bath until only a small bit of ice remained. Prewarmed compete F-12K media was added to the cryopreservation tube and the cell solution was transferred to a conical tube. Cells were pelleted by centrifuging at 1057 x g for 5 minutes and the DMSO F-12K media supernatant was aspirated. The cells were resuspended in fresh F-12K media, transferred to a T-25 tissue culture flask, and incubated in a humidified 37 °C environment with 5% CO_2.

2.4.4 Guide RNA Design

Guide RNA were selected using the *C. griseus* genome *(100, 194)* and software developed by Benchling Inc., CHOPCHOP *(195)*, and CRISPy *(196)*. These programs utilize algorithms *(197-199)* to minimize off-target effects and maximize the likelihood of the gRNA hitting the target site in the genome. Only gRNA preceding the canonical PAM, 5'-NGG-3', were selected. Guide RNA targeting earlier exons proximal to the N-terminus side were chosen to minimize the possibility of a partially functional protein being translated. The first exon was also avoided to prevent an alternative ATG initiation codon from enabling translation of the target protein. Although, gRNA with lengths between 16 – 24 base pairs can be effective, only gRNA with a 20 base pair length were chosen because research has indicated this length is optimal *(200)*. Finally, all selected gRNA were compared directly to the *C. griseus* genome using the Basic Local Alignment Search Tool (BLAST) to verify each gRNA candidate only had a high degree of sequence homology to the target site. For each gene target (i.e. *Gne* and *Renbp*) two gRNA were selected in the event one is unable to generate indels (**Table 2.1**).

Table 2.1 Sequences of gRNA designed to knockout *Gne* and *Renbp*.

Sequence (5' → 3')	Gene target	Exon Location	Gene Location (base pairs from N-terminus)	Strand	PAM (5'→3')
GCTACACACGATCGTTAGAG	*Gne*	2	4388	Sense +	GGG
GTTCGAGTGATGCGGAAGAA	*Gne*	4	12641	Sense +	GGG
CGGCATCTAGAAGCTCAGCG	*Renbp*	3	702	Antisense -	AGG
TGTGCTAGAGAATGTATCAG	*Renbp*	6	2694	Sense +	AGG

2.4.5 Cloning the gRNA oligos into the pSpCas9(BB) vector

The methods for constructing the gRNA-Cas9 plasmid were adapted from previous work *(185, 201, 202)*. The vector pSpCas9(BB)-2A-GFP (PX458) (Addgene, #48138) was graciously provided by Feng Zhang *(185)*. This vector contains the Cas9 from *Streptococcus pyogenes* along with 2A-EGFP (green fluorescent protein) and ampicillin selection markers (**Fig. 2.3**). Four additional base pairs were added to each gRNA oligo and its reverse complement to provide overlap regions with two *BbsI* restriction sites in the pSpCas9(BB)-2A-GFP vector (**Table 2.2**). The modified gRNA oligos and their reverse complements were ordered from Integrated DNA Technologies. The gRNA oligos were resuspended in nuclease- and protease-free water to a final concentration of 100 μM. The gRNA oligos were combined with the master mix outlined in **Table 2.3** and subsequently phosphorylated and annealed in a T100 thermocycler (Bio-Rad) using the following parameters: 37 °C for 30 minutes, 95 °C for 5 minutes, decrease to 25 °C at a rate of 5 °C per minute. The resulting duplex oligos were then diluted in nuclease- and protease-free water at a 1:200 ratio. The pSpCas9(BB)-2A-GFP vector was digested and the gRNA oligo duplex was ligated into the vector between two *BbsI* restriction sites using the reaction mixture outlined in **Table 2.4**. The digestion and ligation mixture was incubated for 60 minutes using the following cycle repeated six times: 37 °C for 5 minutes, 21 °C for 5 minutes. The ligated plasmid was transformed into *E. coli* strain Stbl3 in a competent state using standard heat shock methods. After transformation super optimal broth with catabolite repression (SOC) media

was added and the *E. coli* were plated at two different densities on lysogeny broth (LB) plates with 100 μg mL^{-1} ampicillin. Untransformed *E. coli* and *E. coli* transformed with the linearized but unligated plasmid were plated as negative controls. *E. coli* transformed with the unaltered pSpCas9(BB)-2A-GFP vector were plated as a positive control. All plates were incubated for ~24 hours at 37 °C. The following day plates were inspected for bacterial growth and single colonies were selected for expansion via LB liquid cultures supplemented with 100 μg mL^{-1} ampicillin. Liquid bacterial cultures were incubated for ~18 hours at 37 °C with agitation (200 rpm). The following day plasmid was isolated from the liquid cultures (**2.4.6 Plasmid Isolation**) and sent for Sanger sequencing to verify correct gRNA insertion. The remaining liquid culture was used to make bacterial glycerol stocks for long-term cryogenic storage by combining sterile 50% (v/v) glycerol with the bacterial liquid culture in a 1:1 ratio and freezing at -80 °C. Sanger sequencing was performed by the Johns Hopkins School of Medicine Genetic Resources Core Facility (GRCF) using the U6-Fwd primer: 5'-GAGGGCCTATTTCCCATGATTCC-3'.

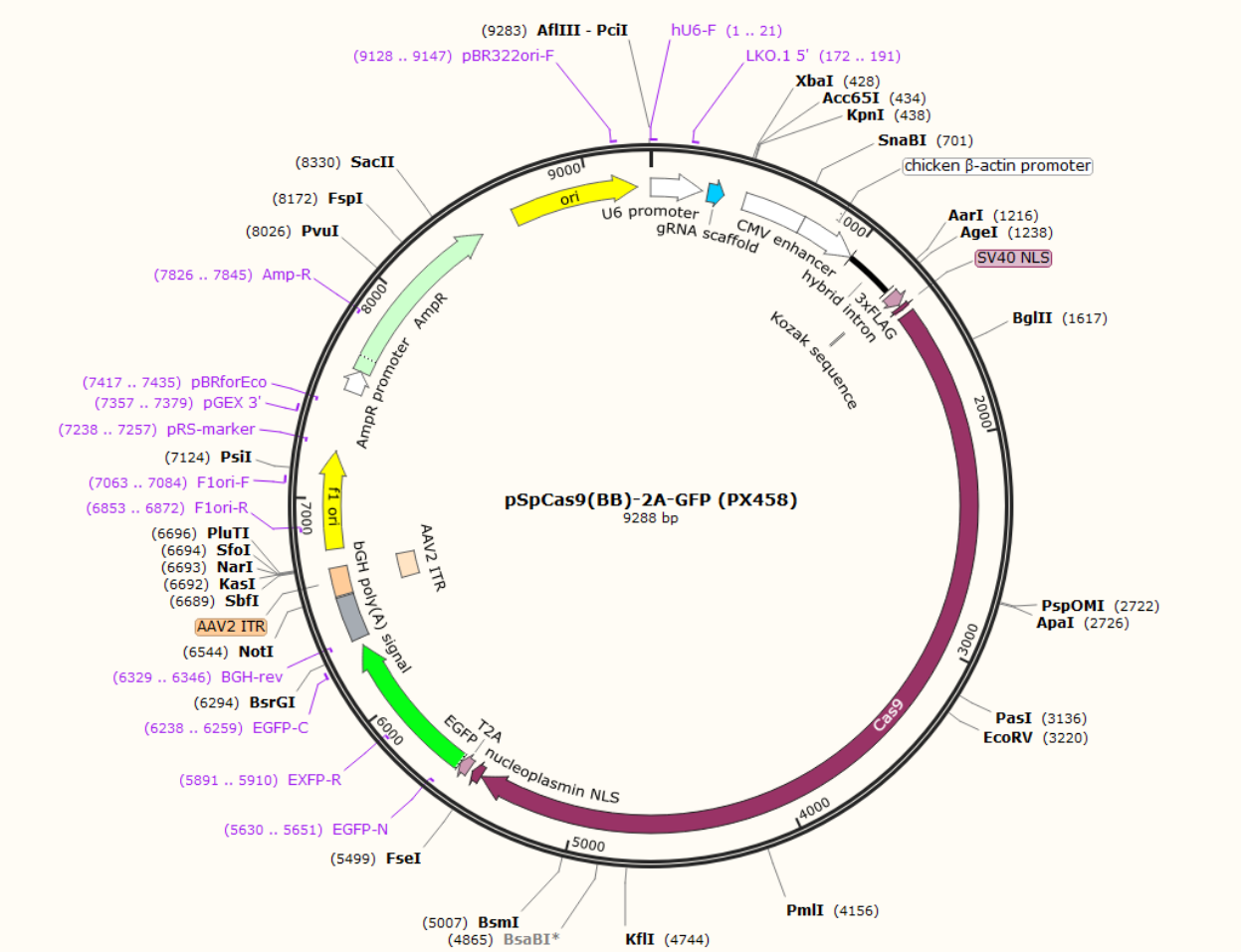

Figure 2.3 Vector map of the pSpCas9(BB)-2A-GFP (PX258) plasmid used for knocking out target proteins in CHO-K1 cells. The pSpCas9(BB)-2A-GFP is a 9300 base pair vector containing the *S. pyogenes* Cas9 gene under the control of the U6 promotor with a CMV enhancer and both GFP and ampicillin genes for selection purposes. Guide RNA were cloned between two *BbsI* restriction sites directly downstream from the U6 promotor. The pSpCas9(BB)-2A-GFP was originally designed and constructed by Feng Zhang *(185)*.

Table 2.2 Sequences of DNA oligos (sense and anti-sense) cloned into the pSpCas9(BB)-2A-GFP (PX258) plasmid. Base pairs in bold text were added to provide overlap between the gRNA and destination vector.

gRNA Sequence (5' → 3')	gRNA Reverse Complement Sequence (5' → 3')	Gene target
CACCGCTACACACGATCGTTAGAG	**AAAC**CTCTAACGATCGTGTGTAGC	*Gne*
CACCGTTCGAGTGATGCGGAAGAA	**AAAC**TTCTTCCGCATCACTCGAAC	*Gne*
CACCCGGCATCTAGAAGCTCAGCG	**AAAC**CGCTGAGCTTCTAGATGCCG	*Renbp*
CACCTGTGCTAGAGAATGTATCAG	**AAAC**CTGATACATTCTCTAGCACA	*Renbp*

Table 2.3 Reaction used to anneal and phosphorylate the gRNA oligos.

Component	Volume (µL)
gRNA (100 µM)	1
gRNA reverse complement (100 µM)	1
T4 ligation buffer, 10x	1
T4 polynucleotide kinase	1
Nuclease- and protease-free H_2O	6
Total	10

Table 2.4 Reaction used to clone the annealed and phosphorylated gRNA oligos into the pSpCas9(BB)-2A-GFP (PX258) plasmid.

Component	Volume (µL)
pSpCas9(BB)-2A-GFP	100 ng
Diluted oligo duplex	2
Tango buffer, 10x	2
DTT, 10 mM	1
ATP, 10 mM	1
FastDigest *BbsI*	1
T7 ligase	0.5
Nuclease- and protease-free H_2O	To 20 µL
Total	20

2.4.6 Plasmid Isolation

All plasmids were isolated from bacteria using the QIAprep Spin Miniprep Kit (Qiagen, 27106) per the manufacturer's instructions. To summarize, bacterial liquid cultures were pelleted via centrifugation at 6,800 x g for 3 minutes at room temperature. The bacterial pellet was resuspended in 250 µL Buffer P1, lysed with 250 µL Buffer P2, and neutralized with 350 µL Buffer N3. This mixture was centrifuged for 10 minutes at 17,900 x g and the resulting supernatant was transferred to a

QIAprep 2.0 spin column. The sample was processed using a vacuum manifold and washed with Buffer PB and Buffer PE. The column then was centrifuged for 1 minute at 17,900 x g to remove residual Buffer PE and eluted using nuclease- and protease-free water. The plasmid concentration was determined using a Nanodrop 2000 (Thermo Fisher Scientific).

2.4.7 Transfection

The day before transfection CHO-K1 cells were seeded in 6-well plates at a density of 1.5 x 10^6 cells mL^{-1}. The following day Lipofectamine 2000 (Thermo Fisher Scientific, 11668027) and sequence verified pSpCas9(BB)-2A-GFP plasmid with the appropriate gRNA inserted were combined to transfect the CHO-K1 cells. For each target protein (i.e. *Gne* and *Renbp*) both constructed plasmids were used to co-transfect the CHO cells to increase the likelihood of indel generation and protein knockout. For each well to be transfected 2500 ng of each plasmid DNA was diluted in 250 µL Opti-Mem I reduced serum medium and 2.5 µL of Lipofectamine 2000 was diluted in 250 µL Opti-Mem I reduced serum medium. The diluted plasmid DNA and Lipofectamine 2000 solutions were combined in a 1:1 ratio and incubated at room temperature for 20 minutes to allow for complexation of DNA and Lipofectamine. During incubation the spent media from the 6-well plates with CHO-K1 cells was aspirated and the cells were washed once with PBS. The wells were replenished with 1.5 mL of F-12K media without FBS and antibiotic-antimycotic solution. Once the DNA-Lipofectamine complexes had formed 500 µL of the complex was added to each well. DNA plasmid and lipofectamine were also individually added to one well each to serve as negative controls. The cells were incubated for 24 hours at 37 °C in a humidified environment with 5% CO_2. After 24 hours the media was aspirated and replaced with fresh F-12K media supplemented with 10% (v/v) FBS and 1% (v/v) antibiotic-antimycotic solution. Forty-eight hours post-transfection the cells were examined for GFP expression using an EVOS FL Imaging System (Thermo Fisher Scientific) and harvested for fluorescent activated cell sorting (FACS).

2.4.8 Fluorescent Activated Cell Sorting

Forty-eight hours post-transfection CHO cells were detached and pelleted as described in the **2.4.1 Cell Culture** section. The pelleted cells were resuspended in 2% (w/v) bovine serum albumin (BSA) in Hanks' buffered salt solution (HBSS) to prevent cell aggregation during the sorting process. Cells were sorted using a Becton Dickinson FACS Canto II (3 laser, 8 color) (BD Biosciences). All FACS experiments were performed with the assistance of Hao Zhang in the Johns Hopkins Bloomberg School of Public Health Flow Cytometry and Immunology Core facility. Each sample was filtered with a sterile 35 μm nylon mesh strainer and combined with 10 μg mL^{-1} of propidium iodide (PI). Each sample was sorted based on the following parameters: morphology, granularity, PI negative, and GFP positive. Single sorted cells were then seeded in 96-well plates with 100 μL of F-12K media supplemented with 10% (v/v) FBS and 1% (v/v) antibiotic-antimycotic solution in order to obtain monoclonal cell lines. The monoclonal cell lines were supplemented with 50 μL of media every three days for a total of 12-14 days. Monoclonal cell lines exhibiting positive growth were expanded to 6-well plates for downstream analysis and validation of protein knockout.

2.4.9 Genomic DNA Extraction and Amplification

Following cell expansion 1 x 10^5 cells were collected from each monoclonal population for genomic DNA (gDNA) extraction and the remaining cells were cryopreserved (**2.4.2 Mammalian Cell Cryopreservation**). Each sample was centrifuged at 1057 x g for 5 minutes, washed once with PBS, and resuspended in 50 μL QuickExtract DNA Extraction Solution (Lucigen, QE0950). The gDNA was isolated by heating in a T100 thermocycler (Bio-Rad) at 65 °C for 10 minutes followed by 98 °C for 5 minutes and then diluted in 100 μL of nuclease- and protease-free water. Primers were designed to amplify a 600 – 1000 base pair amplicon with greater than 100 base pairs flanking the CRISPR cut site. The primers were designed using Integrated DNA Technologies PrimerQuest Tool using the following target parameters: optimal primer T_m = 62 °C, optimal GC% = 50%, and optimal primer size

= 22 nucleotides (**Table 2.5**). Each sample's isolated gDNA was combined in the reaction mix outlined in **Table 2.6** and amplified using a T100 thermocycler (Bio-Rad) with the cycle given in **Table 2.7**. The resulting PCR products were analyzed using a 1% (w/v) agarose gel in 1x tris boric ethylenediaminetetraacetic acid with 0.5 μg mL^{-1} ethidium bromide. Each sample was combined with 5x loading dye and loaded after the gel had solidified. The gel was run at ~120 volts for 60 minutes and the products were visualized with ultraviolet light at 300 or 360 nm.

Table 2.5. Primers used to amplify a region of genomic DNA near the Cas9 cut site of each gene target.

Primer sequence (5' → 3')	Amplification site	Length (base pairs)	T_m (°C)	GC content (%)
GTAACAGTGGGAATCAGGTAGAA	*Gne* Exon 2	23	54.0	43.5
AGCAAGAGCCGTGAAGTAAA	*Gne* Exon 2	20	54.3	45.0
ACTGTGGTATCCTACCCTATCC	*Gne* Exon 4	22	55.0	50.0
CGAACTCCACAGCTGCTATT	*Gne* Exon 4	20	55.0	50.0
CACTCCCATGACCAGGAATATG	*Renbp* Exon 3	22	55.1	50.0
GGTGAGGGCTTGGAATATACTG	*Renbp* Exon 3	22	55.1	50.0
TCTGTGGGCATTCAACTCTATC	*Renbp* Exon 6	22	54.5	45.5
CCAAGCATCTGAGGGCTTTA	*Renbp* Exon 6	20	54.9	50.0

Table 2.6. PCR used to amplify genomic DNA near the Cas9 cut site of each gene target.

Component	Volume (µL)
Genomic DNA	4 (~40 ng)
Forward Primer (9 µM stock)	1 (final conc. 300 nM)
Reverse Primer (9 µM stock)	1 (final conc. 300 nM)
OneTaq Hot Start 2X Master Mix	15
Nuclease free H_2O	9 (to 30 µL)
Total	30

Table 2.7. PCR cycle used to amplify genomic DNA near the Cas9 cut site of each gene target.

Step	Temperature (°C)	Time (min:sec)	Cycles
Denature	95	5:00	1
Denature	95	0:30	40
Anneal	58	0:30	
Extend	72	0:30	
Extend	72	5:00	1
Store	4	∞	NA

2.4.10 PCR Reaction Purification

If the desired PCR product was the only one observed using gel electrophoresis the remaining PCR reaction was purified using a QIAquick PCR Purification Kit (Qiagen, 28104) per the manufacturer's instructions. To briefly summarize, 5 volumes of Buffer PB was added to 1 volume of PCR reaction and if the reaction color turned orange or violet, 3 M sodium acetate, pH 5.0 was added. The reaction was transferred to a QIAquick column and the DNA was bound to the membrane using a vacuum manifold. The bound DNA was washed once with Buffer PE, centrifuged at 17,900 x g for 1

minute to remove residual buffer, and eluted with nuclease- and protease-free water. The purified DNA product concentration was determined using a Nanodrop 2000 (Thermo Fisher Scientific). The purified PCR products were submitted for Sanger sequencing (Johns Hopkins School of Medicine GRCF) using the corresponding forward and reverse primer pair used to amplify the product.

2.4.11 Gel Extraction

If multiple PCR products were observed using gel electrophoresis the target amplicon was isolated using the QIAquick Gel extraction Kit (Qiagen, 28115) per the manufacturer's instructions. To summarize, the target DNA fragment was excised from the gel, weighed, and combined with 3 volumes Buffer QG. The gel buffer mix was incubated at 50 °C for 10 minutes with periodic vortexing; if the mixture turned violet or orange, 3 M sodium acetate, pH 5.0 was added. One volume of 2-propanol was added and each sample was transferred to a QIAquick spin column. The DNA was bound to the column membrane using a vacuum manifold, washed once with Buffer QG and Buffer PE, and centrifuged at 17,900 x g for 1 minute to remove any residual wash buffer. The DNA was eluted from the membrane with nuclease- and protease-free water and the concentration was determined using a Nanodrop 2000 (Thermo Fisher Scientific). The purified PCR products were submitted for Sanger sequencing (Johns Hopkins School of Medicine GRCF) using the corresponding forward and reverse primer pair used to amplify the product.

2.4.12 TOPO-TA Cloning

Monoclonal cells lines whose PCR products sequencing results showed indel generation were further validated by cloning the PCR amplicon into a pCR 4-TOPO vector using the TOPO TA Cloning Kit for Sequencing (Thermo Fisher Scientific, K4575J10). The purified PCR products were ligated to the pCR 4-TOPO vector using the reaction mix outlined in **Table 2.8** and incubated for 15 minutes at room temperature. The ligated plasmid was transformed into Top10 chemically competent *E. coli* using standard heat shock methods. The transformed *E. coli* were supplemented with SOC media and

incubated at 37 °C for 1 hour at 200 rpm. The transformed *E. coli* were plated at two different densities on LB plates with 100 μg mL^{-1} ampicillin and incubated for ~24 hours in a 37 °C. The next day 10 single colonies were selected per sample and used to inoculate LB liquid cultures supplemented with 100 μg mL^{-1} ampicillin. Liquid bacterial cultures were incubated for ~18 hours at 37 °C at 200 rpm. The following day plasmid was isolated from the liquid cultures (**2.4.6 Plasmid Isolation**) and sent for Sanger sequencing (Johns Hopkins School of Medicine GRCF).

Table 2.8 Reaction mix for TOPO cloning.

Component	Volume (μL)
Fresh PCR product	0.5 – 4
Salt solution	1
Nuclease- and protease- free water	add to a total volume of 5 μL
pCR 4-TOPO vector	1 μL
Total	**6**

2.4.13 Western Blotting

Approximately 1 x 10^6 cells were harvested (**2.3.1 Cell Culture**), transferred to a microcentrifuge tube, washed once with PBS, and resuspended in 10 – 25 μL of radioimmunoprecipitation assay buffer (RIPA) supplemented with protease inhibitor cocktail (Sigma Aldrich, P8340-5ml). The samples were incubated on ice for 30 minutes and each sample was vortexed every 10 minutes to promote cell lysis. The samples were centrifuged at ~22,000 x g at 4 °C for 15 minutes and the resulting supernatant was transferred to a fresh microcentrifuge tube. Each protein sample was quantified via the bicinchoninic acid (BCA) assay *(203)*. To summarize, eight BSA standards ranging from 20-20,000 μg mL^{-1} were made in PBS via serial dilutions and 10 μL were added to a 96-well plate in duplicate. One microliter of protein sample was combined with 9 μL PBS and added to the same 96-well plate in duplicate. The Peirce BCA Assay Reagent (Thermo Fisher Scientific, 23225) was

prepared per the manufacturer's instructions and 100 µL was added to each standard and protein sample. The 96-well plate was incubated at 37 °C for ~45 minutes and each wells absorbance was measured at 562 nm using a Synergy HTX Multi-Mode Microplate Reader (BioTek).

Fifteen micrograms of each protein sample was combined with 4x laemmli concentrate supplemented with 2-mercaptoethanol and diluted to 30 µL with RIPA buffer and protease inhibitor cocktail solution. The samples were denatured by heating at 90 °C for 10 minutes and loaded onto a Mini-PROTEAN TGX 4-15% gradient gel with a 10-well comb and 30 µL well volume. The gel was run in 1x tris/glycine/SDS buffer (Biorad, 161-0772) for ~60 minutes at 100 volts. The protein was subsequently transferred to a 0.45 µM nitrocellulose membrane using standard wet transfer techniques with all components being equilibrated with 1x tris/glycine buffer (Biorad, 161-0771) with 20% (v/v) methanol. The transfer was run in 1x tris/glycine buffer with 20% (v/v) methanol on ice at exactly 100 volts for 60 minutes. The membrane was blocked in 5% (w/v) BSA in tris buffered saline with 0.1% (v/v) Tween 20 (TBST) at room temperature for 60 minutes with agitation. The primary antibodies were diluted in 5% (w/v) BSA in TBST to the recommended concentration and added to the blot for overnight incubation at 4 °C with agitation. The primary antibodies used for western blots in this chapter and their dilution ratios are listed in **Table 2.9**. The next day the blot was washed three times with TBST for 10 minutes each with agitation. The appropriate horse radish peroxidase (HRP) linked secondary antibody (anti-mouse IgG, [Cell Signaling, 7076] or anti-rabbit IgG, [Cell Signaling, 7074]) was diluted in 5% (w/v) BSA in TBST at a 1:10,000 ratio, added to the blot, and incubated for 60 minutes at room temperature with agitation. After incubation the blot was washed three times with TBST for 10 minutes each with agitation. While washing, the enhanced chemiluminescent substrate was prepared by combining SuperSignal West Pico PLUS Luminol/Enhancer solution (Thermo Fisher Scientific, 1863098) with SuperSignal West Pico PLUS Stable Peroxidase solution (Thermo Fisher Scientific, 1863099) in a 1:1 ratio. After the third TBST wash, the blot was incubated with the enhanced chemiluminescent substrate for ~30 s and

transferred to a plastic sheet protector in a film cassette for imaging using Blu-C autoradiography films (Stellar Scientific, BLC-810-100).

After imaging the blot was stripped for 15 minutes using Gentle Review Stripping Buffer (Amresco, A611-N552-13), washed three times with TBST for 10 minutes each and reblocked with 5% (w/v) BSA in TBST for 60 minutes at room temperature with agitation. As a loading control, β actin (Cell Signaling, 3700) diluted in 5% (w/v) BSA in TBST at a 1:10,000 ratio was added to the blot and incubated at room temperature for 30 minutes with agitation. The blot was washed three times with TBST for 10 minutes each and HRP-linked anti-mouse IgG diluted 1:10,000 in 5% (w/v) BSA in TBST was added to the blot for 30 minutes. The blot was washed three times with TBST for 10 minutes and imaged via autoradiography as described above. Western blotting to assess protein level knockouts of Gne and Renbp were repeated in biological triplicate for each cell line.

Table 2.9 Primary antibodies used to assess protein level knockout of Gne and Renbp.

Antibody	Protein	Manufacturer	Catalog number	Dilution Concentration
GNE Polyclonal Antibody	Gne	Thermo Fisher Scientific	PA5-55559	0.4 μg mL^{-1} (1:250)
Anti-RENBP antibody	Renbp	Abcam	ab77081	0.7 μg mL^{-1} (1:1000)

2.4.14 Densitometry

ImageJ (National Institute of Health) was used to compare and quantify the density (intensity) of the bands for each western blot sample. Gel images were saved as TIFF files, opened in ImageJ, and converted to an 8-bit gray-scale image (*Image→Type→8-bit*). The rectangle tool was used to select the first lane and it was defined as lane 1 by selecting *Analyze→Gels→Select First Lane*. The first rectangle was copied and dragged to surround the second lane and it was defined as lane 2 by selecting *Analyze→Gels→Select Next Lane*. This process was repeated for all subsequent lanes. After

all lanes were selected the intensity was analyzed by selecting *Analyze→Gels→Plot*. The output profile plot represents the relative density of the rectangle surrounding each lane. The line tool was used to enclose the peak at the baseline to eliminate background signal. The size of each peak was quantified by using the Wand tool to highlight each peak. The peaks were labeled with their size as a percentage relative to the total size of all peaks by selecting *Analyze→Gels→Label Peaks*. The density of each peak was then expressed relative to the peak intensity for the wild type CHO sample and adjusted based on the peak intensity of the β actin loading control.

2.4.15 ManNAx Chemical Analog Synthesis

The 1,3,4-O-Bu_3ManNAc and 1,3,4-O-Bu_3ManNAz analogs used throughout this chapter were synthesized as described in previous work *(156)*. The chemical analogs used in these experiments were synthesized and characterized by Christian Agatemor and Chris Saeui.

2.4.16 Periodate Resorcinol Assay

Forty-eight hours before performing the periodate resorcinol assay 1.5 x 10^6 cells were seeded in 100 mm x 20 mm tissue culture dishes using F-12K nutrient mixture supplemented with 10% (v/v) FBS and 1% (v/v) antibiotic-antimycotic solution. Twenty-four hours before performing the assay the cells were treated with 1,3,4-O-Bu_3ManNAc to final concentrations of 100 μM, 300 μM, and 500 μM. Untreated controls were given a volume of 200 proof ethanol (the solvent vehicle) equivalent to the highest treatment group (i.e. 500 μM). The analogs were resuspended in F-12K nutrient mixture supplemented with 1% (v/v) FBS and no antibiotics and added to the corresponding culture dishes. Free intracellular sialic acid levels were quantified using the previously developed periodate resorcinol assay adapted to a 96-well plate format using an 10-point standard curve *(132, 204)*. The treated cells were harvested by aspirating the media, washing three times with PBS, and detaching nonenzymatically using CellStripper Dissociation Reagent (Corning, 25056CI). Cell density of each sample was determined using a Beck Z2™ Coulter Particle Count and Size Analyzer (Beckman-

Coulter) and normalized such that each sample contained 2.5 x 10^6 cells. The samples were centrifuged at 3000 x g for 3 minutes, resuspended in 300 µL of PBS, and lysed by freeze-thawing three times using liquid nitrogen. The cell lysates and sialic acid standards (0 – 250 µM) were oxidized with 0.4 M periodic acid and cooled on ice for 10 minutes. A resorcinol mixture containing 10% (v/v) 0.5 M resorcinol, 10% (v/v) 2.5 mM $CuSO_4$, 44% (v/v) concentrated HCl, and 36% (v/v) MilliQ water was prepared. After oxidation, 500 µL of the resorcinol mixture was added to each sample and the samples were heated at 100 °C for 10 minutes. After heating, the samples were cooled on ice and 500 µL of tert-butyl was added to each sample to stop the reaction. The samples were centrifuged for two minutes at 16000 x g and 100 µL of each was added to a 96-well plate in triplicate. The absorbance was measured at 630 nm using a Synergy HTX Multi-Mode Microplate Reader (BioTek). Free intracellular sialic acid levels were then determined by creating a standard curve and expressed as molecules of sialic acid per cell.

2.4.17 Azide Incorporation Flow Cytometry Assay

Forty-eight hours before performing the assay 1.5 x 10^5 cells mL^{-1} of each sample were seeded in 6-well plates using F-12K nutrient mixture supplemented with 10% (v/v) FBS and 1% (v/v) antibiotic-antimycotic solution. Twenty-four hours before the assay was performed the cells were treated with 1,3,4-O-Bu_3ManNAz to final concentrations of 100 µM, 200 µM, and 300 µM. Untreated controls were given a volume of 200 proof ethanol (the solvent vehicle) equivalent to the highest treatment group (i.e. 300 µM). The analogs were resuspended in F-12K nutrient mixture supplemented with 1% (v/v) FBS and no antibiotics and added to the corresponding wells. Approximately twenty-four hours post-treatment the media was aspirated and each well was washed three time with PBS. Dibenzocyclooctyne-Cy5 (DBCO-Cy5) (Sigma-Aldrich, 777374) was resuspended in DMSO to a stock concentration of 1 mg mL^{-1} which was in turn diluted to a final concentration of 16.5 µM in F-12K media without FBS or antibiotics. The DBCO-Cy5 solution was

protected from light for all subsequent steps to prevent fluorophore photobleaching. One milliliter of the diluted DBCO-Cy5 solution was added to each well of the 6-well plate and incubated at 37 °C for 30 minutes. The DBCO-Cy5 can react with azide groups in a strain-promoted copper-free azide-alkyne cycloaddition reaction. After incubation, the DBCO-Cy5 solution was aspirated and each well was washed three times with PBS. Following the final wash 300 µL of trypsin-EDTA was added to each well and incubated at 37 °C for 3 minutes. PBS was added to each well and the cells were transferred to microcentrifuge tubes. The cells were pelleted via centrifugation at 376 x g for 5 minutes and resuspended in 200 µL of sterile filtered (0.22 µm) 2% (w/v) BSA in HBSS. Approximately 100 µL of each sample was transferred to a clear V-bottom 96-well culture plate and Cy5 signal was measured using a CytoFLEX flow cytometer (Beckman Coulter). The azide incorporation assay was performed in biological triplicate for each cell line.

2.4.18 Azide Incorporation Plate Reading Assay

Forty-eight hours before performing the assay 1.5 x 10^5 cells mL^{-1} of each sample were seeded in 6-well plates using F-12K nutrient mixture supplemented with 10% (v/v) FBS and 1% (v/v) antibiotic-antimycotic solution. Twenty-four hours before the assay was performed the cells were treated with 1,3,4-O-Bu_3ManNAz to final concentrations of 100 µM, 200 µM, and 300 µM. Untreated controls were given a volume of 200 proof ethanol (the solvent vehicle) equivalent to the highest treatment group (i.e. 300 µM). The analogs were resuspended in F-12K nutrient mixture supplemented with 1% (v/v) FBS and no antibiotics and added to the corresponding culture dishes. Twenty-four hours post-treatment the cells were washed three times with PBS and 1 mL of 16.5 µM DBCO-Cy5 solution was added to each well (prepared as described in **2.4.17 Azide Incorporation Flow Cytometry Assay**). The cells were incubated with DBCO-Cy5 at 37 °C for 30 minutes. After incubation each sample was washed three times with PBS and detached by treating with trypsin-EDTA solution for 3 minutes at 37 °C. Each sample was transferred to a microcentrifuge tube and centrifuged at 376 x g for 5 minutes. The supernatant was aspirated, each sample was resuspended

in 100 µL of PBS, and transferred to a black flat bottom 96-well plate. Cy5 fluorescence was measured using a Synergy HTX Multi-Mode Microplate Reader (BioTek) and each measurement was normalized based on cell number per sample. The plate reading assay was performed in biological triplicate for each sample.

2.4.19 Live-Cell Imaging of Azide-Labeled Glycans

Forty-eight hours before performing the assay 1.5 x 10^5 cells mL^{-1} of each sample were seeded in 6-well plates using F-12K nutrient mixture supplemented with 10% (v/v) FBS and 1% (v/v) antibiotic-antimycotic solution. Twenty-four hours before the assay was performed the cells were treated with 1,3,4-O-Bu_3ManNAz to final concentrations of 100 µM, 200 µM, and 300 µM. Untreated controls were given a volume of 200 proof ethanol (the solvent vehicle) equivalent to the highest treatment group (i.e. 300 µM). The analogs were resuspended in F-12K nutrient mixture supplemented with 1% (v/v) FBS and no antibiotics and added to the corresponding wells. Twenty-four hours post-treatment the media was aspirated and the cells were washed three times with PBS. Alexa Fluor 488 DBCO (AF-DBCO) (Click Chemistry Tools, 1278-1) was resuspended in DMSO to a stock concentration of 1 mg mL^{-1} which was in turn diluted to a working concentration of 25 µM in F-12K media without FBS or antibiotics. After the final PBS wash, one milliliter of AF-DBCO solution was added to each well and incubated at 37 °C for 30 minutes. Each sample was washed three times with PBS and imaged using an EVOS FL Imaging System (Thermo Fisher Scientific).

2.5 Results & Discussion

2.5.1 Construction of gRNA-pSpCas9(BB)-2A-GFP Plasmids

For each protein target (i.e. Gne and Renbp) two gRNA were designed in the event one did not efficiently home Cas9 to the genomic target region (**Table 2.1**). Each gRNA sequence was modified to contain four base pairs of overlap with the pSpCas9(BB)-2A-GFP vector and was cloned into the pSpCas9(BB)-2A-GFP vector between two *BbsI* restriction sites. The transformation showed modest

efficiency with between 10 – 25 colonies for each construct. Multiple colonies were selected for plasmid isolation and Sanger sequencing to verify correct gRNA insertion in the pSpCas9(BB)-2A-GFP vector. Correct gRNA insertion was verified using the Multiple Sequence Alignment tool (MUSCLE). Sanger sequencing indicated the gRNA targeting exon 2 of *Gne* and the gRNA targeting exon 4 of *Gne* were successfully cloned into the pSpCas9(BB)-2A-GFP vector. The sequencing results for both *Gne* gRNA plasmids had quality scores greater than 20 for the gRNA insertion region indicating greater than 99% probability the inferred base pair is correct (**Fig. 2.4**) (**Fig. 2.5**). Similarly, the Sanger sequencing results indicated the gRNA targeting exon 3 of *Renbp* and the gRNA targeting exon 6 of *Renbp* were successfully cloned into the pSpCas9(BB)-2A-GFP vector. The sequencing results for both *Renbp* gRNA had quality scores greater than 30 for the gRNA insertion region indicating greater than 99.9% probability the inferred base pair is correct (**Fig. 2.6**) (**Fig. 2.7**). These cloning results corroborate and demonstrate the reproducibility of the cloning methods originally developed and elucidated by Ran *et al. (185)*.

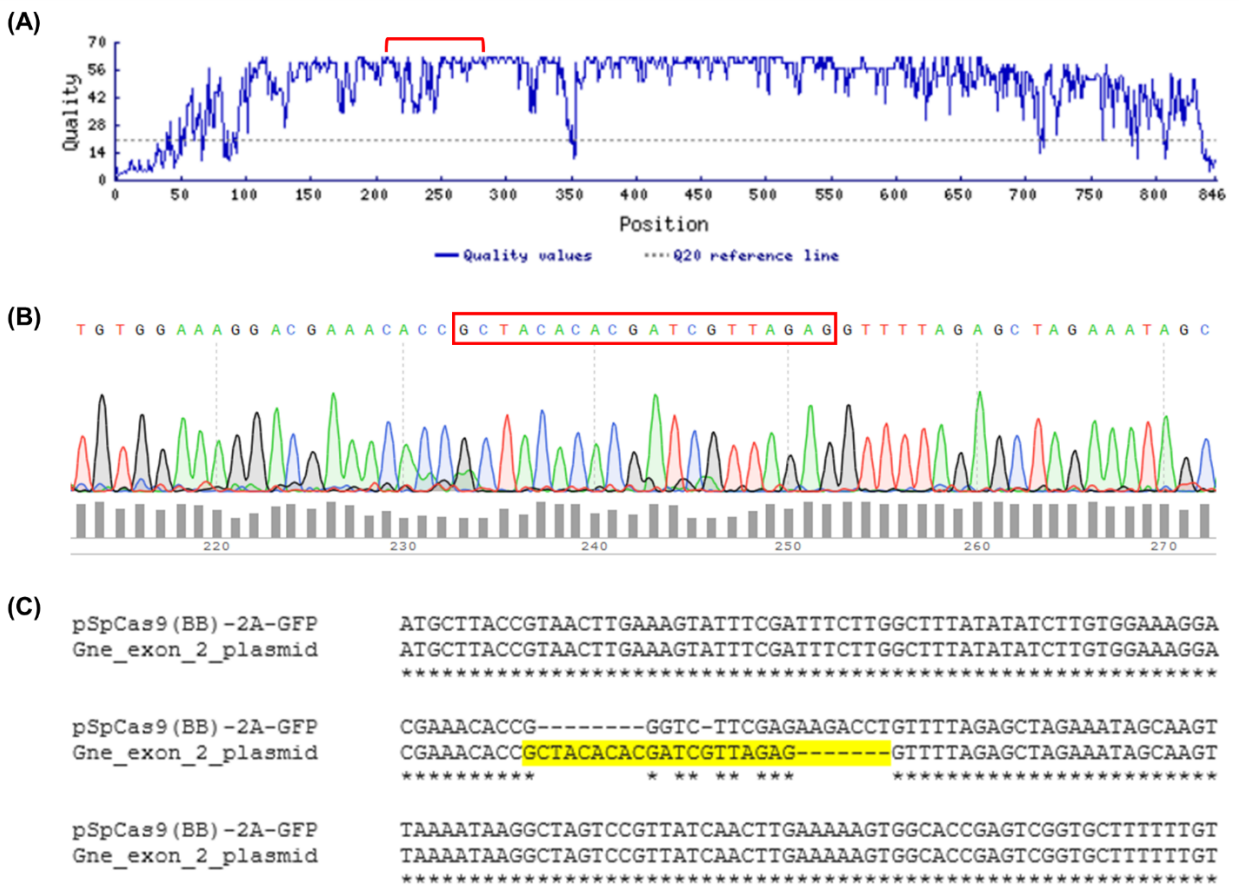

Figure 2.4 Sequencing data for cloning the gRNA targeting *Gne* exon 2 into the pSpcas9(BB)-2A-GFP plasmid. (A) The top panel shows the read quality for each nucleotide from the Sanger sequencing run. (B) The middle panel shows the chromatogram for the region where the gRNA was inserted into the pSpCas9(BB)-2A-GFP vector (gRNA sequence boxed in red). All nucleotides in and immediately surrounding the insertion region had quality scores exceeding 20 meaning there is at least a 99% probability the inferred base pair is correct. (C) The bottom panel shows the MUSCLE alignment between the unaltered pSpCas9(BB)-2A-GFP vector and the plasmid with the gRNA sequence inserted (highlighted in yellow).

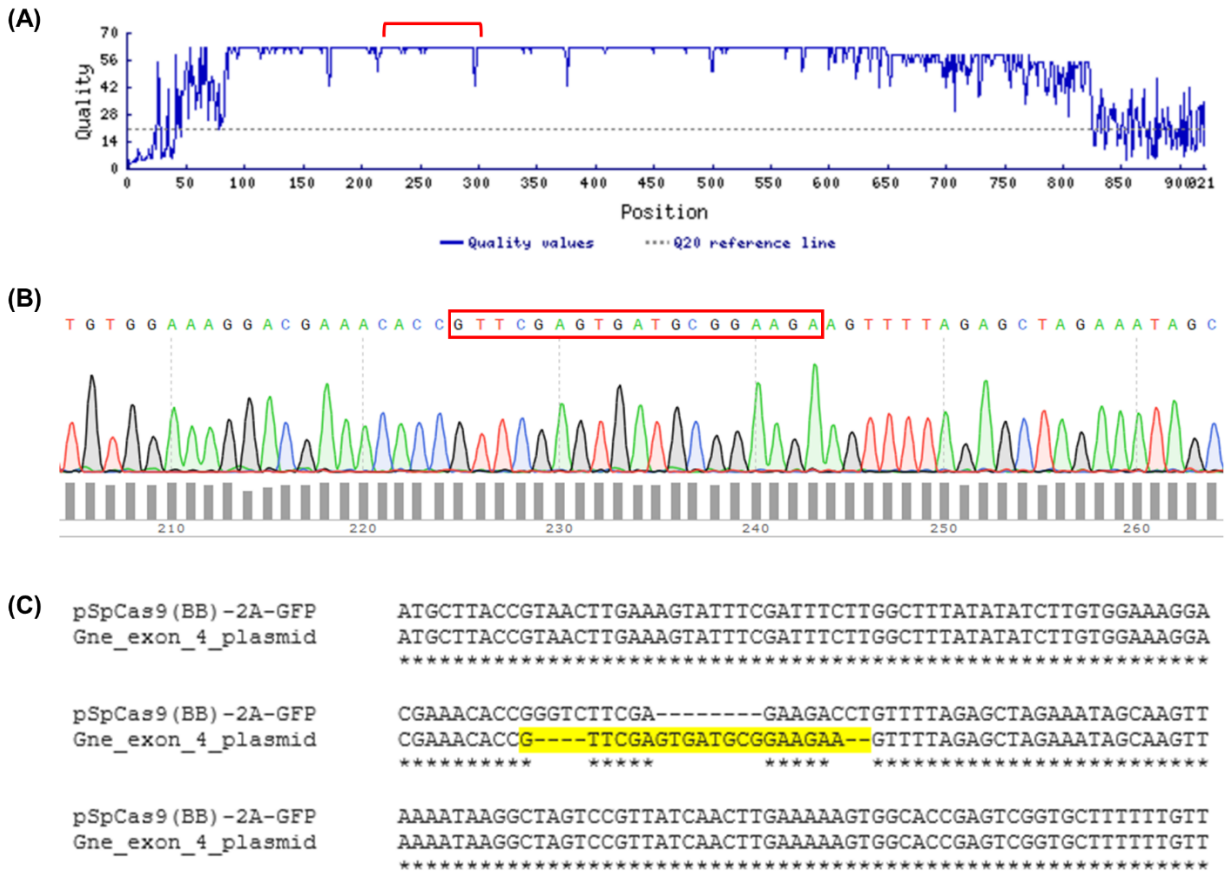

Figure 2.5 Sequencing data for cloning the gRNA targeting *Gne* exon 4 into the pSpcas9(BB)-2A-GFP plasmid. (A) The top panel shows the read quality for each nucleotide from the Sanger sequencing run. (B) The middle panel shows the chromatogram for the region where the gRNA was inserted into the pSpCas9(BB)-2A-GFP vector (gRNA sequence boxed in red). All nucleotides in and immediately surrounding the insertion region had quality scores exceeding 30 meaning there is at least a 99.9% probability the inferred base pair is correct. (C) The bottom panel shows the MUSCLE alignment between the unaltered pSpCas9(BB)-2A-GFP vector and the plasmid with the gRNA sequence inserted (highlighted in yellow).

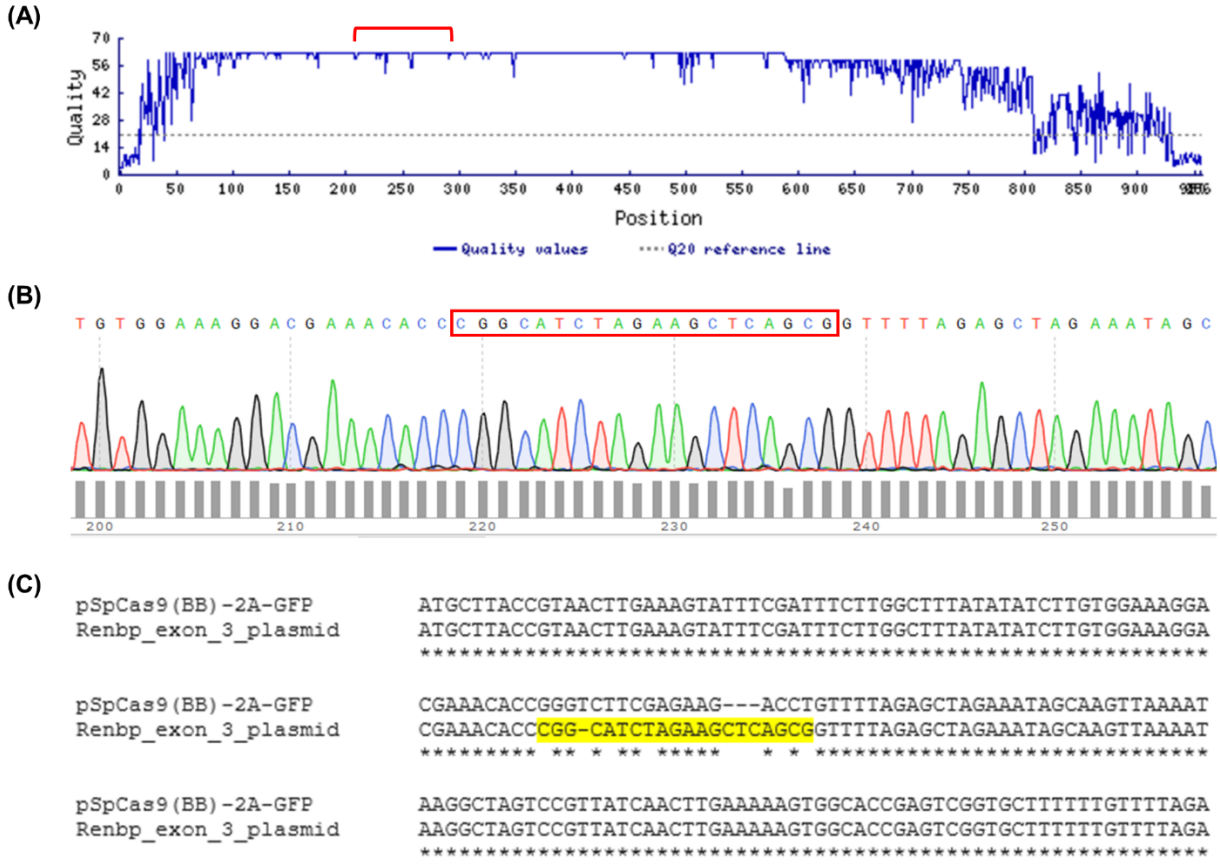

Figure 2.6 Sequencing data for cloning the gRNA targeting *Renbp* exon 3 into the pSpcas9(BB)-2A-GFP plasmid. (A) The top panel shows the read quality for each nucleotide from the Sanger sequencing run. (B) The middle panel shows the chromatogram for the region where the gRNA was inserted into the pSpCas9(BB)-2A-GFP vector (gRNA sequence boxed in red). All nucleotides in and immediately surrounding the insertion region had quality scores exceeding 30 meaning there is at least a 99.9% probability the inferred base pair is correct. (C) The bottom panel shows the MUSCLE alignment between the unaltered pSpCas9(BB)-2A-GFP vector and the plasmid with the gRNA sequence inserted (highlighted in yellow).

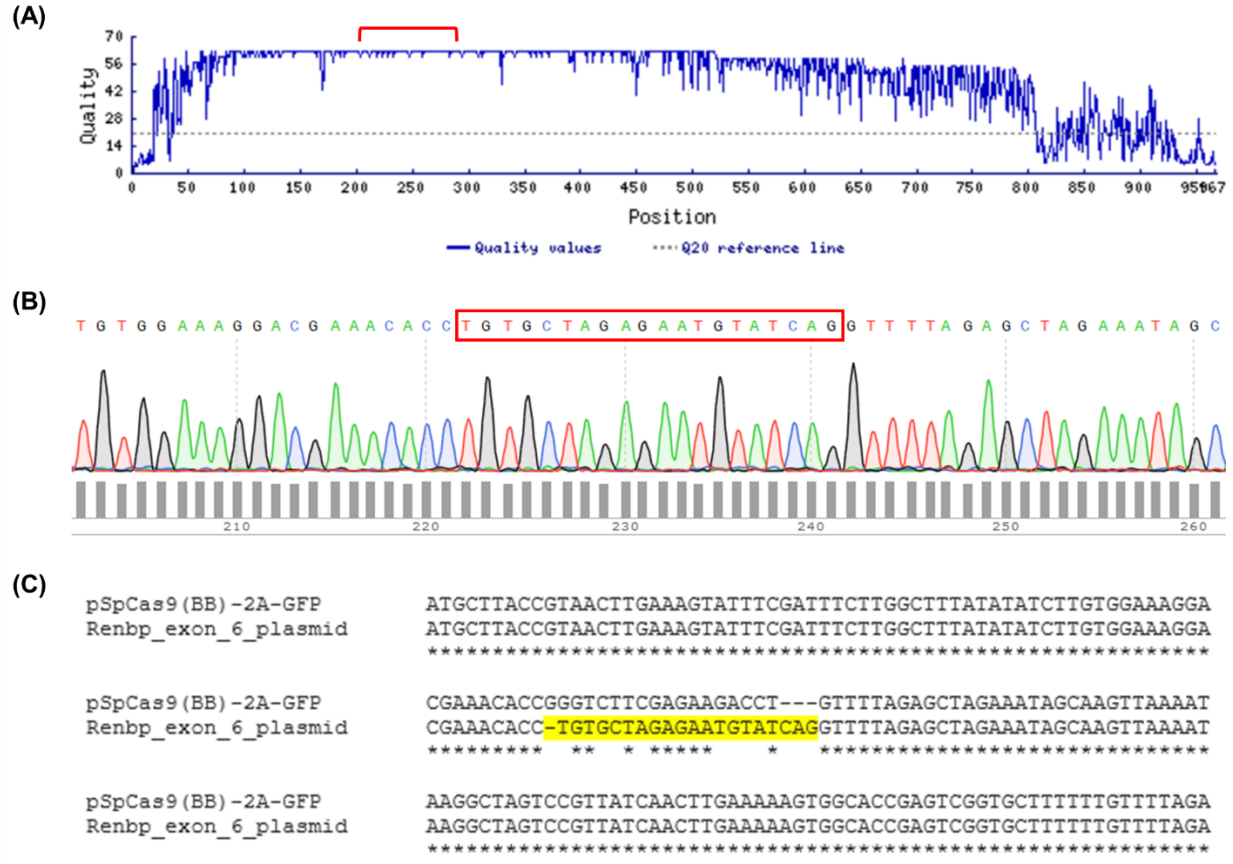

Figure 2.7 Sequencing data for cloning the gRNA targeting *Renbp* exon 6 into the pSpcas9(BB)-2A-GFP plasmid. (A) The top panel shows the read quality for each nucleotide from the Sanger sequencing run. (B) The middle panel shows the chromatogram for the region where the gRNA was inserted into the pSpCas9(BB)-2A-GFP vector (gRNA sequence boxed in red). All nucleotides in and immediately surrounding the insertion region had quality scores exceeding 30 meaning there is at least a 99.9% probability the inferred base pair is correct. (C) The bottom panel shows the MUSCLE alignment between the unaltered pSpCas9(BB)-2A-GFP vector and the plasmid with the gRNA sequence inserted (highlighted in yellow).

2.5.2 Transfection

CHO-K1 cells were transfected with the pSpCas9(BB)-2A-GFP plasmids with gRNA inserts in order to knockout *Gne* and *Renbp*. A co-transfection strategy utilizing both of the pSpCas9(BB)-2A-GFP plasmids with gRNA targeting *Gne* or *Renbp* was chosen to increase the probability of knocking out the target protein if one gRNA proves ineffective. Forty-eight hours post-transfection each sample was imaged using fluorescence microscopy to verify GFP expression. The sample that was transfected with both *Gne* targeting plasmids (i.e. gRNA targeting exon 2 and 4 of *Gne*) and Lipofectamine 2000 showed robust GFP expression while control samples treated with either only Lipofectamine 2000

or only the *Gne* targeting plasmids showed no GFP expression (**Fig. 2.8**). The sample that was transfected with both *Renbp* targeting plasmids (i.e. gRNA targeting exon 3 and 6 of *Renbp*) and Lipofectamine 2000 showed robust GFP expression while control samples treated with either only Lipofectamine 2000 or only the *Renbp* targeting plasmids showed no GFP expression (**Fig. 2.9**).

Once a CHO-K1 cell line with Gne knocked out (CHO^{-Gne}) was engineered and validated the CHO^{-Gne} cell line was transfected with both *Renbp* targeting plasmids in order to create a CHO-K1 cell line with both Gne and Renbp knocked out ($CHO^{-Gne/-Renbp}$). Again, forty-eight hours post-transfection this sample was imaged using fluorescence microscopy to verify GFP expression. The CHO^{-Gne} sample that was transfected with both *Renbp* targeting plasmids and Lipofectamine 2000 exhibited GFP expression while control samples treated with either only Lipofectamine 2000 or only the *Renbp* targeting plasmids showed no GFP expression (**Fig. 2.10**). Utilization of GFP as a marker for gene expression is a common technique that was originally pioneered by Chalfie *et al. (205)*. In all cases the fluorescence microscopy images obtained following transfection with Lipofectamine indicate strong GFP expression due to uptake of the pSpCas9(BB)-2A-GFP vector. Furthermore, GFP expression implies concurrent expression of the gRNA-Cas9 complex also coded on the pSpCas9(BB)-2A-GFP vector.

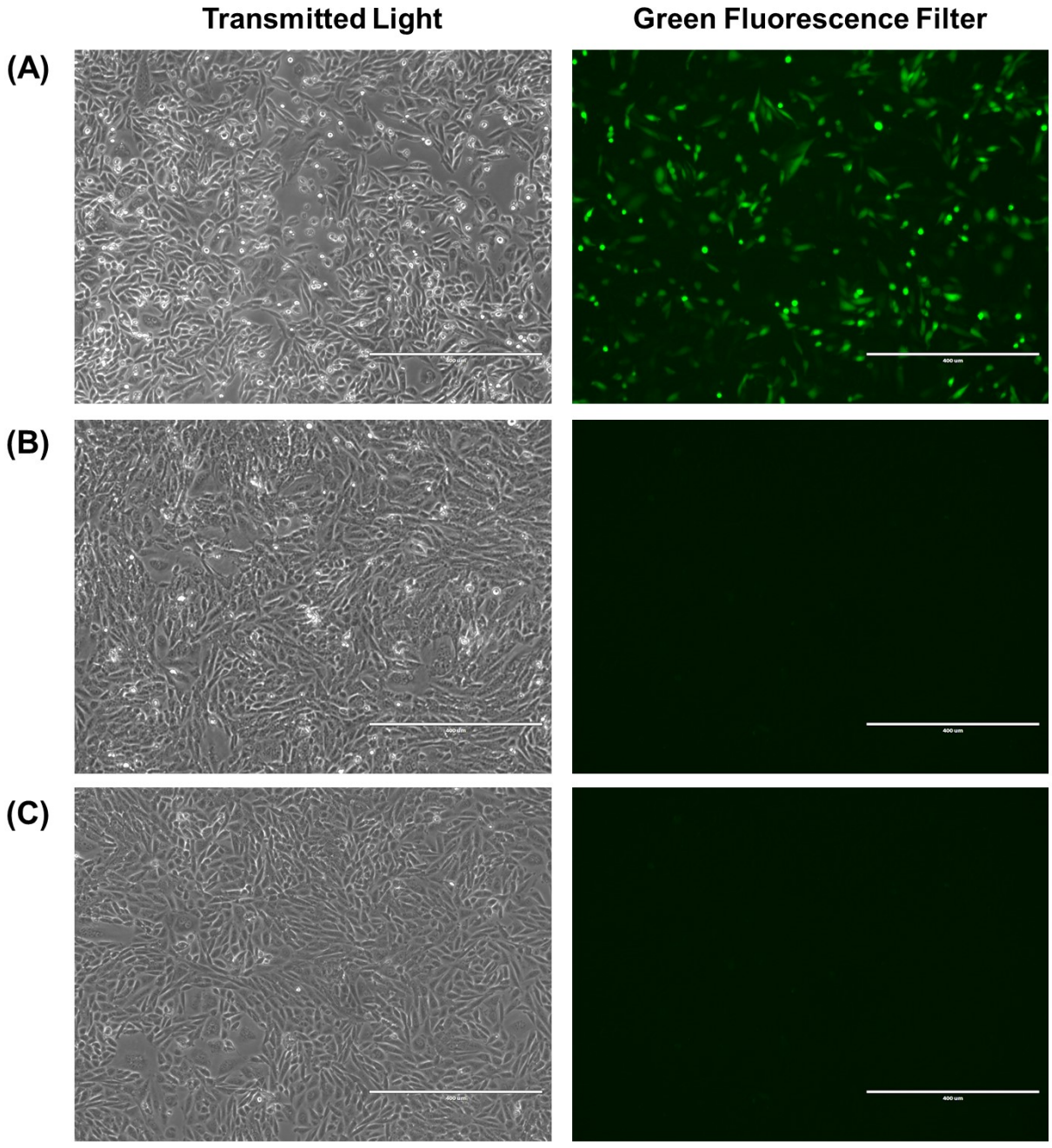

Figure 2.8 Transmitted light and fluorescence microscopy images of wild type CHO-K1 cells 48 hours after transfection with the pSpCas9(BB)-2A-GFP plasmids with gRNA inserts targeting *Gne*. (A) Wild type CHO-K1 cells were transfected with Lipofectamine 2000 and both pSpCas9(BB)-2A-GFP plasmids with gRNA inserts targeting exons 2 and 4 in *Gne*. Wild type CHO-K1 cells were also transfected with (B) Lipofectamine 2000 alone and (C) plasmids alone as negative controls. Scale bars represent 400 µm.

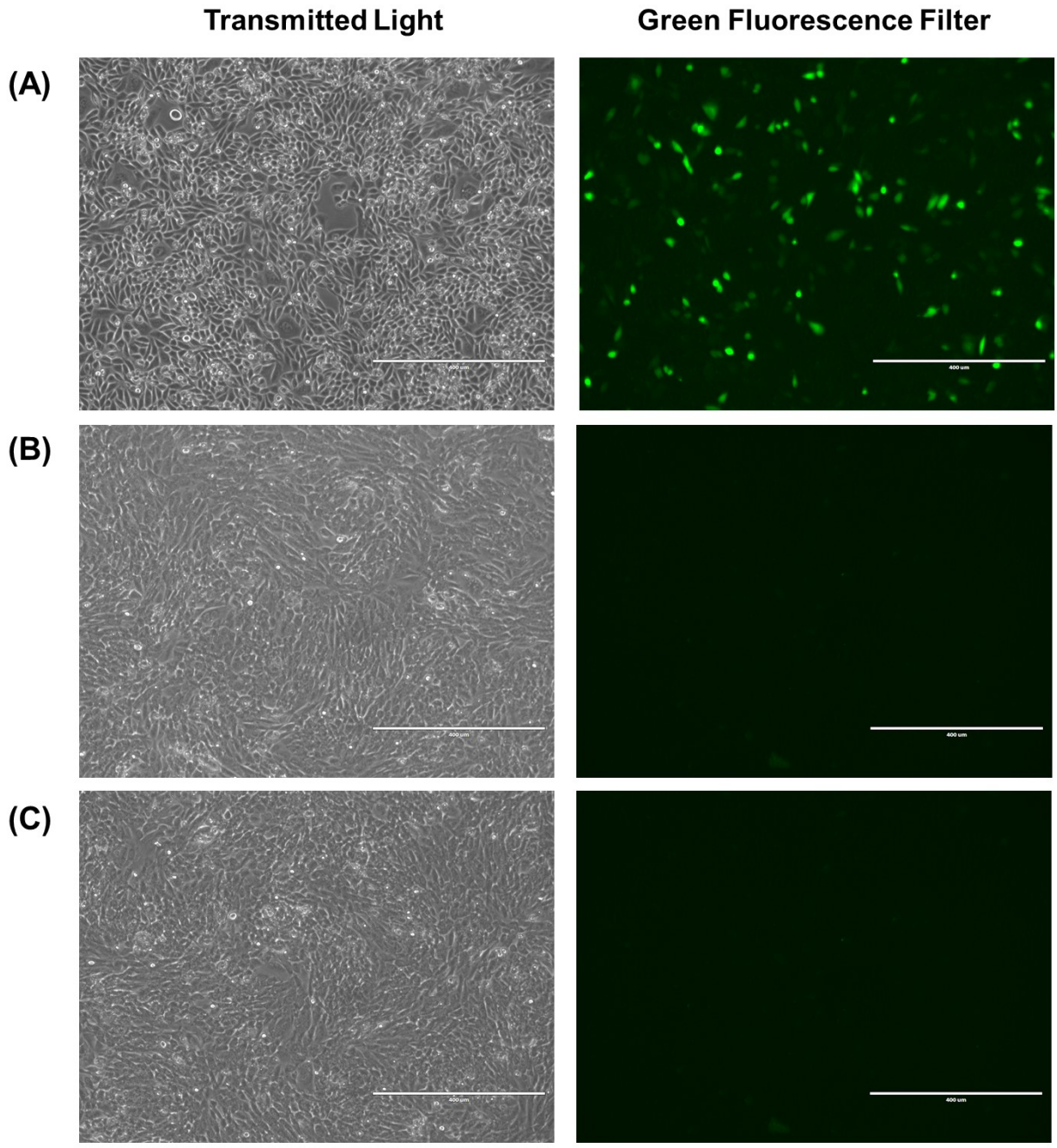

Figure 2.9 Transmitted light and fluorescence microscopy images of wild type CHO-K1 cells 48 hours after transfection with the pSpCas9(BB)-2A-GFP plasmids with gRNA inserts targeting *Renbp*. (A) Wild type CHO-K1 cells were transfected with Lipofectamine 2000 and both pSpCas9(BB)-2A-GFP plasmids with gRNA inserts targeting exons 3 and 6 in *Renbp*. Wild type CHO-K1 cells were also transfected with (B) Lipofectamine 2000 alone and (C) plasmids alone as negative controls. Scale bars represent 400 µm.

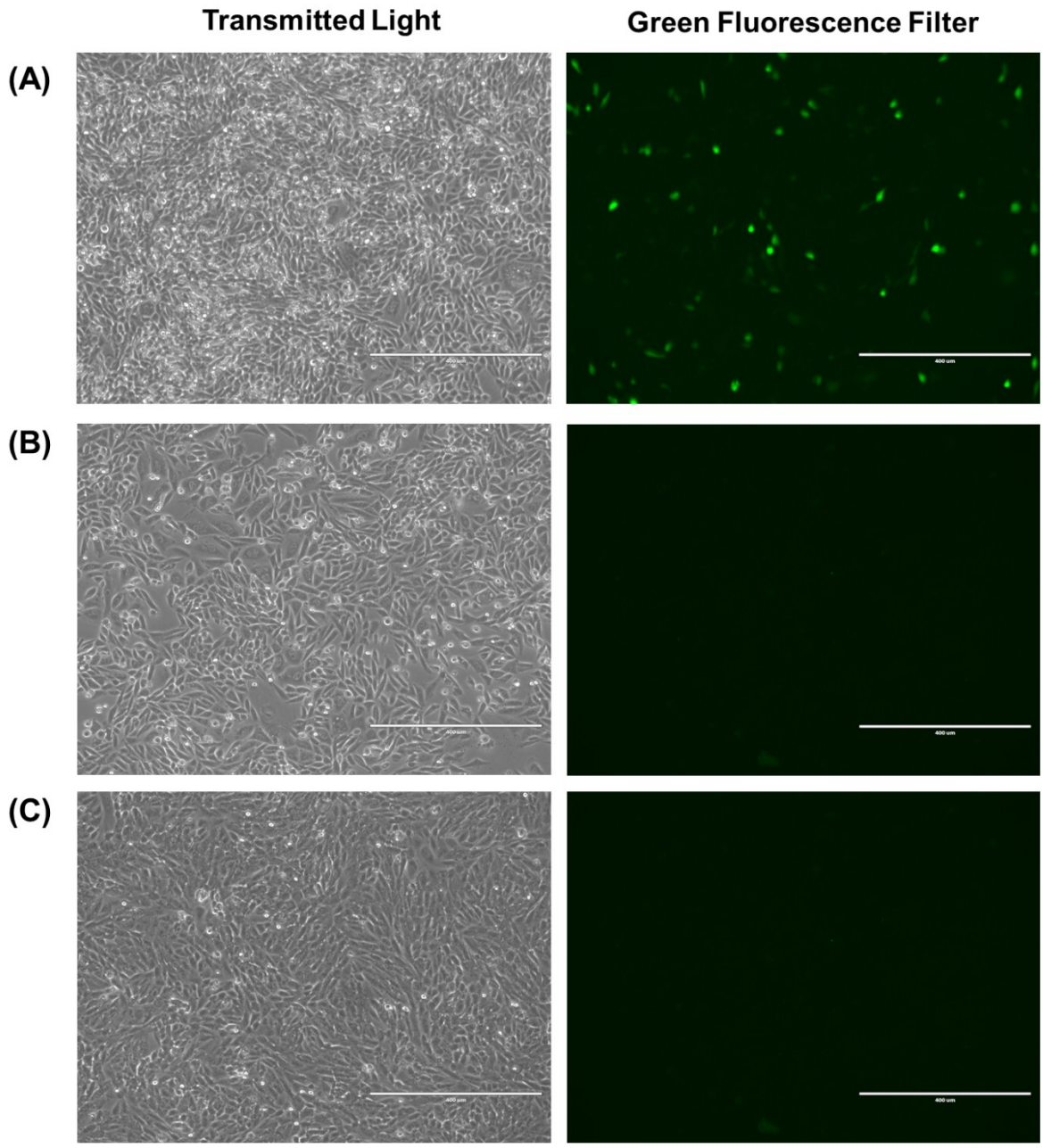

Figure 2.10 Transmitted light and fluorescence microscopy images of CHO^{-Gne} cells 48 hours after transfection with the pSpCas9(BB)-2A-GFP plasmids with gRNA inserts targeting *Renbp*. (A) CHO^{-Gne} were transfected with Lipofectamine 2000 and both pSpCas9(BB)-2A-GFP plasmids with gRNA inserts targeting exons 3 and 6 in *Renbp*. CHO^{-Gne} cells were also transfected with (B) Lipofectamine 2000 alone and (C) plasmids alone as negative controls. Scale bars represent 400 µm.

2.5.3 Fluorescent Activated Cell Sorting

Forty-eight hours post-transfection the CHO-K1 cells were harvested for FACS in order to isolate monoclonal cell populations with either Gne, Renbp, or both proteins knocked out. Each sample was gated based on multiple parameters to ensure viable, GFP positive, single cells were seeded. Cells with the correct morphology and size were selected by measuring forward-scattered light (FSC) pulse height and side-scattered light (SSC) pulse height; for all samples at least 90% of the cells exhibited the correct morphology characteristic of CHO-K1 cells. Singlet cells were selected by measuring SSC pulse width and height and gating accordingly. Again, in all cases greater than 90% of cells in each sample were singlets. Viable cells were selected by staining with PI since it is not permeant to live cells and for all samples greater than 99% were PI negative. Finally, cells expressing GFP were selected be measuring excitation/emission at 488 nm/510 nm and sorting accordingly. Depending on the sample the percentage of each cell population strongly expressing GFP varied between 1.30% to 1.48% (**Fig. 2.11**). The flow cytometry results provide additional confirmation of GFP expression in transfected samples. All samples had a relatively low transfection efficiency, however, in this case the variation is unproblematic because each sample contained a sufficient quantity of cells for seeding multiple 96-well plates.

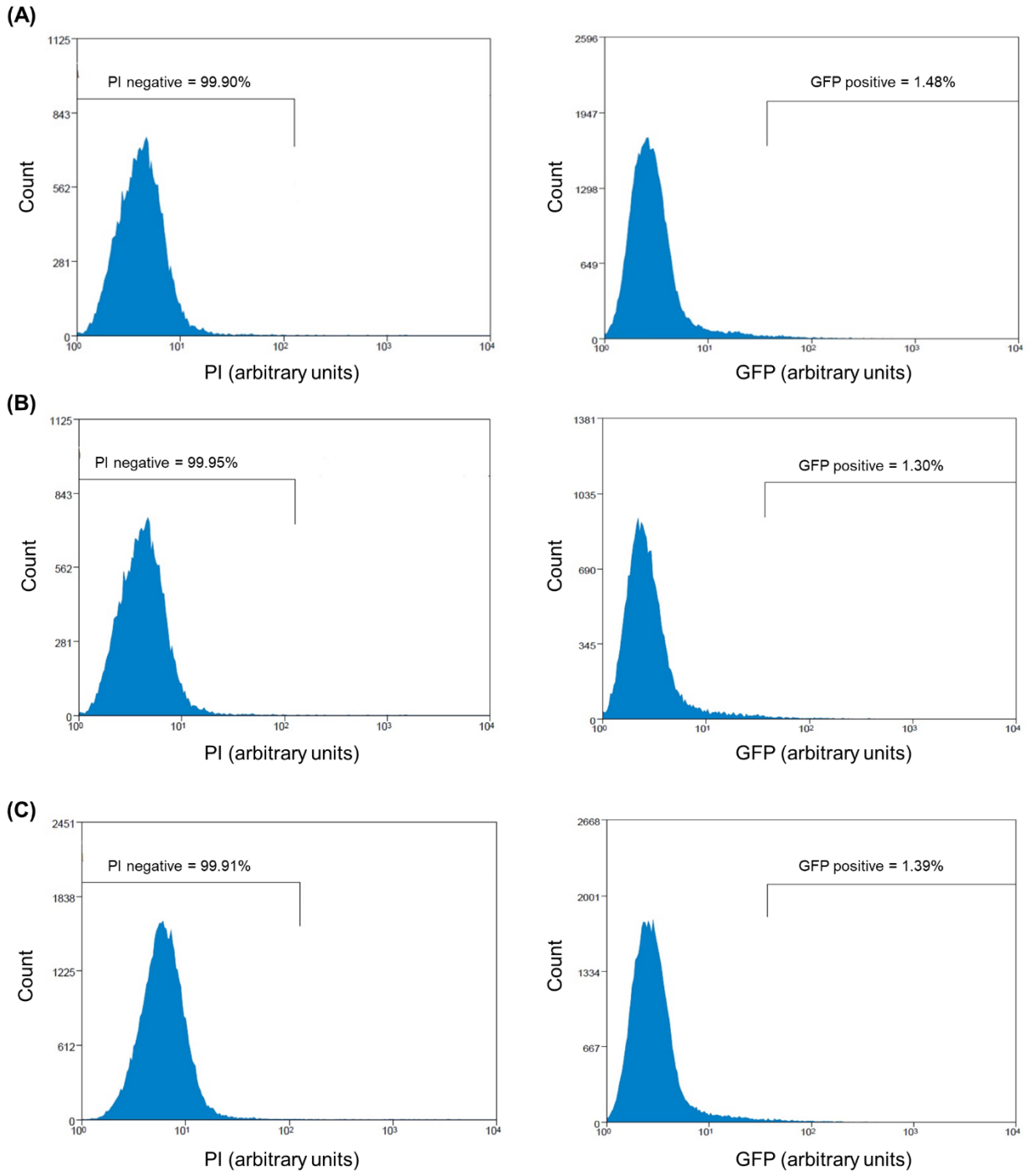

Figure 2.11 FACS data for sorting CHO cells transfected with gRNA-Cas9 plasmids. All samples were sorted and gated based on morphology, granularity, PI negative, and GFP positive. (A) PI and GFP histograms for CHO^{WT} cells co-transfected with the gRNA-Cas9 plasmids targeting exon 2 and exon 4 of *Gne*. (B) PI and GFP histograms for CHO^{WT} cells co-transfected with the gRNA-Cas9 plasmids targeting exon 3 and exon 6 of *Renbp.* (C) PI and GFP histograms CHO^{-Gne} cells co-transfected with the gRNA-Cas9 plasmids targeting exon 3 and exon 6 of *Renbp*.

2.5.4 Genetic Analysis of Indel Generation

After single cells of each sample were sorted and seeded each monoclonal cell line was grown for 10 – 14 days before expansion to 6-well plates and subsequent genetic analysis. In order to analyze potential indel generation in each monoclonal population a 600 – 1000 base pair region of the genomic DNA containing the gRNA cut site was amplified. Gel electrophoresis was used to verify successful amplification of the target genomic DNA sequence. Each amplicon was isolated and directly Sanger sequenced to give a preliminary indication of indel generation in each monoclonal cell population (data not shown). Of the amplicons sequenced a variety of different indels were found including base pair insertions, deletions, and a mix of both. In all cases the genomic edits occurred between 3-5 base pairs upstream of the PAM motif indicating the edits were made by Cas9 double stranded breaks. Of these samples, monoclonal cell populations with indels resulting in frame shifts were selected for more rigorous genetic analysis. Of the wild type CHO cell lines (CHO^{WT}) transfected with the *Gne* targeting CRISPR plasmids a monoclonal population with a one base pair deletion on exon 2 and a one base pair insertion on exon 4 was selected (CHO^{-Gne}). Of the wild type CHO cell lines transfected with the *Renbp* targeting CRISPR plasmids a monoclonal population with a one base pair insertion on exon 3 and a one base pair insertion on exon 6 was selected (CHO^{-Renbp}). Of the CHO^{-Gne} cell lines transfected with the *Renbp* targeting CRISPR plasmids a monoclonal population with a one base pair insertion on exon 3 and a one base pair insertion on exon 6 was selected ($CHO^{-Gne/-Renbp}$). For all samples the nucleotides within and directly surrounding the edited site had quality scores greater than or equal to 20 indicating greater than 99% probability the inferred base pair is correct.

The CHO^{-Gne}, CHO^{-Renbp}, and $CHO^{-Gne/-Renbp}$ cell lines were further validated by cloning the genomic DNA amplicons into an empty vector via TOPO cloning. For each edited genomic site, plasmid was isolated from 10 bacteria colonies and Sanger sequenced. All 10 plasmids with the amplicon insert derived from exon 2 of the CHO^{-Gne} cell line showed deletion of a thymine residue five base pairs upstream of the PAM motif (quality scores ≥ 20) indicating a homozygous gene edit (**Fig. 2.12**). All

10 plasmids with the amplicon insert derived from exon 4 of the CHO^{-Gne} cell line showed insertion of one adenine nucleotide five base pairs upstream of the PAM motif implying a homozygous gene edit (**Fig. 2.12**). For the plasmids with an amplicon insert from exon 3 of the CHO^{-Renbp} cell line nine showed an insertion of one thymine residue while one plasmid had an insertion of a cytosine residue in the same location. The inserted thymine and cytosine residues had sequencing quality scores greater than 20 suggesting that this monoclonal cell line may have a heterozygous gene edit (**Fig. 2.13**). Similarly, for the plasmids with an amplicon insert from exon 6 of the CHO^{-Renbp} cell line nine exhibited insertion of one thymine residue while the remaining plasmid showed insertion of a cytosine residue at the same location. Since the quality scores exceeded 20 for all inserted residues this again suggests the gene mutation at this location is heterozygous (**Fig. 2.13**). Interestingly, the 10 plasmids with inserts from exon 3 and exon 6 of Renbp derived from the CHO$^{-Gne/-Renbp}$ line exclusively showed a thymine insertion 3 and 4 nucleotides away from the PAM motif, respectively (**Fig. 2.14**). This is a strong indication of homozygous gene edits at both locations and demonstrates that even when using the same gRNA the homo- or heterozygous nature of the gene edit can vary depending on the monoclonal cell line. Overall, this sequencing data provides strong evidence that Gne and Renbp were successfully knocked out in CHO cells, however more rigorous genetic analysis would be needed to fully elucidate whether the gene edits are truly homo- or heterozygous.

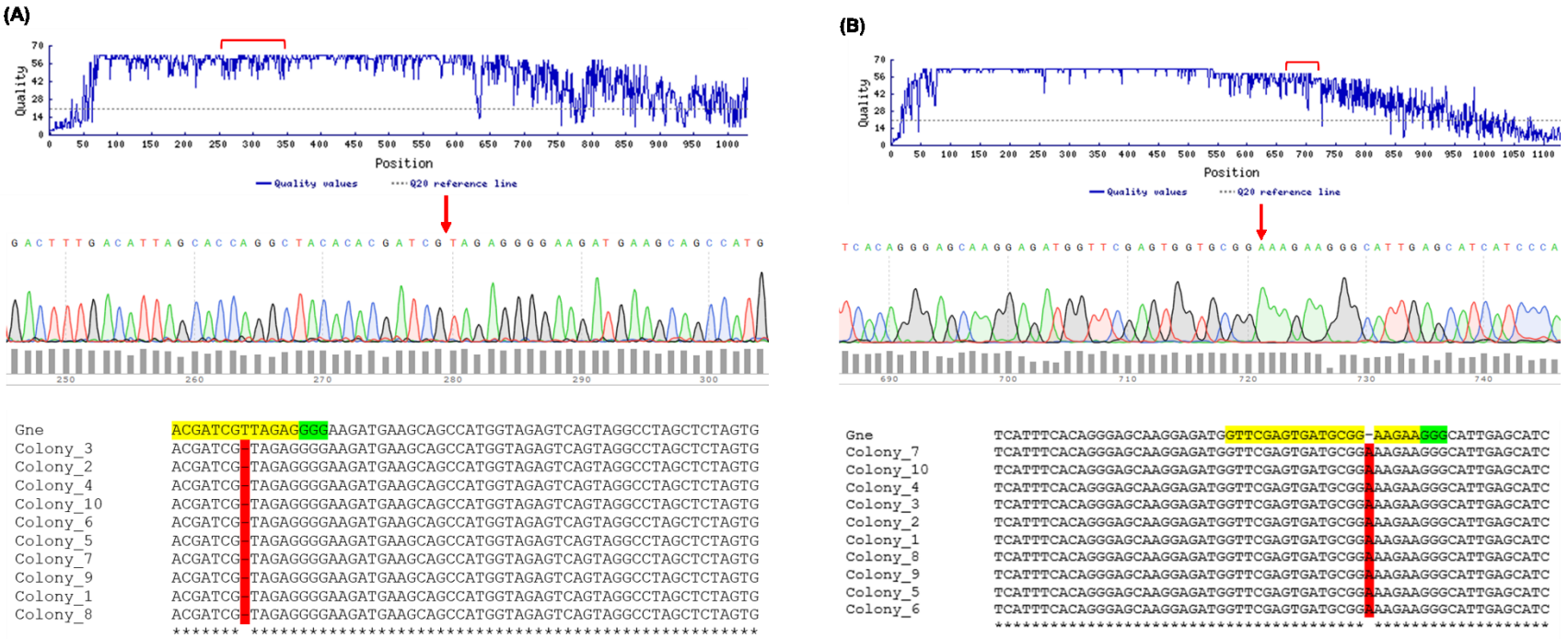

Figure 2.12 Genetic analysis of indel generation in CHO^{-Gne} cells. The region on exon 2 and exon 4 of *Gne* targeted by the gRNA was amplified and cloned into an empty vector. Plasmid was isolated from 20 bacteria colonies (10 per gRNA target site) and Sanger sequenced. (A) For the exon 2 site, all plasmids showed deletion of one thymine residue five base pairs upstream of the PAM motif. (B) For the exon 4 site, all plasmids showed insertion of one adenine residue five base pairs upstream of the PAM motif. The quality score graph and chromatogram are shown for one representative plasmid for each target site and the MUSCLE alignment of all plasmids with *Gne* is show on the bottom. The gRNA is highlighted in yellow, the PAM sequence is highlighted in green and the gene edit is highlighted in red.

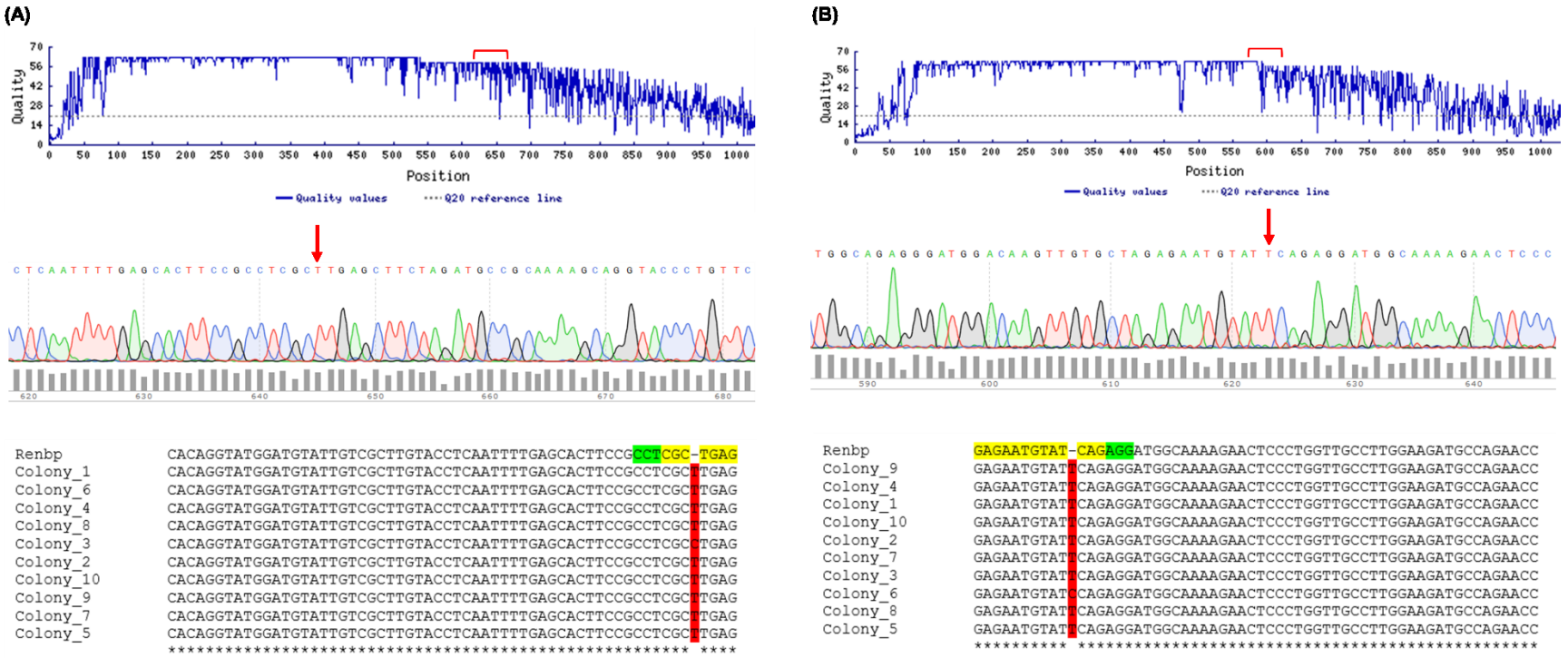

Figure 2.13 Genetic analysis of indel generation in CHO$^{\text{-Renbp}}$ cells. The region on exon 3 and exon 6 of *Renbp* targeted by the gRNA was amplified and cloned into an empty vector. Plasmid was isolated from 20 bacteria colonies (10 per gRNA target site) and Sanger sequenced. (A) For the exon 3 site, nine plasmids showed insertion of one thymine residue while one plasmid showed insertion of a cytosine residue at the same location. (B) For the exon 6 site, nine plasmids showed insertion of one thymine residue, while one plasmid showed insertion of a cytosine residue at the same location. The quality score graph and chromatogram are shown for one representative plasmid for each target site and the MUSCLE alignment of all plasmids with *Renbp* is show on the bottom. The gRNA is highlighted in yellow, the PAM sequence is highlighted in green and the gene edit is highlighted in red.

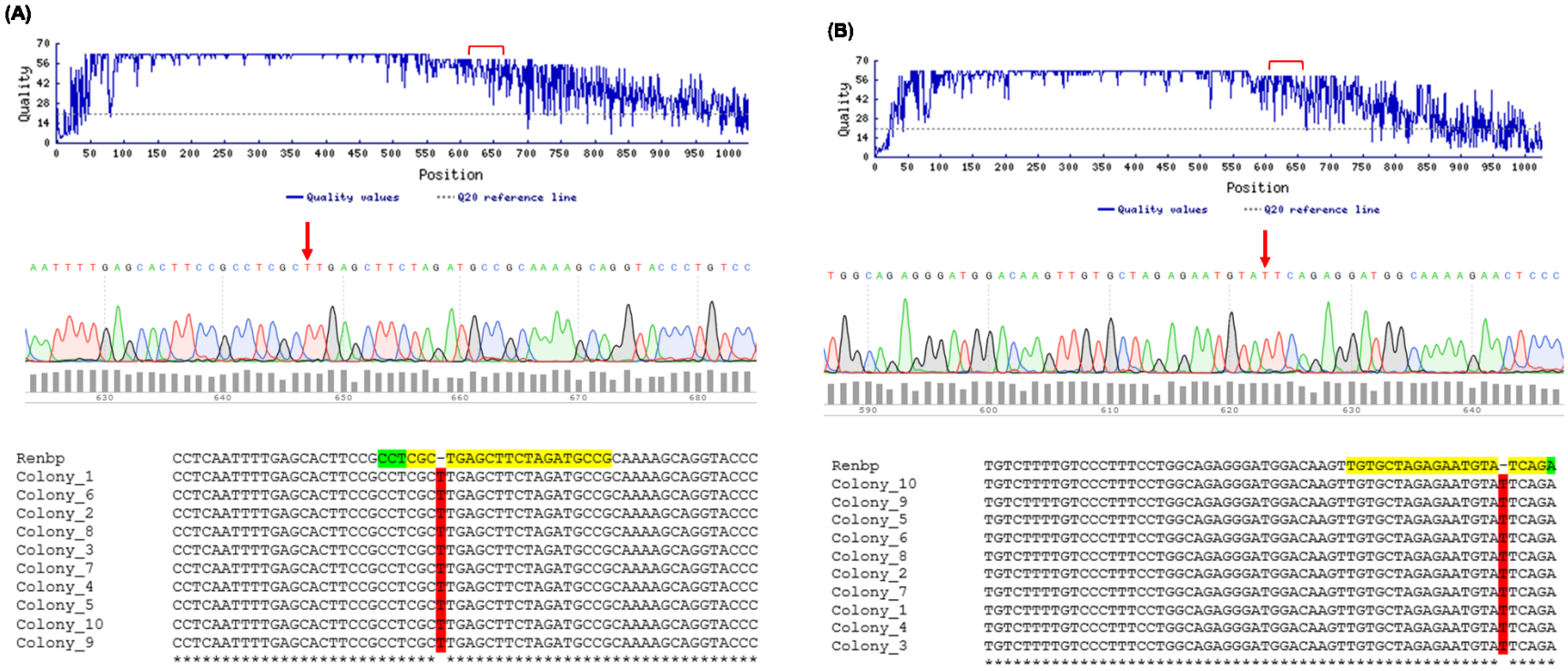

Figure 2.14 Genetic analysis of indel generation in CHO$^{-Gne/-Renbp}$ cells. The region on exon 3 and exon 6 of *Renbp* targeted by the gRNA was amplified and cloned into an empty vector. Plasmid was isolated from 20 bacteria colonies (10 per gRNA target site) and Sanger sequenced. (A) For the exon 3 site, all plasmids showed insertion of one thymine residue three base pairs after the PAM motif. (B) For the exon 6 site, all plasmids showed insertion of one thymine residue four base pairs upstream of the PAM motif. The quality score graph and chromatogram are shown for one representative plasmid for each target site and the MUSCLE alignment of all plasmids with *Renbp* is show on the bottom. The gRNA is highlighted in yellow, the PAM sequence is highlighted in green and the gene edit is highlighted in red

2.5.5 Protein Level Knockout Validation

In order to validate the sequencing data and to verify protein level knockout of the target protein immunoblotting was performed. Protein extracted from each sample was probed with a polyclonal GNE antibody (Thermo Fisher Scientific, PA5-55559) at a concentration of 0.4 μg mL^{-1}. Both the CHO^{-Gne} and $CHO^{-Gne/-Renbp}$ cell lines lacked a band at ~74 kDa while the CHO^{WT} and CHO^{-Renbp} cell lines showed a robust band at this location (**Fig. 2.15**). The intensity of each band was quantified and expressed relative to the CHO^{WT} signal and adjusted based on the corresponding β actin loading control (**Fig. 2.16A**). Both the bands for CHO^{-Gne} and $CHO^{-Gne/-Renbp}$ gave an average density less than 0.01 relative to CHO^{WT} and were significantly less than the CHO^{-Rnebp} cells ($p<0.001$) suggesting that no signal was present for these samples. The small basal signal can likely be attributed to background and nonspecific signal. The CHO^{-Renbp} bands yielded an average density of ~1.2 suggesting that this cell line may have higher Gne expression relative to CHO^{WT}, however it is more likely this difference is simply variation in the western blotting process.

Similarly, protein extracted from each sample was probed with a polyclonal RENBP antibody (Abcam, ab77081) at a concentration of 0.7 μg mL^{-1}. Surprisingly, visible bands around 52 kDa were seen for all cell lines even those with sequencing data that had indicated that Renbp was knocked out (**Fig. 2.15**). Again, the intensity of each band was quantified and expressed relative to the CHO^{WT} signal and adjusted based on the corresponding β actin loading control (**Fig. 2.16B**). The CHO^{-Renbp} and $CHO^{-Gne/-Renbp}$ cell lines both had an average density slightly less than one relative to CHO^{WT}, which could indicate a partial knockdown of Renbp in these cell lines. However, because the standard error of means is large for all samples it is more likely this difference is due to slight variations in the western blotting and densitometry analysis process. Additionally, the band intensities of CHO^{-Renbp} and $CHO^{-Gne/-Renbp}$ were not significantly different from the CHO^{-Gne} band intensity. The presence of a band for the Renbp knockout cell lines could be due to several reasons. First, it is possible that *Renbp* expresses multiple transcript variants and some of these variants may have avoided the CRIPSR-Cas9

mediated gene edits. However, if this was the case it would be expected that the bands for the Renbp knockout lines would at least have a more pronounced reduction in signal relative to the wild type cells. Another possible explanation is Renbp has a long half-life, yet no reduction in signal was observed even after multiple (>5) passages of the cell lines. Another possibility is a partial, nonfunctional version of Renbp is still being translated which the antibody is capable of binding to, thus yielding a signal during immunoblotting. However, this is unlikely because the observed band is at the expected size of 52 kDa, whereas a partial version of Renbp would be expected to give a signal at a lower molecular weight. A final explanation is the antibody used to probe for Renbp is nonspecifically binding to another protein of similar molecular weight. This could be because the antibody was designed to bind human RENBP and although human and *C. griseus* have considerable genomic homology some variations do exist. Taking into account the sequencing and immunoblotting data it is probable Renbp was successfully knocked out, however more rigorous screening will be needed to fully validate the knockout.

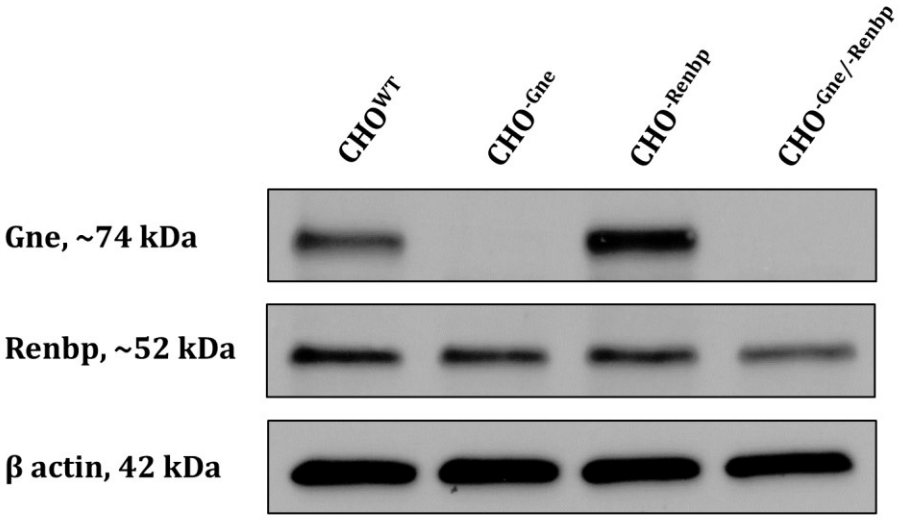

Figure 2.15 Representative western blot analysis of protein level knockout of Gne and Renbp in CHO cells. The engineered cells lines CHO^{-Gne}, CHO^{-Renbp}, and CHO$^{-Gne/-Renbp}$ with sequence verified indel generation were probed for protein level expression of Gne and Renbp. Western blot analysis was repeated in biological triplicate for each cell line.

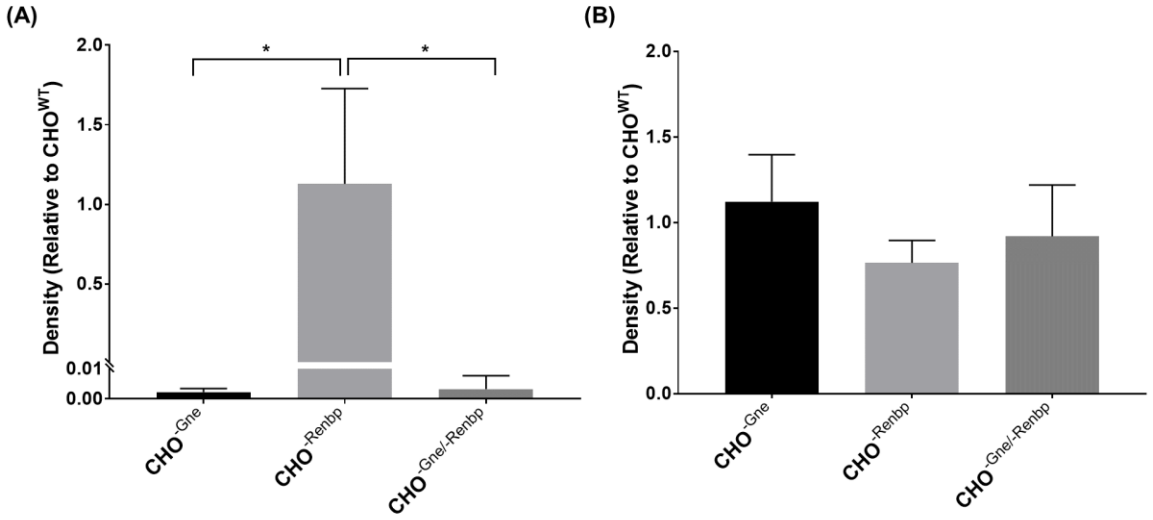

Figure 2.16 Densitometry quantification of western blot band intensities. ImageJ was used to measure band intensity. Each measurement was adjusted based on the β actin loading control and expressed as density relative the CHO^{WT} signal. (A) When the samples were probed for Gne both CHO^{-Gne} and $CHO^{-Gne/Renbp}$ yielded a band intensity less than 0.01 relative to CHO^{WT} while the CHO^{-Renbp} band intensity was ~1.2 relative to CHO^{WT}. The band intensity of CHO^{-Gne} and $CHO^{-Gne/-Renbp}$ was significantly less than the CHO^{-Renbp} intensity ($p<0.001$) (indicated by *) (B) When samples were probed for Renbp all three engineered cell lines yielded band intensities approximately equal to 1 relative the CHO^{WT}. Error bars represent the standard error of the mean between three independent biological replicates.

2.5.6 Periodate Resorcinol Assay

The periodate resorcinol assay was used to quantify differences in free intracellular sialic acid levels between the engineered cell lines when treated with varying concentrations of 1,3,4-O-Bu_3ManNAc. Equal amounts of each of the three engineered CHO lines (i.e. CHO^{-Gne}, CHO^{-Renbp}, $CHO^{-Gne/-Renbp}$) and the wild type CHO line were tested at concentrations of 0 μM, 100 μM, 300 μM, and 500 μM of 1,3,4-O-Bu_3ManNAc. Three biological replicates were performed for each of the 16 samples (**Fig. 2.17**). For all cell lines the level of free intracellular sialic acid increased in a concentration-dependent manner upon supplementation with 1,3,4-O-Bu_3ManNAc. The largest increase in sialic acid production occurred between 0 and 100 μM 1,3,4-O-Bu_3ManNAc for all of the cell lines with further smaller and cell-line-dependent increases observed at 300 and 500 μM. These trends are in agreement previous work from our group showing supplementation with similar concentrations of

1,3,4-O-Bu_3ManNAc increases flux through the SABP leading to increased sialylation levels *(156, 157, 159)*.

Both the CHO^{-Gne} and $CHO^{-Gne/-Renbp}$ cell lines had noticeably lower levels of free intracellular sialic acid at all concentrations of 1,3,4-O-Bu_3ManNAc. This difference is unsurprising considering that in addition to the epimerization of UDP-GlcNAc to ManNAc, Gne also subsequently phosphorylates this monosaccharide to ManNAc-6-phosphate. Importantly, unlike the first epimerization step, the phosphorylation step is not compensated by the addition of exogenous ManNAc. Nevertheless, even in the absence of Gne, sialylation levels were able to increase more than 7-fold when treated with an external source of ManNAc (i.e. 1,3,4-O-Bu_3ManNAc). The levels of sialic acid in any of the 1,3,4-O-Bu_3ManNAc-treated cells, in fact, were higher than in the non-supplemented CHO^{WT} line. This result indicates nonspecific kinases exist that can phosphorylate ManNAc in the absence of Gne, albeit less efficiently. Specifically, GlcNAc kinase may be able phosphorylate ManNAc in the absence of Gne *(189)*. GlcNAc kinase has a millimolar K_m for ManNAc while a micromolar K_m for GlcNAc (its natural substrate) meaning it could phosphorylate ManNAc obtained from non-Gne sources which would explain the low but nonzero levels of sialylation in untreated cells lacking Gne. Then supplementation with 1,3,4-O-Bu_3ManNAc could lead to an increase in the reaction velocity of GlcNAc kinase catalyzed phosphorylation of ManNAc resulting in the observed increase in sialylation levels. In theory, to reach the measured $\sim 1 \times 10^{10}$ sialic acid molecules per cell for CHO^{-Gne} and $CHO^{-Gne/-Renbp}$ lines would require an internal ManNAc concentration of ~166 mM assuming a cell volume of 1 pL. This number might even understate the actual requisite internal ManNAc concentration because it assumes perfect conversion of ManNAc to sialic acid without any diversion to other biochemical pathways. Critically, this level of intracellular ManNAc is within the millimolar K_m of GlcNAc kinase suggesting from an enzymatic kinetics standpoint it could phosphorylate ManNAc in the absence of Gne. GlcNAc kinase offers one possible explanation for the basal sialylation measured even in the absence of Gne; alternatively, this basal sialylation could be a product of metabolic salvage pathways such as sialic

acid lyase or an artifact from using serum in the cell culture media or even background signal *(192, 206)*.

Knocking out Renbp appeared to have little to no effect on free intracellular sialic acid levels in both treated and untreated cells. In both the CHO^{WT} and CHO^{-Renbp} cell lines sialylation increased in a concentration-dependent manner upon supplementation with 1,3,4-O-Bu_3ManNAc, but was not significantly different at any treatment level. This result was expected because the Renbp catalyzed interconversion of ManNac and GlcNAc is a secondary source of ManNAc, and GlcNAc is the thermodynamically favored product. The CHO^{-Gne} and $CHO^{-Gne/-Renbp}$ cell lines had lower sialylation levels (relative to CHO^{WT} and CHO^{-Renbp}) that increased in a concentration-dependent manner following treatment with 1,3,4-O-Bu_3ManNAc, but did not significantly differ at any treatment level. This result was also expected because in the absence of Gne GlcNAc levels will increase which will increase the GlcNAc to ManNAc ratio pushing the reaction toward ManNAc production. Supplementing these cells with an exogenous ManNAc source will in turn lower the GlcNAc to ManNAc ratio which could push the equilibrium back toward GlcNAc production. The results of this experiment suggest that the build-up of GlcNAc outweighs the exogenous supply of ManNAc pushing the reaction toward ManNAc production. However, a previous study showed that when wild type Jurkat cells and Jurkat cells lacking Renbp were treated with 10 mM ManNAc the cells lacking Renbp produced less sialic acid *(191)*. These two possible mechanisms are not necessarily mutually exclusive and will depend on the dynamic changes in GlcNAc and ManNAc levels. Alternatively, the discrepancies between that study and these experiments could be due to inherent variations between Jurkat and CHO cells. Another feasible explanation is the CRISPR-Cas9 methodology failed to completely knockout Renbp (even if genomic analysis suggests otherwise) thus resulting in the observed effect.

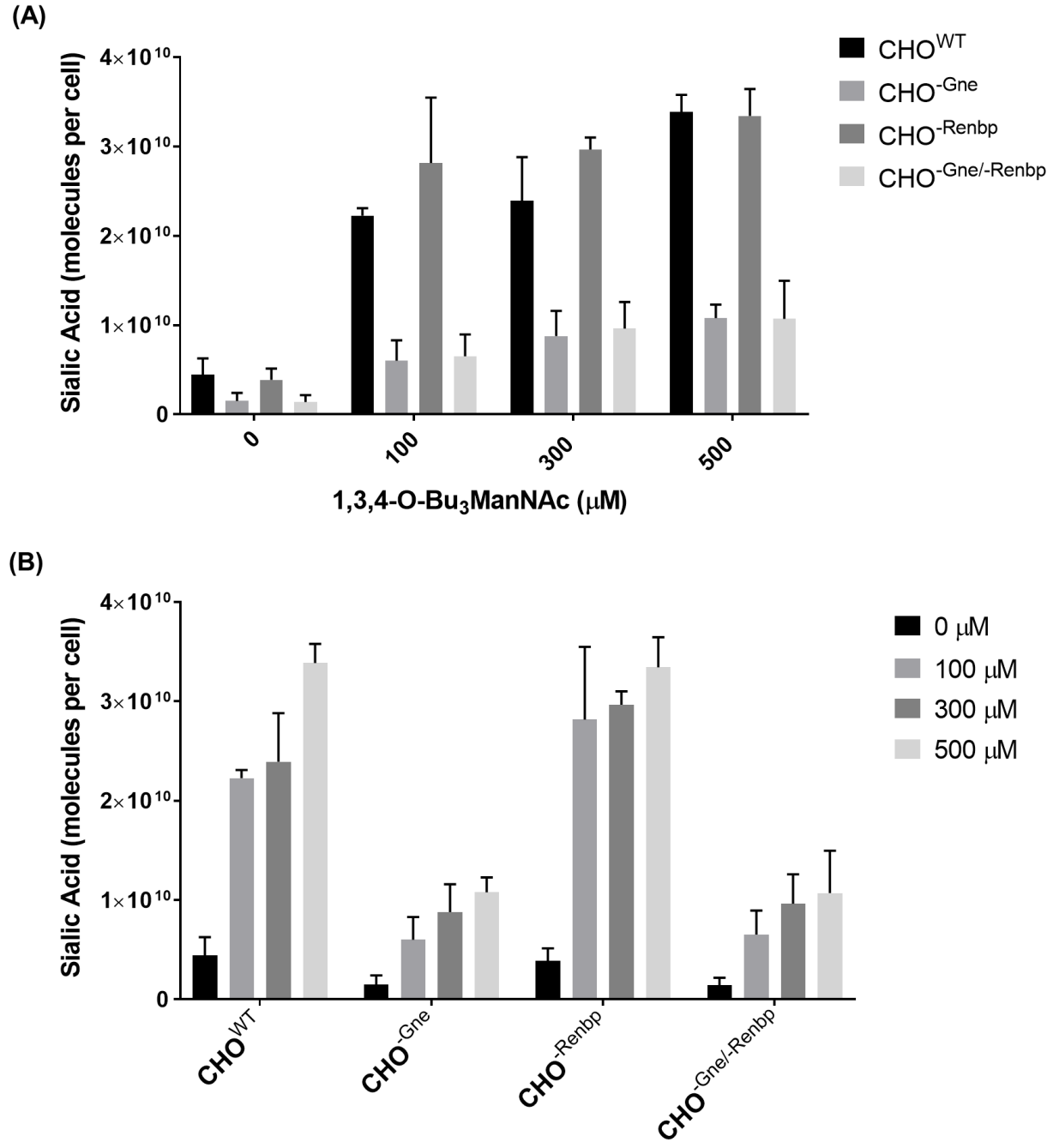

Figure 2.17 Comparison of free intracellular sialic acid levels in various engineered CHO cell lines treated with 1,3,4-O-Bu$_3$ManNAc grouped by analog concentration (A) and cell line (B). CHO^{WT}, CHO^{-Gne}, CHO^{-Renbp}, and CHO$^{-Gne/-Renbp}$ cell lines were treated with various concentrations of 1,3,4-O-Bu$_3$ManNAc (100 μM, 300 μM, 500 μM) or an equivalent volume of the solvent vehicle, ethanol. Twenty-four hours post-treatment 2.5 x 10^6 cells were used to determine free intracellular sialic acid levels using the periodate resorcinol method. Error bars represent the standard error of means between three biological replicates.

2.5.7 Azide Incorporation Flow Cytometry Assay

Flow cytometry was used in order to measure the ability of the different engineered cell lines (CHO^{WT}, CHO^{-Gne}, CHO^{-Renbp}, $CHO^{-Gne/-Renbp}$) to incorporate 1,3,4-O-Bu_3ManNAz into cellular glycosylation. Flow Cytometry was used to quantify azide incorporation after incubating treated and untreated cells with the cyclooctyne, DBCO, conjugated to the fluorophore Cy5. DBCO-Cy5 can react with azide moieties in a strain-promoted copper-free azide-alkyne cycloaddition reaction at physiological conditions (**Fig. 2.18**) *(207)*. All cells lines treated with the solvent vehicle (ethanol) exhibited similar basal Cy5 fluorescence levels. When each cell line was treated with 1,3,4-O-Bu_3ManNAz mean fluorescence intensity (MFI) increased by approximately two orders of magnitude relative to untreated samples. There were minimal differences in MFI between each cell line and MFI did not increase with concentration of 1,3,4-O-Bu_3ManNAz indicating the pathway is saturated at 100 μM (**Fig. 2.19**). Despite the CHO^{-Gne} and $CHO^{-Gne/-Renbp}$ cell lines producing less intracellular sialic acid following treatment with 1,3,4-O-Bu_3ManNAc, these cell lines exhibited similar levels of azide incorporation following treatment with 1,3,4-O-Bu_3ManNAz compared to the CHO^{WT} and CHO^{-Renbp} cell lines. This suggests that when treated with 1,3,4-O-Bu_3ManNAz the CHO^{-Gne} and $CHO^{-Gne/-Renbp}$ cell lines have a higher percent of their sialylation containing the azide moiety relative to CHO^{WT} and CHO^{-Renbp}. These results provide preliminary evidence that knocking out Gne followed by treatment with ManNAc analogs can yield more homogenous glycoprofiles. Knocking out Renbp had minimal effect on sialic acid production levels relative to CHO^{WT} and showed a similar MFI suggesting that azide incorporation levels are not different than the CHO^{WT} line. Interestingly, incorporation of the azide analog decreased as analog concentration increased in all of the cell lines. This decrease may be attributed to the cytotoxicity of 1,3,4-O-Bu_3ManNAz at higher concentrations *(157)*. Furthermore, it appears that incorporation of the azide analog into cellular glycosylation saturates at or before a concentration of 100 μM.

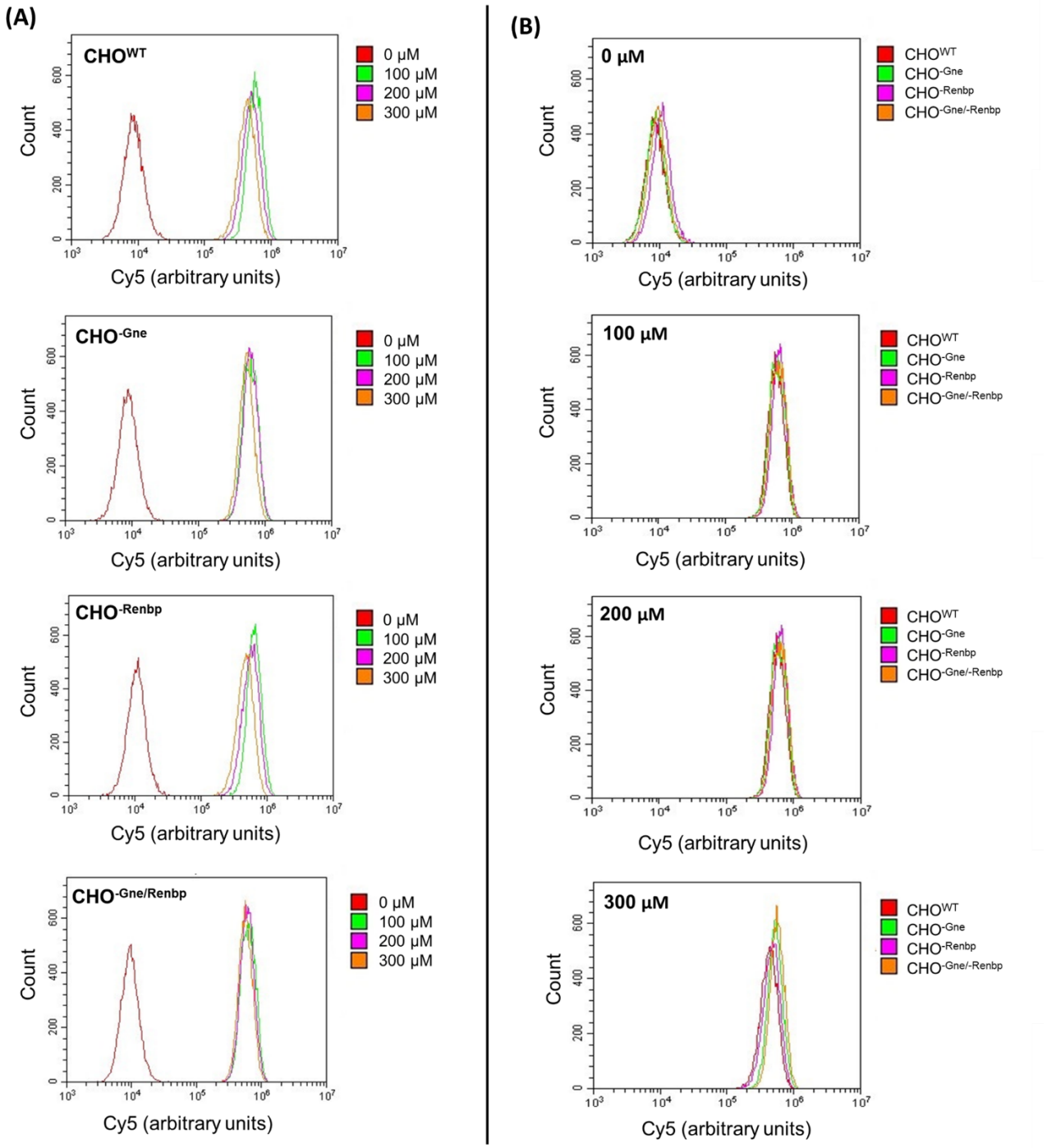

Figure 2.18 Representative flow cytometry data for CHO^{WT}, CHO^{-Gne}, CHO^{-Renbp}, and CHO$^{-Gne/-Renbp}$ cells treated with 1,3,4-O-Bu$_3$ManNAz. (A) Histogram overlays for each cell line treated with 0 µM, 100 µM, 200 µM, or 300 µM of 1,3,4-O-Bu$_3$ManNAz. (B) Histogram overlays for each cell line at each of the 1,3,4-O-Bu$_3$ManNAz concentrations.

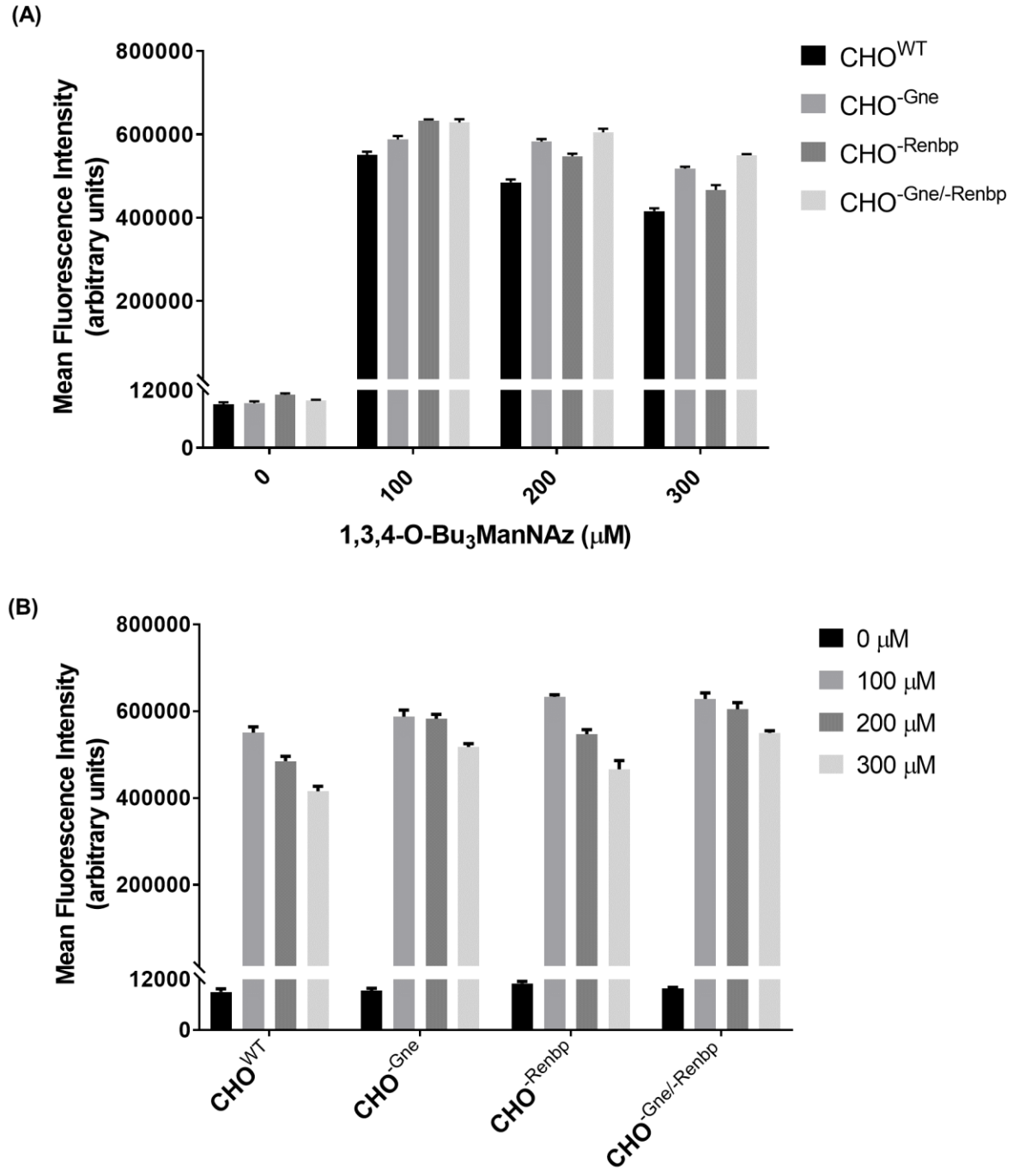

Figure 2.19 Flow cytometry mean fluorescence intensity of CHO^{WT}, CHO^{-Gne}, CHO^{-Renbp}, and $CHO^{-Gne/-Renbp}$ cells treated with 1,3,4-O-Bu_3ManNAz grouped by analog concentration (A) and cell line (B). Each cell line was treated with 0 μM, 100 μM, 200 μM, or 300 μM of 1,3,4-O-Bu_3ManNAz, surface-labeled with DBCO-Cy5, and Cy5 fluorescence levels were measured using flow cytometry. The azide incorporation flow cytometry assay was performed in biological triplicate for each cell line. Error bars represent the standard error of means.

2.5.8 Azide Incorporation Plate Reading Assay

The level of azide incorporation for each cell line was also measured using a plate reading assay. Again, each cell line was treated with 0 – 300 μM of 1,3,4-O-Bu_3ManNAz and reacted with DBCO-Cy5 which was then quantified using a fluorescence plate reader (**Fig. 2.20**). For each cell line the plate reading data exhibited a more pronounced decrease in MFI as concentration of 1,3,4-O-Bu_3ManNAz increased, but in general followed the same overall trends as the flow cytometry data. Again, both the CHO^{-Gne} and $CHO^{-Gne/Renbp}$ cell lines showed similar MFI levels as the wild type cells despite producing less free intracellular sialic acid. This supports the conclusion that knocking out Gne leads to a higher percent of cell surface glycans containing the azide moiety. Interestingly, the CHO^{-Renbp} and $CHO^{-Gne/-Renbp}$ cell lines yielded a measurably higher (although not significantly different) MFI at 100 and 200 μM relative to the CHO^{-Gne} and CHO^{-Renbp}. Furthermore, this trend was also observed in the flow cytometry data, albeit to a smaller extent. This pattern may be due to knocking out Renbp which would further limit endogenous flow of ManNAc into the SABP leading to increased usage of the exogenously supplied 1,3,4-O-Bu_3ManNAz analog. Alternatively, this may simply be due to random fluctuation within the assay itself. Previous work *(157)* and the reduction in MFI at higher concentrations (i.e. 200 and 300 μM) suggests that the non-natural azide analog is cytotoxic above 100 μM which could explain the lower incorporation levels.

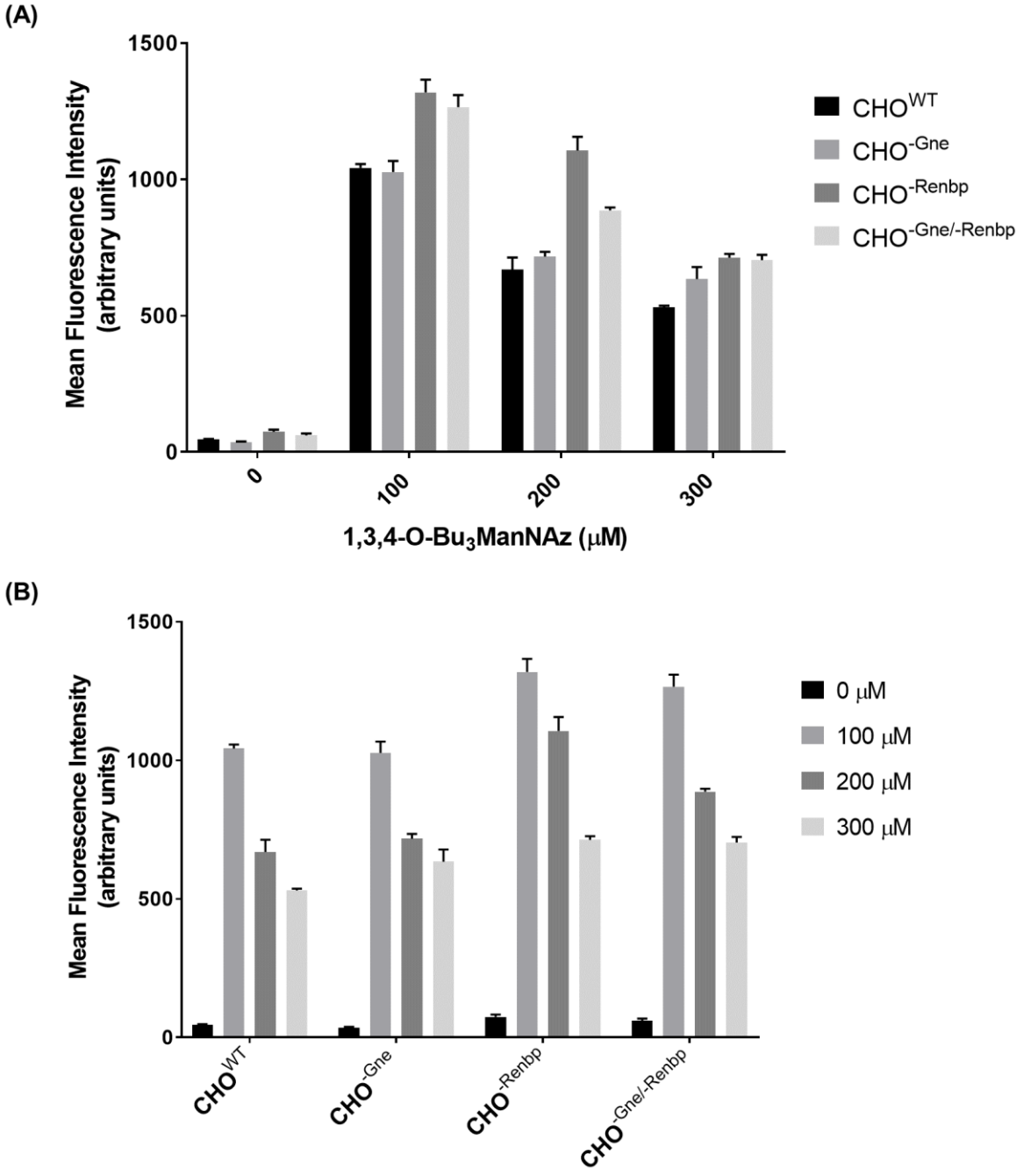

Figure 2.20 Plate reading mean fluorescence intensity of CHO^{WT}, CHO^{-Gne}, CHO^{-Renbp}, and CHO$^{-Gne/-Renbp}$ cells treated with 1,3,4-O-Bu$_3$ManNAz grouped by analog concentration (A) and cell line (B). Each cell line was treated with 0 μM, 100 μM, 200 μM, or 300 μM of 1,3,4-O-Bu$_3$ManNAz and reacted with DBCO-Cy5. Cy5 fluorescence levels were measure for all cells in each well and MFI measurements were adjusted based on cell density. Error bars represent the standard error of means between three independent biological replicates.

2.5.9 Live-Cell Imaging of Azide-Labeled Glycans

To further corroborate the flow cytometry and plate reading azide incorporation data the engineered cell lines were treated with Alexa fluor 488 conjugated to DBCO and imaged using fluorescence microscopy (**Fig. 2.21**). The images verify that all cell lines incorporated the 1,3,4-O-Bu_3ManNAz metabolites into cell surface glycans. There was negligible fluorescence in the control cell lines treated with ethanol. The basal fluorescence levels in untreated cells is consistent with the autofluorescence of mammalian cells or to random uptake of AF-DBCO into the cell membrane because it is nonpolar. Qualitatively, fluorescence appears to be highest for the 100 μM and 200 μM groups. The decrease could be due to the relative cytotoxicity of the analog at higher concentrations which would reduce the overall fluorescence in the image *(157)*. There were not obvious differences in labeling observed when comparing the flow cytometry and fluorescent microscopy data, providing independent evidence that Gne knockdown increases the proportion of azide-labeled sialic acids in 1,3,4-O-Bu_3ManNAz treated cells.

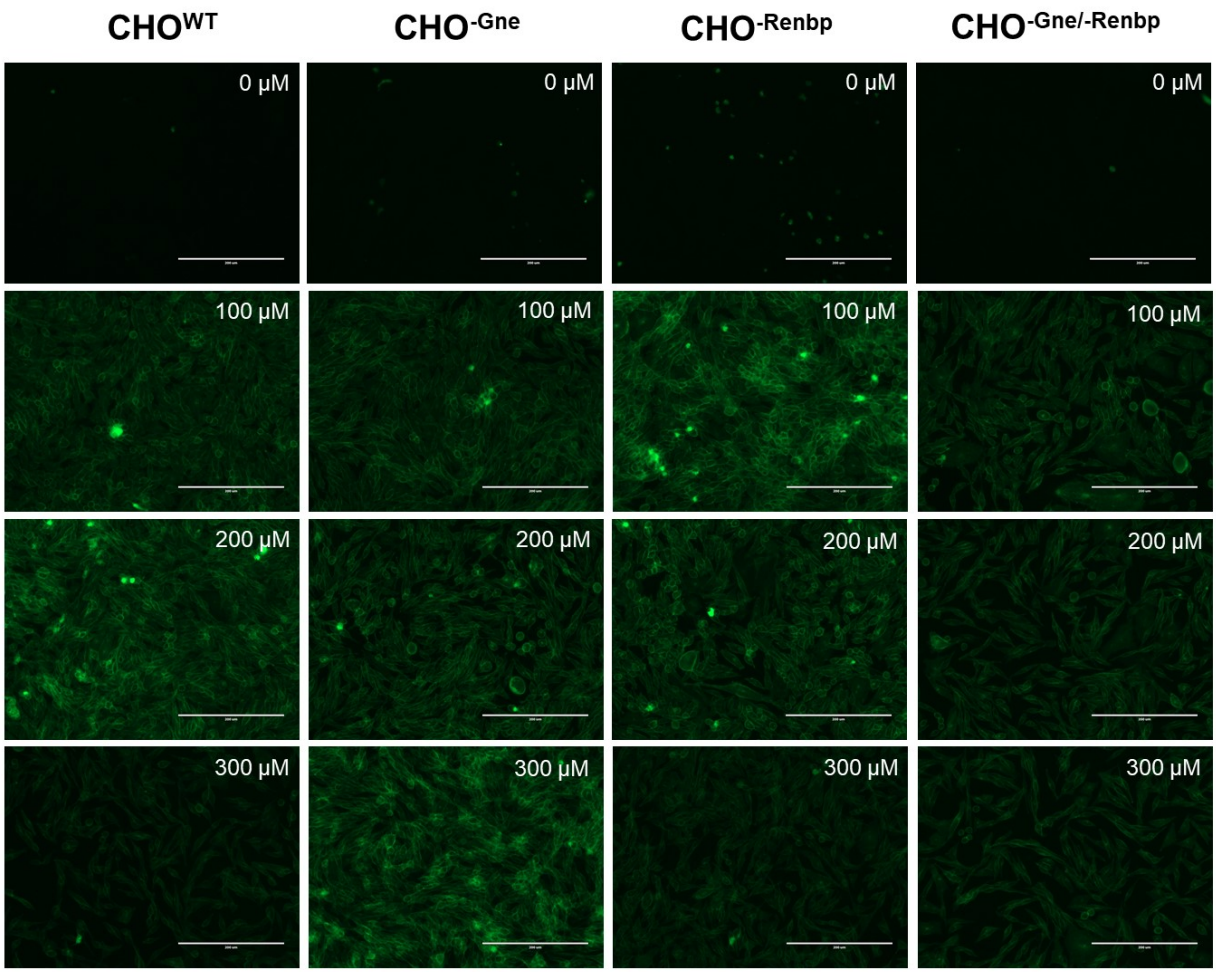

Figure 2.21 Representative fluorescence microscopy images of CHO^{WT}, CHO^{-Gne}, CHO^{-Renbp}, and CHO$^{-Gne/-Renbp}$ cells treated with varying concentrations of 1,3,4-O-Bu$_3$ManNAz. Twenty-four hours after treatment with 1,3,4-O-Bu$_3$ManNAz all samples were treated with AF-DBCO and imaged using an EVOS FL Imaging System. Live-cell imaging was performed in biological triplicate. Scale bars represent 200 μm.

2.6 Concluding Remarks

The goal of this project was to develop and implement a combined genetic engineering and MGE strategy to gain enhanced control over the magnitude and type of sialylation produced by CHO cells. To achieve this aim Gne and Renbp were targeted for CRISPR-Cas knockout to eliminate the primary and secondary routes by which ManNAc is introduced into the SABP. Gne was successfully knocked based on genomic and protein level analysis, however knockout of Renbp was less conclusive as

genomic analysis indicated indel generation but protein level analysis suggested the protein was still present.

MGE technology was applied to these engineered cell line to modulate sialylation quantity and to introduce non-natural chemical groups onto sialic acid. When treated with 1,3,4-O-Bu_3ManNAc each cell line produced more free intracellular sialic acid in a concentration dependent manner, however the Gne knockout CHO cells produced significantly less sialic acid. This supports the idea that Gne is the primary route by which ManNAc can enter the SABP and shows that nonspecific kinases must exist that can phosphorylate ManNAc in the absence of Gne. When each cell line was treated with 1,3,4-O-Bu_3ManNAz azide incorporation onto cell surface glycosylation was similar for all cell lines even the Gne knockout CHO cells. This strongly suggests that the for Gne knockout cells the proportion of surface sialic acids containing the azide moiety was higher compared to wild type CHO cells.

Overall these results demonstrate that reducing endogenous ManNAc flux into the SABP via Gne knockout enhances the ability of MGE to control the composition of sialylation. The system could be extremely useful for creating cells and glycoprotein therapeutics with more controllable and homogenized glycoprofiles. Furthermore, this strategy can increase the percent of surface sialic acids containing non-natural chemical groups which could be a powerful tool for developing novel ADCs with better antibody to drug ratios.

2.7 Future Directions

This project yielded many interesting results and like most research has generated more questions than answers. The final section of this chapter discusses next steps for this project and potential future directions to build off the results of this study.

2.7.1 Engineer CHO Cells with Validated Renbp Knockout

Genomic and protein level analysis of Renbp knockout CHO cells gave conflicting results regarding whether Renbp had been successfully knocked out. Before any definitive conclusions can be made about how knocking out Renbp in CHO cells impacts sialylation this knockout needs to be fully validated. As a first measure the genomic and protein level analysis could be repeated to verify the results obtained in this study are accurate. The western blot could also be tested with positive and negative control cell lines to verify the antibody is indeed binding Renbp. If these analyses are still in disagreement the presence of Renbp could be assessed at the mRNA level by performing qRT-PCR experiments. If these experiments fail to provide a consensus regarding whether Renbp is truly knocked out it would be necessary to reengineer CHO cells using a different set of gRNA.

2.7.2 Corroborate Periodate Resorcinol Assay Data

These studies indicated that the CHO^{-Gne} and $CHO^{-Gne/-Renbp}$ cells produced less intracellular free sialic acid relative to the CHO^{WT} and CHO^{-Renbp} cells when treated with 1,3,4-O-Bu_3ManNAc. This data could be corroborated by performing *Maackia amurensis* or *Limax flavus* lectin blot analysis to determine if changes in free sialic acid manifest as changes in glycoprotein sialylation levels. Also, changes in surface glycosylation following 1,3,4-O-Bu_3ManNAc treatment could be determined through *Maackia amurensis* or *Limax flavus* lectin flow cytometry experiments. These experiments should be repeated using the 1,3,4-O-Bu_3ManNAz analog to determine if the same or similar changes in sialyation are observed with a non-natural analog.

2.7.3 Measure Azide Incorporation at Lower 1,3,4-O-Bu_3ManNAz Concentrations

These studies measured the level of azide incorporation into cell surface glycosylation following treatment with 100, 200, and 300 μM 1,3,4-O-Bu_3ManNAz. These experiments determined analog incorporation was highest at 100 μM with higher concentrations showing reduced incorporation. Based on these results and previous work from our group *(157)* this is likely attributable to the

cytotoxicity of 1,3,4-O-Bu_3ManNAz at concentrations exceeding 100 μM. While these studies indicated azide incorporation was highest at 100 μM it is possible incorporation could be higher at lower concentrations or between 100 and 200 μM. For this reason the flow cytometry, plate reading, and live-cell imaging experiments should be repeated but for 1,3,4-O-Bu_3ManNAz concentrations between 0 – 150 μM. This would reveal the optimal analog concentration for maximum azide incorporation and indicate if the proportion of azide incorporation is titratable.

2.7.4 Knockout Sialic Acid Lyase

As previously mentioned (**2.3 Specific Aims**), ManNAc is endogenously fluxed into the SABP by three different enzymes: Gne, Renbp, and sialic acid lyase. This project aimed to knockout Gne and Renbp but did not consider eliminating sialic acid lyase. A natural extension and further optimization of this study would be to utilize CRISPR-Cas to knockout sialic acid lyase in order to obtain a CHO cell line with all possible endogenous routes for ManNAc to enter the SABP eliminated. In theory, this could further augment the ability of MGE technology to control protein sialylation levels and homogeneity.

Chapter 3: Developing Recombinant Factor IX with an Extended Serum Half-life

3.1 Overview

The third chapter provides a description of a secondary project pursued for this thesis project including rationale for the project, methods, results, and discussion of the current state of the project. The overarching goal of this project was to create coagulation FIX with a prolonged serum half-life. This chapter begins with some brief background information which is followed by the specific aims, methods used, results, and a discussion on the current status of the project.

3.2 Background

This section briefly covers background information relevant to this chapter that was not extensively covered in the introduction. This section begins by describing hemophilia and FIX with an emphasis on how glycosylation, specifically sialic acid, can improve the pharmacokinetic properties of FIX. This is followed by a description of sialyltransferases and how they dictate the orientation sialic acid is added to a glycoprotein. Finally, this section explains how MGE technology could be utilized to increase FIX sialylation to improve serum half-life.

3.2.1 Hemophilia and Factor IX

Hemophilia is an inherited genetic bleeding disorder resulting from deficiencies in coagulation factors. There are two types of hemophilia; hemophilia A (deficiency in Factor VIII) is more common with an incidence rate of 1 in 5,000 male births, while hemophilia B (deficiency in FIX) has an incidence rate of about 1 in 30,000 male births. Hemophilia is not predisposed to any ethic group or geographical location *(208, 209)*. Hemophilia B is of particular interest because of the potential for glycosylation to improve the pharmacokinetic properties of its deficient coagulation factor, FIX (discussed more below).

FIX (sometimes called the Christmas factor) is a 57 kDa vitamin K-dependent glycoprotein with glycosylation contributing to approximately 17% of its molecular weight. In a healthy adult human, the average plasma concentration of FIX is 2.5 – 5 μg mL^{-1} and its serum half-life is just 24 hours. Currently, prophylactic treatment of hemophilia B requires intravenous injection one to four times a week with FIX. There are currently 10 different FIX products available worldwide split into two types: plasma-derived or recombinantly produced *(208, 209)*. The requisite for frequent intravenous injection is burdensome to patients and contributes to the relatively high payer cost of treatment, with some studies estimating this to be $350,000 per year *(208, 210)*. Substantial efforts are being made to increase the serum half-life of recombinantly produced FIX to alleviate patient burden caused by continuous injection and reduce treatment cost to increase global availability. Three products currently on the market (ALPROLIX [Biogen Idec], IDELVION [CSL Behring] and REBINYN [Nova Nordisk]), have been shown to increase serum half-life between 2.5 – 5-fold *(208)*. ALPROLIX is recombinant FIX fused to a Fc region of an IgG enabling the modified protein to evade degradation in similar fashion to how an Fc receptor protects IgG antibodies *(208, 211)*. IDELVION is recombinant FIX fused to human albumin that extends the half-life of FIX through pH-dependent binding of albumin to Fc receptors enabling the protein to avoid lysosomal degradation *(212-216)*. REBINYN is a version of recombinant FIX that has been selectively PEGylated via GlycoPEGylation technology thereby prolonging serum half-life *(208, 217)*.

A relatively unexplored approach to augment recombinant FIX is to modify its glycosylation to prolong serum-half life. Previous research has shown that enzymatic removal of N-glycans increases the rate of catabolism of FIX and as described earlier N-glycan sialylation is known to improve serum half-life of recombinant glycoproteins including FIX *(218-221)*. One study engineered additional N-glycosylation sites into FIX and found that one hyperglycosylated FIX variant had a 2.4-fold higher serum half-life and a 5.4-fold reduction in clearance rate in mice relative to wild type FIX *(221)*. Another study built on this approach by examining 251 potential hyperglycosylated variants and

identified three variants that exhibited a 2.4-fold higher serum half-life and a 4.5-fold reduction in clearance rate in mice relative to wild type FIX *(222)*. Collectively, this work shows that modulating glycosylation can be an efficacious strategy for developing versions of FIX with improved pharmacokinetic properties.

3.2.2 Sialyltransferases

Sialyltransferases are a family of enzymes responsible for catalyzing the transfer of sialic acid from its activated nucleotide sugar donor, CMP, to an acceptor substrate which in most cases is a galactose, GalNAc, or sialic acid residue. In humans, sialic acid can be added to an acceptor substrate in three different orientations α(2,3), α(2,6), or less commonly α(2,8). To accommodate the diversity stemming from different glyosidic linkages and acceptor substrates humans produce 20 different sialyltransferases split into four main classes: (i) β-galactoside α(2,3)-sialyltransferases (ST3GAL I-IV), (ii) β-galactoside α(2,6)-sialyltransferases (ST6GAL I-II), (iii) GalNAc α(2,6) sialyltransferases (ST6GALNAC I-VI), and (iv) α(2,8)-sialyltransferases *(44, 45)*.

CHO cells produce glycosylation similar to human cells, but as discussed in section **1.3.1.4 Chinese Hamster Ovary Cells** subtle yet important differences exist between human and CHO glycosylation. Of particular importance for this chapter the *St6gal1* gene in CHO cells is inactive meaning CHO cells are unable to add sialic acid to acceptor substrates in an α(2,6) orientation *(1)*. To circumvent this issue and "humanize" CHO cells sialylation it is common to engineer CHO cells to express the human ST6GAL1 (**1.3.2 Genetic Glycoegineering**) enabling CHO cells to produce both α(2,3)- and α(2,6)-sialylation. As an added benefit expression of ST6GAL1 has been shown to increase glycoprotein sialylation which can be extremely beneficial for biopharmaceuticals pharmacokinetic properties *(112, 118-120, 122)*. Overexpressing St6gal1 increases sialyltransferase levels thereby increasing the capacity of a cell to sialylate glycoproteins. This enhanced capacity means CHO cells overexpressing ST6GAL1 can benefit even more from MGE technology compared to

wild type CHO cells. This has been demonstrated by studies showing that ST6GAL1 overexpression and MGE act synergistically to increase sialyation. Specifically, multiple studies have shown concomitant overexpression of ST6GAL1 and supplementation with 1,3,4-O-Bu_3ManNAc can increase both free intracellular sialylation and glycoprotein sialylation, including for EPO and IgG *(159-161)*.

3.3 Specific Aims

The overall goal of this project is to demonstrate that our lab's 1,3,4-O-Bu_3ManNAc analog can be used to increase sialylation of glycoproteins from CHO cells expressing ST6GAL1 thereby leading to an extended serum half-life for the target protein. A recent collaboration between our group and Michael Betenbaugh's group demonstrated that treating CHO-K1 cells with 1,3,4-O-Bu_3ManNAc can increase recombinant EPO sialylation levels by ~40% *(159)*. To build on this work and demonstrate the broad applicability of this technology for numerous proteins this project aimed to test if 1,3,4-O-Bu_3ManNAc can be used increase sialylation of FIX recombinantly produced in CHO cells expressing ST6GAL1.

Aim 1: Engineer a CHO-K1 cell line that expresses both ST6GAL1 and FIX. Preconstructed lentiviral particles were utilized to transduce CHO cells to insert the *ST6GAL1* and *FIX* genes. Monoclonal cell populations were isolated via FACS and target protein expression was verified.

Aim 2: Purify and characterize active FIX. Factor IX will be purified via immunoprecipitation and active forms will be isolated using fast protein liquid chromatography (FPLC). Factor IX activity will be verified using a fluorometric assay based on the ability of FIX to generate Factor X.

Aim 3: Determine how supplementation with 1,3,4-O-Bu_3ManNAc effects FIX sialylation levels. The engineered CHO cells will be supplemented with varying concentrations of 1,3,4-O-Bu_3ManNAc and FIX sialylation will be measured.

3.4 Materials & Methods

3.4.1 Cell Culture

The CHO-K1 cell line (ATCC, CCL-61) was used for all cell engineering and experiments performed in this chapter. The CHO-K1 cell line is a subclone of the parental CHO cell line derived by Puck *et al.* from a biopsy of an ovary of an adult *C. griseus* (Chinese hamster) *(193)*. Unless stated otherwise CHO-K1 cells were cultured in an adherent monolayer in F-12K nutrient mixture (Kaighn's modification) (Corning, 10-025-CV) supplemented with 10% (v/v) heat inactivated, sterile filtered FBS, 1% (v/v) antibiotic-antimycotic solution (100x) (Sigma Aldrich, A5955-100ML), and 5% CO_2 in a humidified environment at 37 °C. CHO-K1 cells were kept at or below 1 x 10^5 cells cm^{-2} to prevent them from reaching a confluent and quiescent growth stage. The cells were passaged every three to four days by aspirating the spent media, washing once with phosphate buffered saline (PBS) (pH = 7.4), detached using 0.25% trypsin-EDTA (Gibco, 25200-056), and incubated in a 5% CO_2, humidified 37 °C environment for 5 to 10 minutes. After incubation, cell detachment was verified using a microscope and fresh complete F-12K media was used to transfer cells to a conical tube. Cells were pelleted via centrifugation for 5 minutes at 1057 x g, resuspended in 5 mL of complete F-12K media and seeded at a density of 1 x 10^4 cells cm^{-2}. Cell density was determined using a Beck Z2™ Coulter Particle Count and Size Analyzer (Beckman-Coulter) with a 100 μm aperture, dilution factor of 1:101, and boundaries set between 7 and 25 μm. To measurements were made per sample and averaged to determine cell density. Wild type and all engineered CHO-K1 cells were cryopreserved using the same procedure outlined in section **2.4.2 Mammalian Cell Cryopreservation** and thawed using the procedure described in section **2.4.3 Thawing Cryopreserved Cells.**

3.4.3 Lentiviral Transduction

Twenty-four hours before transduction CHO-K1 cells were seeded at a density of 1.5 x 10^5 cells mL^{-1} in 6-well plates with F-12K media supplemented with 10% (v/v) FBS and 1% (v/v) antibiotic-

antimycotic solution. For the transduction, total transducing units (TU) was calculated using **Equation 3.1** with different multiplicity of infections (MOI) (the number of transducing lentiviral particles per cell) ranging from 0.25 to 2. Then the total volume (mL) of lentiviral particles to be added to each well was calculated using **Equation 3.2**. Twenty-four hours after seeding the cells from two wells were detached, pelleted and counted (**3.4.1 Cell Culture**). The cell density from these wells was assumed to be approximately equivalent to the remaining wells and used to calculate TU. The media was aspirated from the remaining wells, the cells were washed once with PBS, and 1.5 mL of fresh culture media was added to each well. The calculated volume of CD75(ST6GAL1) (NM_173216) Human Tagged ORF Clone Lentiviral Particle (Origene, RC203776L3V) or Factor IX(F9) (NM_000133) Human Tagged ORF Clone Lentiviral Particle (Origene, RC219065L4V), polybrene (final concentration 8 μg mL^{-1}), and culture media (to a final volume of 500 μL) were added to the appropriate well. The transduced cells were incubated for 18-20 hours with 5% CO_2 in a humidified environment at 37 ° C. The ST6GAL1 lentiviral particle contains a Myc-DDK tag and the puromycin selection gene, while the Factor IX lentiviral particle contains a GFP tag and the puromycin selection gene.

$$Total\ transducing\ units\ (TU) = (Total\ number\ of\ cells\ per\ well)\ x\ (Desired\ MOI) \qquad \textbf{Equation 3.1}$$

$$Total\ mL\ of\ lentiviral\ particles\ to\ be\ added\ to\ each\ well = \frac{(Total\ TU\ needed)}{(\frac{TU}{mL})} \qquad \textbf{Equation 3.2}$$

3.4.4 Puromycin Selection

CHO-K1 cells were seeded at a density of 1.5 x 10^5 cells mL^{-1} in 6-well plates with F-12K media supplemented with 10% (v/v) FBS and 1% (v/v) antibiotic-antimycotic solution. Twenty-four hours after seeding the cells were treated with puromycin ranging from 0.5 to 10 μg mL^{-1} to construct a

puromycin kill curve. Based on the puromycin kill curve data the optimal dose of puromycin was determined to be 8 μg mL^{-1}.

Twenty-four hours after transducing the CHO cells with the ST6GAL1 lentiviral particles the media was replaced with fresh F-12K media supplemented with 10% (v/v) FBS and 1% (v/v) antibiotic-antimycotic solution. Forty-eight hours post-transduction the CHO cells were treated with 8 μg mL^{-1} of puromycin to select successfully transduced cells. The puromycin was replaced every third day for a total of 15 days at which point the cells were harvested for sorting and downstream analysis.

3.4.5 Fluorescent Activated Cell Sorting

Twenty-four hours after transducing the CHO cells with the FIX lentiviral particles the media was replaced with fresh F-12K media supplemented with 10% (v/v) FBS and 1% (v/v) antibiotic-antimycotic solution. Forty-eight hours after transducing the CHO cells with the FIX lentiviral particles were detached and pelleted as described in section **3.4.1 Cell Culture**. In contrast, the CHO cells transduced with ST6GAL1 lentiviral particles were detached and pelleted after selecting with puromycin for a 15 day period (**3.4.4 Puromycin Selection**). The pelleted cells were resuspended in 2% (w/v) BSA in HBSS to prevent cell aggregation during the sorting process. All FACS experiments were performed with the assistance of Hao Zhang in the Johns Hopkins Bloomberg School of Public Health Flow Cytometry and Immunology Core facility. Each sample was filtered with a sterile 35 μm nylon mesh strainer and combined with 10 μg mL^{-1} of PI. The samples transduced with FIX lentiviral particles were sorted based on the following parameters: morphology, granularity, PI negative, and GFP positive. While the samples transduced with ST6GAL1 lentiviral particles were sorted based on the following parameters: morphology, granularity and PI negative. Single sorted cells were then seeded in 96-well plates with 100 μL of F-12K media supplemented with 10% (v/v) FBS and 1% (v/v) antibiotic-antimycotic solution in order to obtain monoclonal cell lines. The

monoclonal cell lines were supplemented with 50 μL of media every three days for a total of 12-14 days. Monoclonal cell lines exhibiting positive growth were expanded to 6-well plates for downstream analysis and protein expression validation.

3.4.6 Western Blotting

Approximately 1 x 10^6 cells were harvested, transferred to a microcentrifuge tube, washed once with PBS, and resuspended in 10 – 25 μL of RIPA with protease inhibitor cocktail (Sigma Aldrich, P8340-5ml). The samples were incubated on ice for 30 minutes and each sample was vortexed every 10 minutes to promote cell lysis. The samples were centrifuged at ~22,000 x g at 4 °C for 15 minutes and the resulting supernatant was transferred to a fresh microcentrifuge tube. Each protein sample was quantified via the BCA Assay (**2.4.13 Western Blotting**).

Fifteen micrograms of each protein sample was combined with 4x laemmli concentrate with 2-mercaptoethanol and diluted to 30 μL with RIPA buffer and protease inhibitor cocktail solution. The samples were denatured by heating at 90 °C for 10 minutes and loaded onto a Mini-PROTEAN TGX 4-15% gradient gel with a 10-well comb and 30 μL well volume. The gel was run in 1x tris/glycine/SDS buffer (Biorad, 161-0772) for ~60 minutes at 100 volts. The protein was subsequently transferred to a 0.45 μM nitrocellulose membrane using standard wet transfer techniques with all components being equilibrated with 1x tris/glycine buffer (Biorad, 161-0771) with 20% (v/v) methanol. The transfer was run in 1x tris/glycine buffer (Biorad, 161-0771) with 20% (v/v) methanol on ice at exactly 100 volts for 60 minutes. The membrane was blocked in 5% (w/v) BSA in TBST at room temperature for 60 minutes with agitation. The primary antibodies were diluted in 5% (w/v) BSA in TBST to the recommended concentration and added to the blot for overnight incubation at 4 °C with agitation. The primary antibodies used for western blots in this chapter and their dilution ratios are listed in **Table 3.1**. The next day the blot wash washed three times with TBST for 10 minutes each with agitation. The appropriate HRP linked secondary antibody

(anti-mouse IgG, [Cell Signaling, 7076] or anti-rabbit IgG, [Cell Signaling, 7074]) was diluted in 5% (w/v) BSA in TBST at a 1:10,000 ratio, added to the blot, and incubated for 60 minutes at room temperature with agitation. After incubation the blot was washed three times with TBST for 10 minutes each with agitation. While washing, the enhanced chemiluminescent substrate was prepared by combine SuperSignal West Pico PLUS Luminol/Enhancer solution (Thermo Fisher Scientific, 1863098) with SuperSignal West Pico PLUS Stable Peroxidase solution (Thermo Fisher Scientific, 1863099) in a 1:1 ratio. After the third TBST wash, the blot was incubated with the enhanced chemiluminescent substrate for ~30 seconds and transferred to a plastic sheet protector in a film cassette for imaging using Blu-C autoradiography films (Stellar Scientific, BLC-810-100).

After imaging the blot was stripped for 15 minutes using Gentle Review Stripping Buffer (Amresco, A611-N552-13), washed three times with TBST for 10 minutes each and reblocked with 5% (w/v) BSA in TBST for 60 minutes at room temperature with agitation. As a loading control, β actin (Cell Signaling, 3700) diluted in 5% (w/v) BSA in TBST at a 1:10,000 ratio was added to the blot and incubated at room temperature for 30 minutes with agitation. The blot was washed three times with TBST for 10 minutes each and HRP-linked Anti-mouse IgG diluted 1:10,000 in 5% BSA in TBST was added to the blot for 30 minutes. The blot was washed three times with TBST for 10 minutes and imaged via autoradiography as described above. Western blot analysis was performed in triplicate to verify expression of ST6GAL1 and FIX.

Table 3.1 Primary antibodies used to verify ST6GAL1 and FIX protein expression.

Antibody	Protein	Manufacturer	Catalog number	Dilution Concentration
ST6GAL1 Polyclonal Antibody	ST6GAL1	Thermo Fisher Scientific	PA5-27982	0.44 μg mL^{-1} (1:1000)
Factor IX Antibody (B-3)	FIX	Santa Cruz	sc-377187	0.1 μg mL^{-1} (1:500)

3.4.7 *Sambucus nigra* Lectin Blot

Approximately 1 x 10^6 $CHO^{+ST6GAL1}$ cells were harvested, transferred to a microcentrifuge tube, washed once with PBS, and resuspended in 10 – 25 µL of RIPA with protease inhibitor cocktail (Sigma Aldrich, P8340-5ml). The samples were incubated on ice for 30 minutes and each sample was vortexed every 10 minutes to promote cell lysis. The samples were centrifuged at ~22,000 x g at 4 °C for 15 minutes and the resulting supernatant was transferred to a fresh microcentrifuge tube. Each protein sample was quantified via the BCA assay (**2.4.13 Western Blotting**).

Five micrograms of each protein sample was combined with 4x Laemmli concentrate with 2-mercaptoethanol and diluted to 30 µL with RIPA buffer and protease inhibitor cocktail solution. The samples were denatured by heating at 90 °C for 10 minutes and loaded onto a Mini-PROTEAN TGX 4-15% gradient gel with a 10-well comb and 30 µL well volume. The gel was run in 1x tris/glycine/SDS buffer (Biorad, 161-0772) for ~60 minutes at 100 volts. The protein was subsequently transferred to 0.45 µm polyvinylidene difluoride membrane preequilibrated in methanol using standard wet transfer techniques with all other components being equilibrated with 1x tris/glycine buffer (Biorad, 161-0771) with 20% (v/v) methanol. The transfer was run in 1x tris/glycine buffer (Biorad, 161-0771) with 20% (v/v) methanol on ice at exactly 100 volts for 60 minutes. The membrane was blocked with 3% BSA in PBS with 0.1% (v/v) Tween 20 (PBST) at room temperature for 60 minutes with agitation. Biotin conjugated *Sambucus nigra* (SNA) lectin (B-1305, Vector Laboratories) lectin was diluted in PBST to a concentration of 1 µg mL^{-1} and added to the blot for 1 hour at 4 °C with agitation. After incubation, the blot was washed five times with PBST for 10 minutes each. Streptavidin-HRP (Cell Signaling, 3999S) diluted in PBST at a ratio of 1:100,000 and added to the blot for 30 minutes with agitation. After incubation, the blot was washed five times with PBST for 10 minutes each. While washing, the enhanced chemiluminescent substrate was prepared by combine SuperSignal West Pico PLUS Luminol/Enhancer solution (Thermo Fisher Scientific, 1863098) with SuperSignal West Pico PLUS Stable Peroxidase solution (Thermo Fisher Scientific,

1863099) in a 1:1 ratio. After the last PBST wash, the blot was incubated with the enhanced chemiluminescent substrate for ~30 seconds and transferred to a plastic sheet protector in a film cassette for imaging using Blu-C autoradiography films (Stellar Scientific, BLC-810-100).

After imaging, the blot was washed once with PBST and an inhibitory sugar solution comprised of 150 mM sialic acid and 150 mM lactose was added for 60 minutes with agitation. The inhibitory sugar solution serves as a negative control to verify the lectin is specifically binding to the target glycan motif. After incubating with the inhibitory sugar solution the blot was washed five times with PBST and incubated with streptavidin-HRP (1:100,000) in PBST. The blot was washed five times with PBST for 10 minutes each and imaged exactly as described above for the lectin. The inhibitory sugars should out compete the glycoproteins for lectin binding resulting in no signal when imaging. After imaging, the blot was probed with β actin (Cell Signaling, 3700) as a loading control (**3.4.6 Western Blotting**). After imaging the loading control, the blot was washed once with PBST for 10 minutes and amido black stain solution diluted in deionized water was added for one minute. The blot was destained for 30 minutes using 35% (v/v) 2-propanol, 10% (v/v) acetic acid solution. The blot was air dried for 30 minutes and imaged for another loading control measure. SNA lectin blots were performed in biological triplicate.

3.4.8 Adapting CHO-K1 Cells to Serum Free Suspension Culture

Once a monoclonal population of CHO-K1 cells expressing FIX and ST6GAL1 was engineered and validated the cells were sequentially adapted to serum-free, chemically defined suspension culture conditions. The engineered cells were detached and pelleted as described in section **3.4.1 Cell Culture**. The cells were resuspended in FreeStyle CHO Expression Medium (Thermo Fisher Scientific, 12651014) supplemented with 5% (v/v) FBS, 0.2% (v/v) penicillin streptomycin solution, 8 mM L-glutamine, and 1x Pluronic F-68 (Gibco, 24040032). Cell density was determined using a Beck Z2™ Coulter Particle Count and Size Analyzer and the cells were seeded in a 125 mL suspension culture

vented shaker flask at a density of 5 x 10^5 cells mL^{-1}. The suspension culture was incubated in a humidified environment at 37 °C with 5% CO_2 at 125 rpm. Cell density and viability was monitored every day to establish growth rates of suspension culture. The media was changed every four days and once the culture reached a density of 1 x 10^6 cells mL^{-1} the cells were passaged to a new shaker flask at a density of 5 x 10^5 cells mL^{-1} with half the volume of FBS. This process was repeated until reaching 0.0156% (v/v) FBS at which point the cells were passaged to completely serum free media. Once the suspension culture reached a density of 1 x 10^6 cells mL^{-1} with at least 90% viability the cells were considered adapted and seeding density for all subsequent passages was reduced to 2.5 x 10^5 cells mL^{-1}.

3.5 Results & Discussion

3.5.1 Fluorescent Activated Cell Sorting

CHO-K1 cells transduced with the ST6GAL1 lentiviral particles were selected with puromycin for 15 days and single cells were sorted to isolate a monoclonal population. The ST6GAL1 transduced cells were gated based on multiple parameters to ensure viable, single cells were seeded. Cells with the correct morphology and size were selected by measuring FSC pulse height and SSC pulse height while granularity was accessed by measuring SSC pulse width and height and gating accordingly. At least 80% of the ST6GAL1 transduced CHO cells displayed the correct cellular morphology and greater than 90% of these cells were singlets. Finally, PI staining showed greater than 98% of the cell sample was viable (**Fig. 3.1**).

Once a ST6GAL1 positive CHO cell line was established this cell line was transduced with a FIX lentiviral particle containing a GFP selection marker. The cells transduced with FIX were gated based on multiple parameters to ensure single, viable, GFP positive cells were selected. Over 90% of the cell sample displayed the appropriate cell morphology and approximately 89% were singlets. Interestingly, only 1.46% of the cell sample was GFP positive suggesting transduction was extremely

inefficient (**Fig. 3.1**). This is in contrast to a previous study that was able to achieve up to 95% transduction efficiency in CHO cells *(223)*. These differences could result from not using the optimal MOI and cell density or from differences in the lentiviral plasmids and particles used.

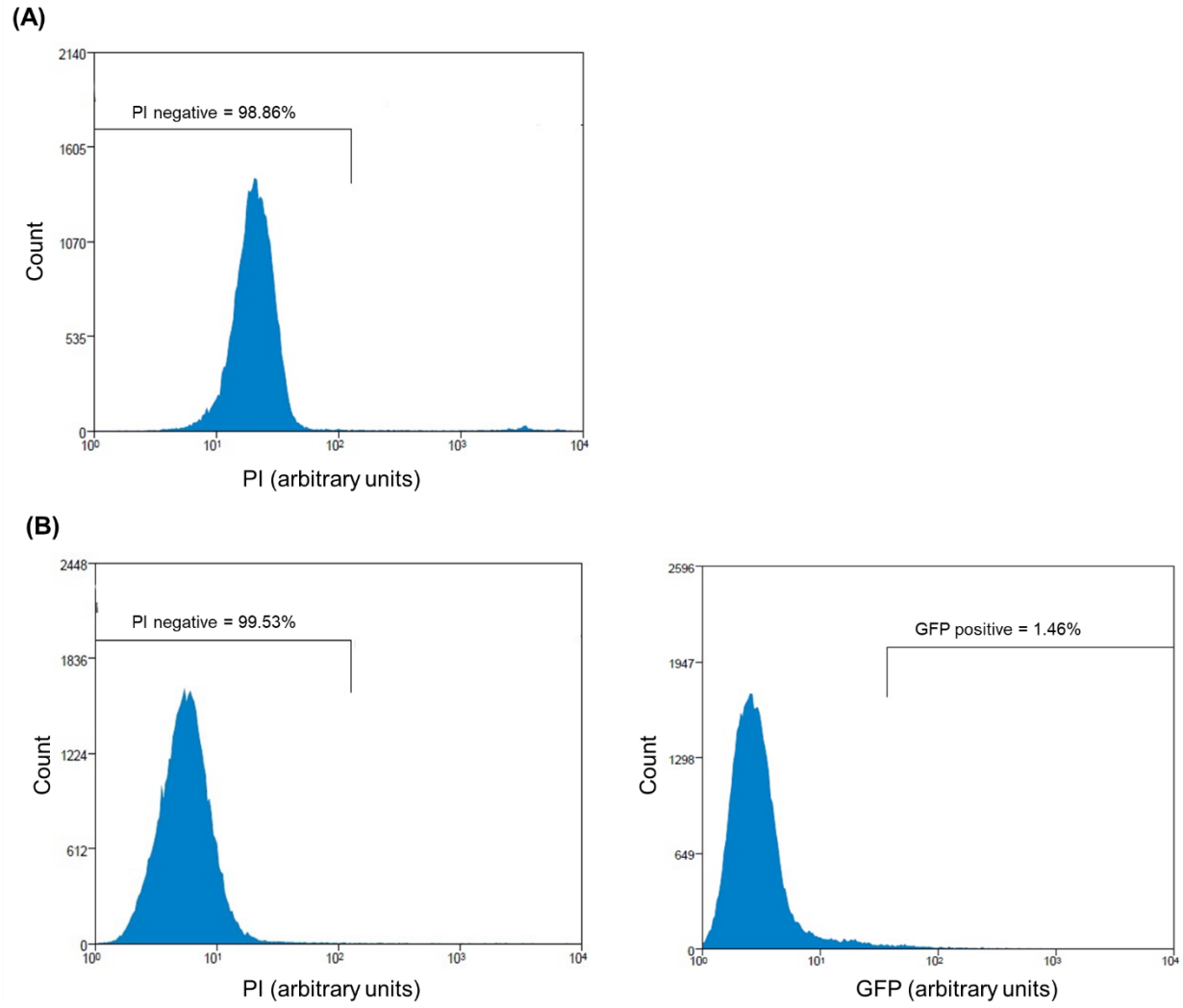

Figure 3.1 FACS data for sorting CHO cells transduced with ST6GAL1 and FIX lentiviral particles. All samples were sorted and gated based on morphology, granularity, and PI negative. (A) PI FACS histogram for CHO^{WT} cells transduced with preconstructed ST6GAL1 lentiviral particles. (B) PI and GFP FACS histograms for $CHO^{+ST6GAL1}$ cells transduced with preconstructed FIX lentiviral particles.

3.5.2 Western Blotting

Immunoblotting was used in order to verify ST6GAL1 expression in transduced CHO-K1 cells. Protein was extracted from monoclonal populations of CHO cells transduced with ST6GAL1 lentiviral particles and probed for expression using an ST6GAL1 polyclonal antibody (Thermo Fisher Scientific, PA5-27982) at a concentration of 0.44 μg mL^{-1}. Approximately 30 monoclonal cell lines were screened with cell lines exhibiting a range of expression levels. From these cell lines a monoclonal population was selected that showed robust ST6GAL1 expression relative to CHO^{WT} (**Fig. 3.2**) (**Fig. 3.3**).

Once a monoclonal population of CHO cells expressing ST6GAL1 was isolated these cells were transduced with FIX lentiviral particles. Again, following FACS, approximately 30 monoclonal cell lines were screened via western blotting with cell lines exhibiting a range of FIX expression levels. Of these cell lines one with high FIX expression ($CHO^{+FIX/+ST6GAL1}$) was selected for downstream applications (**Fig. 3.2**). The observed molecular weight for FIX is typically around 50 kDa, however in this case the observed molecular weight of FIX is approximately 70 kDa since it is conjugated to GFP.

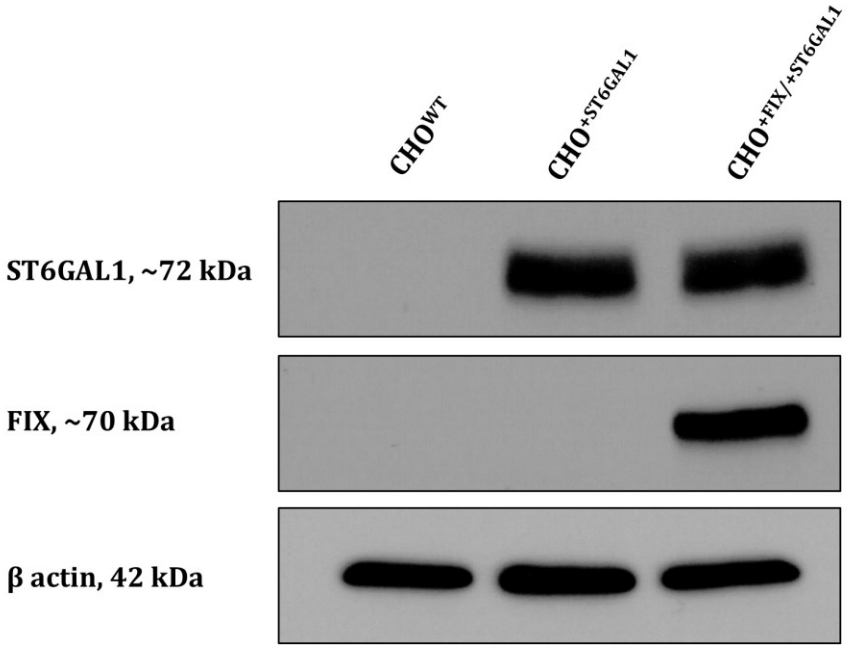

Figure 3.3 Representative western blot showing expression levels of FIX and ST6GAL1 in engineered CHO cells. Monoclonal populations of CHO cells transduced with FIX and/or ST6GAL1 lentiviral particles were isolated and probed for protein expression. Western blot analysis was performed in biological triplicate for each cell line.

3.5.3 *Sambucus nigra* Lectin Blots

SNA lectin blots were performed with the $CHO^{+ST6GAL1}$ cell line in order to provide further evidence of ST6GAL1 expression. The $CHO^{+ST6GAL1}$ sample yielded a stronger signal relative to the CHO^{WT} protein sample, however the CHO^{WT} sample still exhibited some basal signal levels (**Fig. 3.3**). The St6gal1 gene in wild type CHO cells is inactive meaning there should be not be any α2,6-linked sialic acid in CHO^{WT}, however it has been shown that the SNA lectin also nonspecifically binds to α2,3-linked sialic acid *(122)*. Lectin specificity was demonstrated by incubating the blot in a 150 mM sialic acid and lactose solution. Overall the SNA lectin blot data provided further evidence showing the $CHO^{+ST6GAL1}$ cell line does indeed express ST6GAL1.

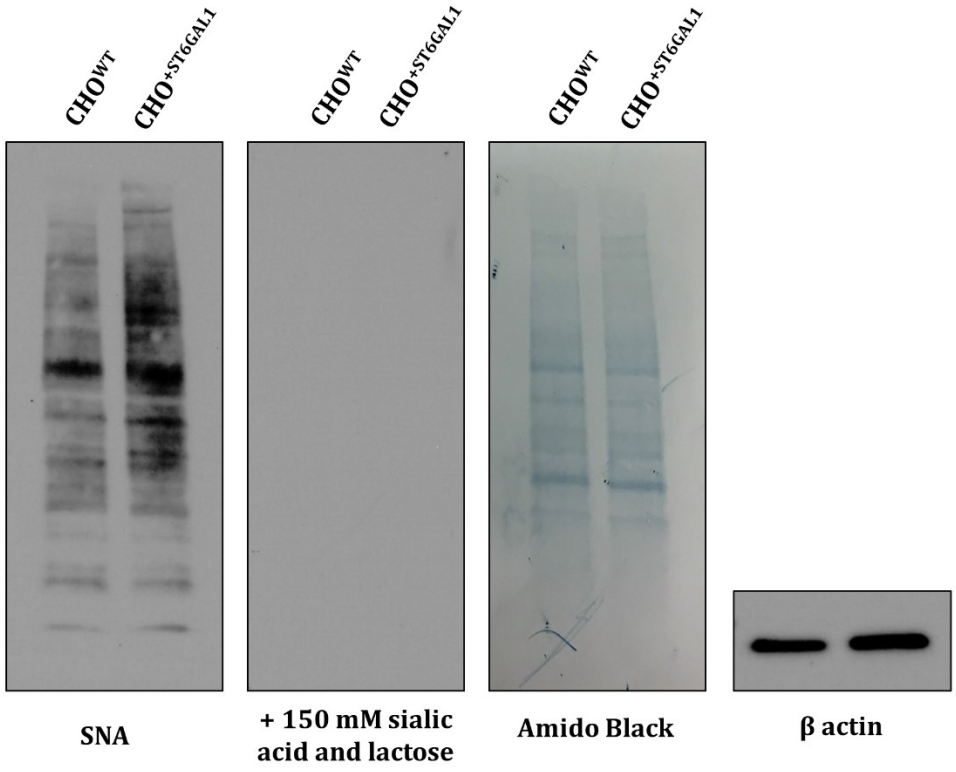

Figure 3.3 Representative SNA lectin blot comparing CHO^{WT} and $CHO^{+ST6GAL1}$ α2,6-linked sialic acid content. Five micrograms of protein for each sample was probed with 1 μg mL^{-1} of SNA lectin. Lectin specificity was demonstrated by adding an inhibitory sugar solution composed of 150 mM sialic and lactose. Equal loading was verified by amido black staining and probing for β actin. SNA lectin blots were performed in biological triplicate.

3.6 Concluding Remark

The goal of this project was to use MGE and genetic engineering to increase the serum half-life of FIX recombinantly produced by CHO cells. Lentiviral transductions were utilized to develop a CHO cell line co-expressing ST6GAL1 and FIX which was verified through immunoblotting. Expression of ST6GAL1 enables to CHO cells to add sialic acid to glycoproteins in the α(2,6) orientation in addition to the α(2,3) orientation as is found in humans. Expressing ST6GAL1 in CHO cells also has the added benefit of enhancing the effectiveness of MGE in increasing sialylation. In sum, this engineered cell line will provide a foundation for demonstrating MGE, specifically our group's 1,3,4-O-Bu_3ManNAc analog, can be used to increase glycoprotein sialylation in order to prolong serum half-life.

3.7 Future Directions

While a CHO cell line expressing both ST6GAL1 and FIX was successfully created, the final two aims of this project were not completed. The final section of this chapter describes next steps to complete the remaining aims of this project. Additionally, this section highlights future studies that can be conducted using glycoengineered FIX.

3.7.1 Purification and Activity Assay

In order to determine if MGE can be used to increase sialylation of recombinantly produced FIX an effective purification process needs to be developed. Previous studies used a two-step approach to purify FIX consisting of an immunoaffinity step followed by anion exchange chromatography to isolate active fractions of FIX *(217, 221, 222, 224-226)*. These studies can be used as a foundation for developing a successful purification process of FIX from CHO cells. After purifying FIX it will also be critical to verify the isolated coagulation factor is active. Multiple activity assays are commercially available which commonly measure FIX activity by measuring its ability to generate Factor X.

3.7.2 Characterize Changes in Sialylation After MGE

Once a FIX purification process has been developed and validated, MGE can be implemented to increase FIX sialylation. Specifically, the CHO cells producing FIX can be treated with 1,3,4-O-Bu_3ManNAc to increase flux through the SABP and in theory increase FIX sialylation. Changes in FIX α(2,3)- and α(2,6)-linked sialylation could be determined via *Maackia amurensis* and SNA lectin blots and mass spectrometry analysis.

3.7.3 *In vivo* Assessment of Serum Half-Life

If MGE technology is able to increase recombinantly produced FIX *in vivo* studies could be used to test if the glycoengineered FIX has a prolonged serum half-life. Serum half-life could be assessed by treating rats with glycoengineered FIX and collecting serum samples at various time points. Since

FIX is conjugated to GFP, protein retention could also be analyzed using fluorescence microscopy to measure GFP levels. If MGE was able to increase FIX sialylation and serum half-life it would represent a promising therapeutic for improving hemophilia B treatment.

References

1. Buettner, M. J.; Shah, S. R.; Saeui, C. T.; Ariss, R.; Yarema, K. J. Improving immunotherapy through glycodesign. *Front. Immunol.* **2018***, 9*, 2485.

2. Seeberger, P. In *Chapter 2: Monosaccharide Diversity;* Varki, A., Cummings, R., Esko, J., Stanley, P., Hart, G., Aebi, M., Darvill, A., Kinoshita, T., Packer, N., Prestegard, J., Schnaar, R. and Seeberger, P., Eds.; Essentials of Glycobiology; Cold Spring Harbor Laboratory Press: Cold Spring Harbor, NY, 2017; .

3. Varki, A.; Kornfeld, S. In *Chapter 1: Historical Background and Overview;* Varki, A., Cummings, R., Esko, J., Stanley, P., Hart, G., Aebi, M., Darvill, A., Kinoshita, T., Packer, N., Prestegard, J., Schnaar, R. and Seeberger, P., Eds.; Essentials of Glycobiology; Cold Spring Harbor Laboratory Press: Cold Spring Harbor, NY, 2017; .

4. Prestegard, J.; Liu, J.; Widmalm, G. In *Chapter 3: Oligosaccharides and Polysaccharides;* Varki, A., Cummings, R., Esko, J., Stanley, P., Hart, G., Aebi, M., Darvill, A., Kinoshita, T., Packer, N., Prestegard, J., Schnaar, R. and Seeberger, P., Eds.; Essentials of Glycobiology; Cold Spring Harbor Laboratory Press: Cold Spring Harbor, NY, 2017; .

5. Bieberich, E. Synthesis, processing, and function of N-glycans in N-glycoproteins. *Adv. Neurobiol.* **2014***, 9*, 47-70.

6. Stanley, P.; Taniguchi, N.; Aebi, M. In *Chapter 9: N-Glycans;* Varki, A., Cummings, R., Esko, J., Pamela, S., Hart, G., Aebi, M., Darvill, A., Kinoshita, T., Packer, N., Prestegard, J., Schnaar, R. and Seeberger, P., Eds.; Essentials of Glycobiology; Cold Spring Harbor Laboratory Press: Cold Spring Harbor, NY, 2017; .

7. Aebi, M. N-linked protein glycosylation in the ER. *Biochim. Biophys. Acta* **2013***, 1833*, 2430-2437.

8. Chojnacki, T.; Dallner, G. The biological role of dolichol. *Biochem. J.* **1988***, 251*, 1-9.

9. Kornfeld, R.; Kornfeld, S. Assembly of asparagine-linked oligosaccharides. *Annu. Rev. Biochem.* **1985***, 54*, 631-664.

10. Bretthauer, R. K. Structure, expression, and regulation of UDP-GlcNAc: dolichol phosphate GlcNAc-1-phosphate transferase (DPAGT1). *Curr. Drug Targets* **2009***, 10*, 477-482.

11. Gao, X. D.; Tachikawa, H.; Sato, T.; Jigami, Y.; Dean, N. Alg14 recruits Alg13 to the cytoplasmic face of the endoplasmic reticulum to form a novel bipartite UDP-N-acetylglucosamine transferase required for the second step of N-linked glycosylation. *J. Biol. Chem.* **2005***, 280*, 36254-36262.

12. Rush, J. S.; Waechter, C. J. Transmembrane movement of a water-soluble analogue of mannosylphosphoryldolichol is mediated by an endoplasmic reticulum protein. *J. Cell Biol.* **1995***, 130*, 529-536.

13. Sanyal, S.; Menon, A. K. Stereoselective transbilayer translocation of mannosyl phosphoryl dolichol by an endoplasmic reticulum flippase. *Proc. Natl. Acad. Sci. U. S. A.* **2010***, 107*, 11289-11294.

14. Kelleher, D. J.; Gilmore, R. An evolving view of the eukaryotic oligosaccharyltransferase. *Glycobiology* **2006***, 16*, 62R.

15. Mohorko, E.; Glockshuber, R.; Aebi, M. Oligosaccharyltransferase: the central enzyme of N-linked protein glycosylation. *J. Inherit. Metab. Dis.* **2011***, 34*, 869-878.

16. Krambeck, F. J.; Betenbaugh, M. J. A mathematical model of N-linked glycosylation. *Biotechnol. Bioeng.* **2005***, 92*, 711-728.

17. Krambeck, F. J.; Bennun, S. V.; Narang, S.; Choi, S.; Yarema, K. J.; Betenbaugh, M. J. A mathematical model to derive N-glycan structures and cellular enzyme activities from mass spectrometric data. *Glycobiology* **2009***, 19*, 1163-1175.

18. Werz, D. B.; Ranzinger, R.; Herget, S.; Adibekian, A.; von der Lieth, C. W.; Seeberger, P. H. Exploring the structural diversity of mammalian carbohydrates ("glycospace") by statistical databank analysis. *ACS Chem. Biol.* **2007***, 2*, 685-691.

19. Krasikov, V. V.; Karelov, D. V.; Firsov, L. M. α-Glucosidases. *Biochemistry (Mosc)* **2001***, 66*, 267-281.

20. Hammond, C.; Braakman, I.; Helenius, A. Role of N-linked oligosaccharide recognition, glucose trimming, and calnexin in glycoprotein folding and quality control. *Proc. Natl. Acad. Sci. U. S. A.* **1994***, 91*, 913-917.

21. Ellgaard, L.; Molinari, M.; Helenius, A. Setting the standards: quality control in the secretory pathway. *Science* **1999***, 286*, 1882-1888.

22. Deprez, P.; Gautschi, M.; Helenius, A. More than one glycan is needed for ER glucosidase II to allow entry of glycoproteins into the calnexin/calreticulin cycle. *Mol. Cell* **2005***, 19*, 183-195.

23. Driouich, A.; Gonnet, P.; Makkie, M.; Laine, A. C.; Faye, L. The role of high-mannose and complex asparagine-linked glycans in the secretion and stability of glycoproteins. *Planta* **1989***, 180*, 96-104.

24. Schachter, H. Biosynthetic controls that determine the branching and microheterogeneity of protein-bound oligosaccharides. *Biochem. Cell Biol.* **1986***, 64*, 163-181.

25. Rose, D. R. Structure, mechanism and inhibition of Golgi α-mannosidase II. *Curr. Opin. Struct. Biol.* **2012***, 22*, 558-562.

26. Dennis, J. W.; Nabi, I. R.; Demetriou, M. Metabolism, cell surface organization, and disease. *Cell* **2009***, 139*, 1229-1241.

27. Kizuka, Y.; Taniguchi, N. Enzymes for N-glycan branching and their genetic and nongenetic regulation in cancer. *Biomolecules* **2016**, *6*, 10.3390/biom6020025.

28. Zhao, Y.; Sato, Y.; Isaji, T.; Fukuda, T.; Matsumoto, A.; Miyoshi, E.; Gu, J.; Taniguchi, N. Branched N-glycans regulate the biological functions of integrins and cadherins. *FEBS J.* **2008**, *275*, 1939-1948.

29. Liu, L. Antibody glycosylation and its impact on the pharmacokinetics and pharmacodynamics of monoclonal antibodies and Fc-fusion proteins. *J. Pharm. Sci.* **2015**, *104*, 1866-1884.

30. Gu, J.; Nishikawa, A.; Tsuruoka, N.; Ohno, M.; Yamaguchi, N.; Kangawa, K.; Taniguchi, N. Purification and characterization of UDP-N-acetylglucosamine: α-6-D-mannoside β 1-6N-acetylglucosaminyltransferase (N-acetylglucosaminyltransferase V) from a human lung cancer cell line. *J. Biochem.* **1993**, *113*, 614-619.

31. Pinho, S. S.; Reis, C. A.; Paredes, J.; Magalhaes, A. M.; Ferreira, A. C.; Figueiredo, J.; Xiaogang, W.; Carneiro, F.; Gartner, F.; Seruca, R. The role of N-acetylglucosaminyltransferase III and V in the post-transcriptional modifications of E-cadherin. *Hum. Mol. Genet.* **2009**, *18*, 2599-2608.

32. Song, Y.; Aglipay, J. A.; Bernstein, J. D.; Goswami, S.; Stanley, P. The bisecting GlcNAc on N-glycans inhibits growth factor signaling and retards mammary tumor progression. *Cancer Res.* **2010**, *70*, 3361-3371.

33. Yoshimura, M.; Nishikawa, A.; Ihara, Y.; Taniguchi, S.; Taniguchi, N. Suppression of lung metastasis of B16 mouse melanoma by N-acetylglucosaminyltransferase III gene transfection. *Proc. Natl. Acad. Sci. U. S. A.* **1995**, *92*, 8754-8758.

34. Yoshimura, M.; Ihara, Y.; Matsuzawa, Y.; Taniguchi, N. Aberrant glycosylation of E-cadherin enhances cell-cell binding to suppress metastasis. *J. Biol. Chem.* **1996**, *271*, 13811-13815.

35. Ihara, Y.; Yoshimura, M.; Miyoshi, E.; Nishikawa, A.; Sultan, A. S.; Toyosawa, S.; Ohnishi, A.; Suzuki, M.; Yamamura, K.; Ijuhin, N.; Taniguchi, N. Ectopic expression of N-acetylglucosaminyltransferase III in transgenic hepatocytes disrupts apolipoprotein B secretion and induces aberrant cellular morphology with lipid storage. *Proc. Natl. Acad. Sci. U. S. A.* **1998**, *95*, 2526-2530.

36. Xu, Q.; Isaji, T.; Lu, Y.; Gu, W.; Kondo, M.; Fukuda, T.; Du, Y.; Gu, J. Roles of N-acetylglucosaminyltransferase III in epithelial-to-mesenchymal transition induced by transforming growth factor beta1 (TGF-β1) in epithelial cell lines. *J. Biol. Chem.* **2012**, *287*, 16563-16574.

37. Pinho, S. S.; Oliveira, P.; Cabral, J.; Carvalho, S.; Huntsman, D.; Gartner, F.; Seruca, R.; Reis, C. A.; Oliveira, C. Loss and recovery of Mgat3 and GnT-III Mediated E-cadherin N-glycosylation is a mechanism involved in epithelial-mesenchymal-epithelial transitions. *PLoS One* **2012**, *7*, e33191.

38. Qasba, P. K.; Ramakrishnan, B.; Boeggeman, E. Structure and function of β-1,4-galactosyltransferase. *Curr. Drug Targets* **2008**, *9*, 292-309.

39. Furukawa, K.; Sato, T. β-1,4-galactosylation of N-glycans is a complex process. *Biochim. Biophys. Acta* **1999***, 1473*, 54-66.

40. Cheng, K.; Zhou, Y.; Neelamegham, S. DrawGlycan-SNFG: a robust tool to render glycans and glycopeptides with fragmentation information. *Glycobiology* **2017***, 27*, 200-205.

41. Javaud, C.; Dupuy, F.; Maftah, A.; Julien, R.; Petit, J. M. The fucosyltransferase gene family: an amazing summary of the underlying mechanisms of gene evolution. *Genetica* **2003***, 118*, 157-170.

42. Stanley, P.; Cummings, R. In *Chapter 14: Structures common to different glycans;* Varki, A., Cummings, R., Esko, J., Stanley, P., Hart, G., Aebi, M., Darvill, A., Kinoshita, T., Packer, N., Prestegard, J., Schnaar, R. and Seeberger, P., Eds.; Essentials of Glycobiology; Cold Spring Harbor Laboratory Press: Cold Spring Harbor, NY, 2017; .

43. Angata, T.; Varki, A. Chemical diversity in the sialic acids and related α-keto acids: an evolutionary perspective. *Chem. Rev.* **2002***, 102*, 439-469.

44. Harduin-Lepers, A.; Vallejo-Ruiz, V.; Krzewinski-Recchi, M. A.; Samyn-Petit, B.; Julien, S.; Delannoy, P. The human sialyltransferase family. *Biochimie* **2001***, 83*, 727-737.

45. Li, Y.; Chen, X. Sialic acid metabolism and sialyltransferases: natural functions and applications. *Appl. Microbiol. Biotechnol.* **2012***, 94*, 887-905.

46. Bork, K.; Horstkorte, R.; Weidemann, W. Increasing the sialylation of therapeutic glycoproteins: the potential of the sialic acid biosynthetic pathway. *J. Pharm. Sci.* **2009***, 98*, 3499-3508.

47. Brockhausen, I.; Stanley, P. In *Chapter 10: O-GalNAc Glycans;* Varki, A., Cummings, R., Esko, J., Stanley, P., Hart, G., Aebi, M., Darvill, A., Kinoshita, T., Packer, N., Prestegard, J., Schnaar, R. and Seeberger, P., Eds.; Essentials of Glycobiology; Cold Spring Harbor Laboratory Press: Cold Spring Harbor, NY, 2017; .

48. Haltiwanger, R.; Wells, L.; Freeze, H.; Stanley, P. In *Chapter 13: Other Classes of Eukaryotic Glycans;* Varki, A., Cummings, R., Esko, J., Stanley, P., Hart, G., Aebi, M., Darvill, A., Kinoshita, T., Packer, N., Prestegard, J., Schnaar, R. and Seeberger, P., Eds.; Essentials of Glycobiology; Cold Spring Harbor Laboratory Press: Cold Spring Harbor, NY, 2017; .

49. Hanisch, F. G. O-glycosylation of the mucin type. *Biol. Chem.* **2001***, 382*, 143-149.

50. Van den Steen, P.; Rudd, P. M.; Dwek, R. A.; Opdenakker, G. Concepts and principles of O-linked glycosylation. *Crit. Rev. Biochem. Mol. Biol.* **1998***, 33*, 151-208.

51. Bennett, E. P.; Mandel, U.; Clausen, H.; Gerken, T. A.; Fritz, T. A.; Tabak, L. A. Control of mucin-type O-glycosylation: a classification of the polypeptide GalNAc-transferase gene family. *Glycobiology* **2012***, 22*, 736-756.

52. Ten Hagen, K. G.; Fritz, T. A.; Tabak, L. A. All in the family: the UDP-GalNAc:polypeptide N-acetylgalactosaminyltransferases. *Glycobiology* **2003***, 13*, 16R.

53. Kong, Y.; Joshi, H. J.; Schjoldager, K. T.; Madsen, T. D.; Gerken, T. A.; Vester-Christensen, M. B.; Wandall, H. H.; Bennett, E. P.; Levery, S. B.; Vakhrushev, S. Y.; Clausen, H. Probing polypeptide GalNAc-transferase isoform substrate specificities by in vitro analysis. *Glycobiology* **2015***, 25*, 55-65.

54. Schachter, H.; Brockhausen, I. The biosynthesis of branched O-glycans. *Symp. Soc. Exp. Biol.* **1989***, 43*, 1-26.

55. Bond, M. R.; Hanover, J. A. A little sugar goes a long way: the cell biology of O-GlcNAc. *J. Cell Biol.* **2015***, 208*, 869-880.

56. Zachara, N.; Akimoto, Y.; Hart, G. In *Chapter 19: The O-GlcNAc Modification;* Varki, A., Cummings, R., Esko, J., Stanley, P., Hart, G., Aebi, M., Darvill, A., Kinoshita, T., Packer, N., Prestegard, J., Schnaar, R. and Seeberger, P., Eds.; Essentials of Glycobiology; Cold Spring Harbor Laboratory Press: Cold Spring Harbor, NY, 2017; .

57. Chiaradonna, F.; Ricciardiello, F.; Palorini, R. The nutrient-sensing hexosamine biosynthetic pathway as the hub of cancer metabolic rewiring. *Cells* **2018***, 7*, 10.3390/cells7060053.

58. Okajima, T.; Irvine, K. D. Regulation of notch signaling by O-linked fucose. *Cell* **2002***, 111*, 893-904.

59. Sheikh, M. O.; Halmo, S. M.; Wells, L. Recent advancements in understanding mammalian O-mannosylation. *Glycobiology* **2017***, 27*, 806-819.

60. Brandenburg, K.; Holst, O. Glycolipids: distribution and biological function. *eLS* **2015**.

61. Schnaar, R.; Kinoshita, T. In *Chapter 11: Glycosphingolipids;* Varki, A., Cummings, R., Esko, J., Stanley, P., Hart, G., Aebi, M., Darvill, A., Kinoshita, T., Packer, N., Prestegard, J., Schnaar, R. and Seeberger, P., Eds.; Essentials of Glycobiology; Cold Spring Harbor Laboratory Press: Cold Spring Harbor, NY, 2017; .

62. Hakomori, S. Structure, organization, and function of glycosphingolipids in membrane. *Curr. Opin. Hematol.* **2003***, 10*, 16-24.

63. D'Angelo, G.; Capasso, S.; Sticco, L.; Russo, D. Glycosphingolipids: synthesis and functions. *FEBS J.* **2013***, 280*, 6338-6353.

64. Kinoshita, T. Glycosylphosphatidylinositol (GPI) anchors: biochemistry and cell biology: introduction to a thematic review series. *J. Lipid Res.* **2016***, 57*, 4-5.

65. Ferguson, M.; Hart, G.; Kinoshita, T. In *Chapter 12: Glycosylphosphatidylinositol Anchors;* Varki, A., Cummings, R., Esko, J., Stanley, P., Hart, G., Aebi, M., Darvill, A., Kinoshita, T., Packer, N., Prestegard, J., Schnaar, R. and Seeberger, P., Eds.; Essentials of Glycobiology; Cold Spring Harbor Laboratory Press: Cold Spring Harbor, NY, 2017; .

66. Paulick, M. G.; Bertozzi, C. R. The glycosylphosphatidylinositol anchor: a complex membrane-anchoring structure for proteins. *Biochemistry* **2008***, 47*, 6991-7000.

67. Walsh, G. Biopharmaceutical benchmarks 2014. *Nat. Biotechnol.* **2014***, 32*, 992-1000.

68. Moorkens, E.; Meuwissen, N.; Huys, I.; Declerck, P.; Vulto, A. G.; Simoens, S. The market of biopharmaceutical medicines: a snapshot of a diverse industrial landscape. *Front. Pharmacol.* **2017***, 8*, 314.

69. Anonymous. Global biopharmaceuticals market. **2018**.

70. Sola, R. J.; Griebenow, K. Glycosylation of therapeutic proteins: an effective strategy to optimize efficacy. *BioDrugs* **2010***, 24*, 9-21.

71. Fitzhugh, D. J.; Lockey, R. F. History of immunotherapy: the first 100 years. *Immunol. Allergy Clin. North. Am.* **2011***, 31*, 57, vii.

72. Plotkin, S. A.; Plotkin, S. L. The development of vaccines: how the past led to the future. *Nat. Rev. Microbiol.* **2011***, 9*, 889-893.

73. Lalonde, M. E.; Durocher, Y. Therapeutic glycoprotein production in mammalian cells. *J. Biotechnol.* **2017***, 251*, 128-140.

74. Baeshen, N. A.; Baeshen, M. N.; Sheikh, A.; Bora, R. S.; Ahmed, M. M.; Ramadan, H. A.; Saini, K. S.; Redwan, E. M. Cell factories for insulin production. *Microb. Cell. Fact.* **2014***, 13*, 0.

75. Hossler, P.; Khattak, S. F.; Li, Z. J. Optimal and consistent protein glycosylation in mammalian cell culture. *Glycobiology* **2009***, 19*, 936-949.

76. Ghaderi, D.; Zhang, M.; Hurtado-Ziola, N.; Varki, A. Production platforms for biotherapeutic glycoproteins. Occurrence, impact, and challenges of non-human sialylation. *Biotechnol. Genet. Eng. Rev.* **2012***, 28*, 147-175.

77. Ladisch, M. R.; Kohlmann, K. L. Recombinant human insulin. *Biotechnol. Prog.* **1992**, *8*, 469-478.

78. Helenius, A.; Aebi, M. Intracellular functions of N-linked glycans. *Science* **2001***, 291*, 2364-2369.

79. Ahmad, M.; Hirz, M.; Pichler, H.; Schwab, H. Protein expression in Pichia pastoris: recent achievements and perspectives for heterologous protein production. *Appl. Microbiol. Biotechnol.* **2014***, 98*, 5301-5317.

80. Nielsen, K. H. Protein expression-yeast. *Methods Enzymol.* **2014***, 536*, 133-147.

81. Meehl, M. A.; Stadheim, T. A. Biopharmaceutical discovery and production in yeast. *Curr. Opin. Biotechnol.* **2014***, 30*, 120-127.

82. Tomiya, N.; Howe, D.; Aumiller, J. J.; Pathak, M.; Park, J.; Palter, K. B.; Jarvis, D. L.; Betenbaugh, M. J.; Lee, Y. C. Complex-type biantennary N-glycans of recombinant human transferrin from Trichoplusia ni insect cells expressing mammalian [β]-1,4-galactosyltransferase and [β]-1,2-N-acetylglucosaminyltransferase II. *Glycobiology* **2003***, 13*, 23-34.

83. Viswanathan, K.; Lawrence, S.; Hinderlich, S.; Yarema, K. J.; Lee, Y. C.; Betenbaugh, M. J. Engineering sialic acid synthetic ability into insect cells: identifying metabolic bottlenecks and devising strategies to overcome them. *Biochemistry* **2003***, 42*, 15215-15225.

84. Granell, A. E.; Palter, K. B.; Akan, I.; Aich, U.; Yarema, K. J.; Betenbaugh, M. J.; Thornhill, W. B.; Recio-Pinto, E. DmSAS is required for sialic acid biosynthesis in cultured Drosophila third instar larvae CNS neurons. *ACS Chem. Biol.* **2011***, 6*, 1287-1295.

85. Scherer, W. F.; Syverton, J. T.; Gey, G. O. Studies on the propagation in vitro of poliomyelitis viruses. IV. Viral multiplication in a stable strain of human malignant epithelial cells (strain HeLa) derived from an epidermoid carcinoma of the cervix. *J. Exp. Med.* **1953***, 97*, 695-710.

86. Goh, J. B.; Ng, S. K. Impact of host cell line choice on glycan profile. *Crit. Rev. Biotechnol.* **2018***, 38*, 851-867.

87. Dumont, J.; Euwart, D.; Mei, B.; Estes, S.; Kshirsagar, R. Human cell lines for biopharmaceutical manufacturing: history, status, and future perspectives. *Crit. Rev. Biotechnol.* **2016***, 36*, 1110-1122.

88. Petricciani, J.; Sheets, R. An overview of animal cell substrates for biological products. *Biologicals* **2008***, 36*, 359-362.

89. Butler, M.; Spearman, M. The choice of mammalian cell host and possibilities for glycosylation engineering. *Curr. Opin. Biotechnol.* **2014***, 30*, 107-112.

90. Galfre, G.; Milstein, C. Preparation of monoclonal antibodies: strategies and procedures. *Methods Enzymol.* **1981***, 73*, 3-46.

91. Potter, M.; Boyce, C. R. Induction of plasma-cell neoplasms in strain BALB/c mice with mineral oil and mineral oil adjuvants. *Nature* **1962***, 193*, 1086-1087.

92. Barnes, L. M.; Bentley, C. M.; Dickson, A. J. Advances in animal cell recombinant protein production: GS-NS0 expression system. *Cytotechnology* **2000***, 32*, 109-123.

93. Chung, C. H.; Mirakhur, B.; Chan, E.; Le, Q. T.; Berlin, J.; Morse, M.; Murphy, B. A.; Satinover, S. M.; Hosen, J.; Mauro, D.; Slebos, R. J.; Zhou, Q.; Gold, D.; Hatley, T.; Hicklin, D. J.; Platts-Mills, T. A. Cetuximab-induced anaphylaxis and IgE specific for galactose-α-1,3-galactose. *N. Engl. J. Med.* **2008***, 358*, 1109-1117.

94. Ghaderi, D.; Taylor, R. E.; Padler-Karavani, V.; Diaz, S.; Varki, A. Implications of the presence of N-glycolylneuraminic acid in recombinant therapeutic glycoproteins. *Nat. Biotechnol.* **2010***, 28*, 863-867.

95. Tangvoranuntakul, P.; Gagneux, P.; Diaz, S.; Bardor, M.; Varki, N.; Varki, A.; Muchmore, E. Human uptake and incorporation of an immunogenic nonhuman dietary sialic acid. *Proc. Natl. Acad. Sci. U. S. A.* **2003***, 100*, 12045-12050.

96. Kim, J. Y.; Kim, Y. G.; Lee, G. M. CHO cells in biotechnology for production of recombinant proteins: current state and further potential. *Appl. Microbiol. Biotechnol.* **2012***, 93*, 917-930.

97. Durocher, Y.; Butler, M. Expression systems for therapeutic glycoprotein production. *Curr. Opin. Biotechnol.* **2009***, 20*, 700-707.

98. Swiech, K.; Picanco-Castro, V.; Covas, D. T. Human cells: new platform for recombinant therapeutic protein production. *Protein Expr. Purif.* **2012***, 84*, 147-153.

99. Berting, A.; Farcet, M. R.; Kreil, T. R. Virus susceptibility of Chinese hamster ovary (CHO) cells and detection of viral contaminations by adventitious agent testing. *Biotechnol. Bioeng.* **2010***, 106*, 598-607.

100. Xu, X.; Nagarajan, H.; Lewis, N. E.; Pan, S.; Cai, Z.; Liu, X.; Chen, W.; Xie, M.; Wang, W.; Hammond, S.; Andersen, M. R.; Neff, N.; Passarelli, B.; Koh, W.; Fan, H. C.; Wang, J.; Gui, Y.; Lee, K. H.; Betenbaugh, M. J.; Quake, S. R.; Famili, I.; Palsson, B. O.; Wang, J. The genomic sequence of the Chinese hamster ovary (CHO)-K1 cell line. *Nat. Biotechnol.* **2011***, 29*, 735-741.

101. Lai, T.; Yang, Y.; Ng, S. K. Advances in mammalian cell line development technologies for recombinant protein production. *Pharmaceuticals (Basel)* **2013***, 6*, 579-603.

102. Bosques, C. J.; Collins, B. E.; Meador, J. W.,3rd; Sarvaiya, H.; Murphy, J. L.; Dellorusso, G.; Bulik, D. A.; Hsu, I. H.; Washburn, N.; Sipsey, S. F.; Myette, J. R.; Raman, R.; Shriver, Z.; Sasisekharan, R.; Venkataraman, G. Chinese hamster ovary cells can produce galactose-α-1,3-galactose antigens on proteins. *Nat. Biotechnol.* **2010***, 28*, 1153-1156.

103. Howard, D. R.; Fukuda, M.; Fukuda, M. N.; Stanley, P. The GDP-fucose:N-acetylglucosaminide 3-α-L-fucosyltransferases of LEC11 and LEC12 Chinese hamster ovary mutants exhibit novel specificities for glycolipid substrates. *J. Biol. Chem.* **1987***, 262*, 16830-16837.

104. Sasaki, H.; Bothner, B.; Dell, A.; Fukuda, M. Carbohydrate structure of erythropoietin expressed in Chinese hamster ovary cells by a human erythropoietin cDNA. *J. Biol. Chem.* **1987***, 262*, 12059-12076.

105. Campbell, C.; Stanley, P. A dominant mutation to ricin resistance in Chinese hamster ovary cells induces UDP-GlcNAc:glycopeptide β-4-N-acetylglucosaminyltransferase III activity. *J. Biol. Chem.* **1984***, 259*, 13370-13378.

106. Patnaik, S. K.; Stanley, P. Lectin-resistant CHO glycosylation mutants. *Methods Enzymol.* **2006***, 416*, 159-182.

107. Jefferis, R. Glycosylation as a strategy to improve antibody-based therapeutics. *Nat. Rev. Drug Discov.* **2009***, 8*, 226-234.

108. Sinclair, A. M.; Elliott, S. Glycoengineering: the effect of glycosylation on the properties of therapeutic proteins. *J. Pharm. Sci.* **2005***, 94*, 1626-1635.

109. Clausen, H.; Wandall, H.; Steentoft, C.; Stanley, P.; Schnaar, R. In *Chapter 56: Glycosylation Engineering;* Varki, A., Cummings, R., Esko, J., Stanley, P., Hart, G., Aebi, M., Darvill, A., Kinoshita, T., Packer, N., Prestegard, J., Schnaar, R. and Seeberger, P., Eds.; Essentials of Glycobiology; Cold Springs Harbor Laboratory Press: Cold Springs Harbor, 2017; .

110. Hamilton, S. R.; Zha, D. Progress in yeast glycosylation engineering. *Methods Mol. Biol.* **2015**, *1321*, 73-90.

111. Chandrasegaran, S.; Carroll, D. Origins of programmable nucleases for genome engineering. *J. Mol. Biol.* **2016**, *428*, 963-989.

112. Wang, Q.; Yin, B.; Chung, C. Y.; Betenbaugh, M. J. Glycoengineering of CHO cells to improve product quality. *Methods Mol. Biol.* **2017**, *1603*, 25-44.

113. Agrawal, P.; Kurcon, T.; Pilobello, K. T.; Rakus, J. F.; Koppolu, S.; Liu, Z.; Batista, B. S.; Eng, W. S.; Hsu, K. L.; Liang, Y.; Mahal, L. K. Mapping posttranscriptional regulation of the human glycome uncovers microRNA defining the glycocode. *Proc. Natl. Acad. Sci. U. S. A.* **2014**, *111*, 4338-4343.

114. Morell, A. G.; Gregoriadis, G.; Scheinberg, I. H.; Hickman, J.; Ashwell, G. The role of sialic acid in determining the survival of glycoproteins in the circulation. *J. Biol. Chem.* **1971**, *246*, 1461-1467.

115. Weiss, P.; Ashwell, G. The asialoglycoprotein receptor: properties and modulation by ligand. *Prog. Clin. Biol. Res.* **1989**, *300*, 169-184.

116. Tang, L.; Persky, A. M.; Hochhaus, G.; Meibohm, B. Pharmacokinetic aspects of biotechnology products. *J. Pharm. Sci.* **2004**, *93*, 2184-2204.

117. Raju, T. S.; Scallon, B. Fc glycans terminated with N-acetylglucosamine residues increase antibody resistance to papain. *Biotechnol. Prog.* **2007**, *23*, 964-971.

118. Lee, E. U.; Roth, J.; Paulson, J. C. Alteration of terminal glycosylation sequences on N-linked oligosaccharides of Chinese hamster ovary cells by expression of β-galactoside α2,6-sialyltransferase. *J. Biol. Chem.* **1989**, *264*, 13848-13855.

119. Minch, S. L.; Kallio, P. T.; Bailey, J. E. Tissue plasminogen activator coexpressed in Chinese hamster ovary cells with α(2,6)-sialyltransferase contains NeuAc α(2,6)Gal β(1,4)Glc-N-AcR linkages. *Biotechnol. Prog.* **1995**, *11*, 348-351.

120. Schlenke, P.; Grabenhorst, E.; Wagner, R.; Nimtz, M.; Conradt, H. S. In *Expression of human α2, 6-sialyltransferase in BHK-21A cells increases the sialylation of coexpressed human erythropoietin: NeuAc-transfer onto GalNAc(βl-4)GlcNAc-R motives;* Carrondo, M. J. T., Griffiths, B. and Moreira, J. L. P., Eds.; Animal Cell Technology: From Vaccines to Genetic Medicine; Springer Netherlands: Dordrecht, 1997; pp 475-480.

121. Jeong, Y. T.; Choi, O.; Lim, H. R.; Son, Y. D.; Kim, H. J.; Kim, J. H. Enhanced sialylation of recombinant erythropoietin in CHO cells by human glycosyltransferase expression. *J. Microbiol. Biotechnol.* **2008**, *18*, 1945-1952.

122. Yin, B.; Gao, Y.; Chung, C. Y.; Yang, S.; Blake, E.; Stuczynski, M. C.; Tang, J.; Kildegaard, H. F.; Andersen, M. R.; Zhang, H.; Betenbaugh, M. J. Glycoengineering of Chinese hamster ovary cells for enhanced erythropoietin N-glycan branching and sialylation. *Biotechnol. Bioeng.* **2015**, *112*, 2343-2351.

123. Weikert, S.; Papac, D.; Briggs, J.; Cowfer, D.; Tom, S.; Gawlitzek, M.; Lofgren, J.; Mehta, S.; Chisholm, V.; Modi, N.; Eppler, S.; Carroll, K.; Chamow, S.; Peers, D.; Berman, P.; Krummen, L. Engineering Chinese hamster ovary cells to maximize sialic acid content of recombinant glycoproteins. *Nat. Biotechnol.* **1999***, 17*, 1116-1121.

124. Bragonzi, A.; Distefano, G.; Buckberry, L. D.; Acerbis, G.; Foglieni, C.; Lamotte, D.; Campi, G.; Marc, A.; Soria, M. R.; Jenkins, N.; Monaco, L. A new Chinese hamster ovary cell line expressing α2,6-sialyltransferase used as universal host for the production of human-like sialylated recombinant glycoproteins. *Biochim. Biophys. Acta* **2000***, 1474*, 273-282.

125. Monaco, L.; Marc, A.; Eon-Duval, A.; Acerbis, G.; Distefano, G.; Lamotte, D.; Engasser, J. M.; Soria, M.; Jenkins, N. Genetic engineering of α2,6-sialyltransferase in recombinant CHO cells and its effects on the sialylation of recombinant interferon-γ. *Cytotechnology* **1996***, 22*, 197-203.

126. Raymond, C.; Robotham, A.; Spearman, M.; Butler, M.; Kelly, J.; Durocher, Y. Production of α2,6-sialylated IgG1 in CHO cells. *MAbs* **2015***, 7*, 571-583.

127. Jassal, R.; Jenkins, N.; Charlwood, J.; Camilleri, P.; Jefferis, R.; Lund, J. Sialylation of human IgG-Fc carbohydrate by transfected rat α2,6-sialyltransferase. *Biochem. Biophys. Res. Commun.* **2001***, 286*, 243-249.

128. Cha, H. M.; Lim, J. H.; Yeon, J. H.; Hwang, J. M.; Kim, D. I. Co-overexpression of Mgat1 and Mgat4 in CHO cells for production of highly sialylated albumin-erythropoietin. *Enzyme Microb. Technol.* **2017***, 103*, 53-58.

129. Fukuta, K.; Yokomatsu, T.; Abe, R.; Asanagi, M.; Makino, T. Genetic engineering of CHO cells producing human interferon-γ by transfection of sialyltransferases. *Glycoconj. J.* **2000***, 17*, 895-904.

130. Fukuta, K.; Abe, R.; Yokomatsu, T.; Kono, N.; Asanagi, M.; Omae, F.; Minowa, M. T.; Takeuchi, M.; Makino, T. Remodeling of sugar chain structures of human interferon-γ. *Glycobiology* **2000***, 10*, 421-430.

131. Seppala, R.; Lehto, V. P.; Gahl, W. A. Mutations in the human UDP-N-acetylglucosamine 2-epimerase gene define the disease sialuria and the allosteric site of the enzyme. *Am. J. Hum. Genet.* **1999***, 64*, 1563-1569.

132. Yarema, K. J.; Goon, S.; Bertozzi, C. R. Metabolic selection of glycosylation defects in human cells. *Nat. Biotechnol.* **2001***, 19*, 553.

133. Hinderlich, S.; Weidemann, W.; Yardeni, T.; Horstkorte, R.; Huizing, M. UDP-GlcNAc 2-Epimerase/ManNAc Kinase (GNE): a master regulator of sialic acid synthesis. *Top. Curr. Chem.* **2015***, 366*, 97-137.

134. Bork, K.; Reutter, W.; Weidemann, W.; Horstkorte, R. Enhanced sialylation of EPO by overexpression of UDP-GlcNAc 2-epimerase/ManAc kinase containing a sialuria mutation in CHO cells. *FEBS Lett.* **2007***, 581*, 4195-4198.

135. Son, Y. D.; Jeong, Y. T.; Park, S. Y.; Kim, J. H. Enhanced sialylation of recombinant human erythropoietin in Chinese hamster ovary cells by combinatorial engineering of selected genes. *Glycobiology* **2011***, 21*, 1019-1028.

136. Wong, N. S.; Yap, M. G.; Wang, D. I. Enhancing recombinant glycoprotein sialylation through CMP-sialic acid transporter over expression in Chinese hamster ovary cells. *Biotechnol. Bioeng.* **2006***, 93*, 1005-1016.

137. Monti, E.; Miyagi, T. Structure and function of mammalian sialidases. *Top. Curr. Chem.* **2015***, 366*, 183-208.

138. Zhang, M.; Koskie, K.; Ross, J. S.; Kayser, K. J.; Caple, M. V. Enhancing glycoprotein sialylation by targeted gene silencing in mammalian cells. *Biotechnol. Bioeng.* **2010***, 105*, 1094-1105.

139. Smith, R. E.,Jr; Jaiyesimi, I. A.; Meza, L. A.; Tchekmedyian, N. S.; Chan, D.; Griffith, H.; Brosman, S.; Bukowski, R.; Murdoch, M.; Rarick, M.; Saven, A.; Colowick, A. B.; Fleishman, A.; Gayko, U.; Glaspy, J. Novel erythropoiesis stimulating protein (NESP) for the treatment of anaemia of chronic disease associated with cancer. *Br. J. Cancer* **2001***, 84 Suppl 1*, 24-30.

140. Bello, N. A.; Lewis, E. F.; Desai, A. S.; Anand, I. S.; Krum, H.; McMurray, J. J.; Olson, K.; Solomon, S. D.; Swedberg, K.; van Veldhuisen, D. J.; Young, J. B.; Pfeffer, M. A. Increased risk of stroke with darbepoetin alfa in anaemic heart failure patients with diabetes and chronic kidney disease. *Eur. J. Heart Fail.* **2015***, 17*, 1201-1207.

141. Song, R.; Oren, D. A.; Franco, D.; Seaman, M. S.; Ho, D. D. Strategic addition of an N-linked glycan to a monoclonal antibody improves its HIV-1-neutralizing activity. *Nat. Biotechnol.* **2013***, 31*, 1047-1052.

142. Campbell, C. T.; Sampathkumar, S. G.; Yarema, K. J. Metabolic oligosaccharide engineering: perspectives, applications, and future directions. *Mol. Biosyst* **2007***, 3*, 187-194.

143. Du, J.; Meledeo, M. A.; Wang, Z.; Khanna, H. S.; Paruchuri, V. D.; Yarema, K. J. Metabolic glycoengineering: sialic acid and beyond. *Glycobiology* **2009***, 19*, 1382-1401.

144. Kayser, H.; Zeitler, R.; Kannicht, C.; Grunow, D.; Nuck, R.; Reutter, W. Biosynthesis of a nonphysiological sialic acid in different rat organs, using N-propanoyl-D-hexosamines as precursors. *J. Biol. Chem.* **1992***, 267*, 16934-16938.

145. Yorke, S. The application of N-acetylmannosamine to the mammalian cell culture production of recombinant human glycoproteins. *Chemistry of New Zealand* **2013**.

146. Hadfield, A. F.; Mella, S. L.; Sartorelli, A. C. N-acetyl-D-mannosamine analogues as potential inhibitors of sialic acid biosynthesis. *J. Pharm. Sci.* **1983***, 72*, 748-751.

147. Schwartz, E. L.; Hadfield, A. F.; Brown, A. E.; Sartorelli, A. C. Modification of sialic acid metabolism of murine erythroleukemia cells by analogs of N-acetylmannosamine. *Biochim. Biophys. Acta* **1983***, 762*, 489-497.

148. Kayser, H.; Geilen, C. C.; Paul, C.; Zeitler, R.; Reutter, W. Incorporation of N-acyl-2-amino-2-deoxy-hexoses into glycosphingolipids of the pheochromocytoma cell line PC 12. *FEBS Lett.* **1992**, *301*, 137-140.

149. Wong, N. S.; Wati, L.; Nissom, P. M.; Feng, H. T.; Lee, M. M.; Yap, M. G. An investigation of intracellular glycosylation activities in CHO cells: effects of nucleotide sugar precursor feeding. *Biotechnol. Bioeng.* **2010**, *107*, 321-336.

150. Baker, K. N.; Rendall, M. H.; Hills, A. E.; Hoare, M.; Freedman, R. B.; James, D. C. Metabolic control of recombinant protein N-glycan processing in NS0 and CHO cells. *Biotechnol. Bioeng.* **2001**, *73*, 188-202.

151. Hills, A. E.; Patel, A.; Boyd, P.; James, D. C. Metabolic control of recombinant monoclonal antibody N-glycosylation in GS-NS0 cells. *Biotechnol. Bioeng.* **2001**, *75*, 239-251.

152. Arnold, J. N.; Wormald, M. R.; Sim, R. B.; Rudd, P. M.; Dwek, R. A. The impact of glycosylation on the biological function and structure of human immunoglobulins. *Annu. Rev. Immunol.* **2007**, *25*, 21-50.

153. Yarema, K. J.; Mahal, L. K.; Bruehl, R. E.; Rodriguez, E. C.; Bertozzi, C. R. Metabolic delivery of ketone groups to sialic acid residues. Application to cell surface glycoform engineering. *J. Biol. Chem.* **1998**, *273*, 31168-31179.

154. Kim, E. J.; Sampathkumar, S. G.; Jones, M. B.; Rhee, J. K.; Baskaran, G.; Goon, S.; Yarema, K. J. Characterization of the metabolic flux and apoptotic effects of O-hydroxyl- and N-acyl-modified N-acetylmannosamine analogs in Jurkat cells. *J. Biol. Chem.* **2004**, *279*, 18342-18352.

155. Jones, M. B.; Teng, H.; Rhee, J. K.; Lahar, N.; Baskaran, G.; Yarema, K. J. Characterization of the cellular uptake and metabolic conversion of acetylated N-acetylmannosamine (ManNAc) analogues to sialic acids. *Biotechnol. Bioeng.* **2004**, *85*, 394-405.

156. Aich, U.; Campbell, C. T.; Elmouelhi, N.; Weier, C. A.; Sampathkumar, S. G.; Choi, S. S.; Yarema, K. J. Regioisomeric SCFA attachment to hexosamines separates metabolic flux from cytotoxicity and MUC1 suppression. *ACS Chem. Biol.* **2008**, *3*, 230-240.

157. Almaraz, R. T.; Aich, U.; Khanna, H. S.; Tan, E.; Bhattacharya, R.; Shah, S.; Yarema, K. J. Metabolic oligosaccharide engineering with N-Acyl functionalized ManNAc analogs: Cytotoxicity, metabolic flux, and glycan-display considerations. *Biotechnol. Bioeng.* **2012**, *109*, 992-1006.

158. Saeui, C. T.; Liu, L.; Urias, E.; Morrissette-McAlmon, J.; Bhattacharya, R.; Yarema, K. J. Pharmacological, physiochemical, and drug-relevant biological properties of short chain fatty acid hexosamine analogues used in metabolic glycoengineering. *Mol. Pharm.* **2018**, *15*, 705-720.

159. Yin, B.; Wang, Q.; Chung, C. Y.; Bhattacharya, R.; Ren, X.; Tang, J.; Yarema, K. J.; Betenbaugh, M. J. A novel sugar analog enhances sialic acid production and biotherapeutic sialylation in CHO cells. *Biotechnol. Bioeng.* **2017**, *114*, 1899-1902.

160. Wang, Q.; Chung, C. Y.; Yang, W.; Yang, G.; Chough, S.; Chen, Y.; Yin, B.; Bhattacharya, R.; Hu, Y.; Saeui, C. T.; Yarema, K. J.; Betenbaugh, M. J.; Zhang, H. Combining butyrated ManNAc with glycoengineered CHO cells improves EPO glycan quality and production. *Biotechnol. J.* **2018**, e1800186.

161. Yin, B.; Wang, Q.; Chung, C. Y.; Ren, X.; Bhattacharya, R.; Yarema, K. J.; Betenbaugh, M. J. Butyrated ManNAc analog improves protein expression in Chinese hamster ovary cells. *Biotechnol. Bioeng.* **2018**, *115*, 1531-1541.

162. Keppler, O. T.; Stehling, P.; Herrmann, M.; Kayser, H.; Grunow, D.; Reutter, W.; Pawlita, M. Biosynthetic modulation of sialic acid-dependent virus-receptor interactions of two primate polyoma viruses. *J. Biol. Chem.* **1995**, *270*, 1308-1314.

163. Werner, A.; Horstkorte, R.; Glanz, D.; Biskup, K.; Blanchard, V.; Berger, M.; Bork, K. Glycoengineering the N-acyl side chain of sialic acid of human erythropoietin affects its resistance to sialidase. *Biol. Chem.* **2012**, *393*, 777-783.

164. Mahal, L. K.; Yarema, K. J.; Bertozzi, C. R. Engineering chemical reactivity on cell surfaces through oligosaccharide biosynthesis. *Science* **1997**, *276*, 1125-1128.

165. Nauman, D. A.; Bertozzi, C. R. Kinetic parameters for small-molecule drug delivery by covalent cell surface targeting. *Biochim. Biophys. Acta* **2001**, *1568*, 147-154.

166. Lee, J. H.; Baker, T. J.; Mahal, L. K.; Zabner, J.; Bertozzi, C. R.; Wiemer, D. F.; Welsh, M. J. Engineering novel cell surface receptors for virus-mediated gene transfer. *J. Biol. Chem.* **1999**, *274*, 21878-21884.

167. Laughlin, S. T.; Baskin, J. M.; Amacher, S. L.; Bertozzi, C. R. In vivo imaging of membrane-associated glycans in developing zebrafish. *Science* **2008**, *320*, 664-667.

168. Hsu, T. L.; Hanson, S. R.; Kishikawa, K.; Wang, S. K.; Sawa, M.; Wong, C. H. Alkynyl sugar analogs for the labeling and visualization of glycoconjugates in cells. *Proc. Natl. Acad. Sci. U. S. A.* **2007**, *104*, 2614-2619.

169. Tanaka, Y.; Kohler, J. J. Photoactivatable crosslinking sugars for capturing glycoprotein interactions. *J. Am. Chem. Soc.* **2008**, *130*, 3278-3279.

170. Yarema, K. J.; Sun, Z. A photochemical snapshot of CD22 binding. *Nat. Chem. Biol.* **2005**, *1*, 69-70.

171. Sampathkumar, S. G.; Jones, M. B.; Yarema, K. J. Metabolic expression of thiol-derivatized sialic acids on the cell surface and their quantitative estimation by flow cytometry. *Nat. Protoc.* **2006**, *1*, 1840-1851.

172. Agarwal, P.; Bertozzi, C. R. Site-specific antibody-drug conjugates: the nexus of bioorthogonal chemistry, protein engineering, and drug development. *Bioconjug. Chem.* **2015**, *26*, 176-192.

173. Zhou, Q. Site-specific antibody conjugation for ADC and beyond. *Biomedicines* **2017**, *5*, 10.3390/biomedicines5040064.

174. Okeley, N. M.; Toki, B. E.; Zhang, X.; Jeffrey, S. C.; Burke, P. J.; Alley, S. C.; Senter, P. D. Metabolic engineering of monoclonal antibody carbohydrates for antibody-drug conjugation. *Bioconjug. Chem.* **2013**, *24*, 1650-1655.

175. Badr, H. A.; Al-Sadek, D. M.; El-Houseini, M. E.; Saeui, C. T.; Mathew, M. P.; Yarema, K. J.; Ahmed, H. Harnessing cancer cell metabolism for theranostic applications using metabolic glycoengineering of sialic acid in breast cancer as a pioneering example. *Biomaterials* **2017**, *116*, 158-173.

176. Badr, H. A.; AlSadek, D. M.; Mathew, M. P.; Li, C. Z.; Djansugurova, L. B.; Yarema, K. J.; Ahmed, H. Nutrient-deprived cancer cells preferentially use sialic acid to maintain cell surface glycosylation. *Biomaterials* **2015**, *70*, 23-36.

177. Saeui, C. T.; Nairn, A. V.; Galizzi, M.; Douville, C.; Gowda, P.; Park, M.; Dharmarha, V.; Shah, S. R.; Clarke, A.; Austin, M.; Moremen, K. W.; Yarema, K. J. Integration of genetic and metabolic features related to sialic acid metabolism distinguishes human breast cell subtypes. *PLoS One* **2018**, *13*, e0195812.

178. Horstkorte, R.; Rau, K.; Laabs, S.; Danker, K.; Reutter, W. Biochemical engineering of the N-acyl side chain of sialic acid leads to increased calcium influx from intracellular compartments and promotes differentiation of HL60 cells. *FEBS Lett.* **2004**, *571*, 99-102.

179. Sampathkumar, S. G.; Li, A. V.; Jones, M. B.; Sun, Z.; Yarema, K. J. Metabolic installation of thiols into sialic acid modulates adhesion and stem cell biology. *Nat. Chem. Biol.* **2006**, *2*, 149-152.

180. Schmidt, C.; Stehling, P.; Schnitzer, J.; Reutter, W.; Horstkorte, R. Biochemical engineering of neural cell surfaces by the synthetic N-propanoyl-substituted neuraminic acid precursor. *J. Biol. Chem.* **1998**, *273*, 19146-19152.

181. Deveau, H.; Garneau, J. E.; Moineau, S. CRISPR/Cas system and its role in phage-bacteria interactions. *Annu. Rev. Microbiol.* **2010**, *64*, 475-493.

182. Horvath, P.; Barrangou, R. CRISPR/Cas, the immune system of bacteria and archaea. *Science* **2010**, *327*, 167-170.

183. Jiang, F.; Doudna, J. A. CRISPR-Cas9 structures and mechanisms. *Annu. Rev. Biophys.* **2017**, *46*, 505-529.

184. Ma, Y.; Zhang, L.; Huang, X. Genome modification by CRISPR/Cas9. *FEBS J.* **2014**, *281*, 5186-5193.

185. Ran, F. A.; Hsu, P. D.; Wright, J.; Agarwala, V.; Scott, D. A.; Zhang, F. Genome engineering using the CRISPR-Cas9 system. *Nat. Protoc.* **2013**, *8*, 2281-2308.

186. Hinderlich, S.; Stasche, R.; Zeitler, R.; Reutter, W. A bifunctional enzyme catalyzes the first two steps in N-acetylneuraminic acid biosynthesis of rat liver. Purification and characterization of UDP-N-acetylglucosamine 2-epimerase/N-acetylmannosamine kinase. *J. Biol. Chem.* **1997**, *272*, 24313-24318.

187. Takahashi, S.; Takahashi, K.; Kaneko, T.; Ogasawara, H.; Shindo, S.; Kobayashi, M. Human renin-binding protein is the enzyme N-acetyl-D-glucosamine 2-epimerase. *J. Biochem.* **1999***, 125*, 348-353.

188. Keppler, O. T.; Hinderlich, S.; Langner, J.; Schwartz-Albiez, R.; Reutter, W.; Pawlita, M. UDP-GlcNAc 2-epimerase: a regulator of cell surface sialylation. *Science* **1999***, 284*, 1372-1376.

189. Hinderlich, S.; Berger, M.; Keppler, O. T.; Pawlita, M.; Reutter, W. Biosynthesis of N-acetylneuraminic acid in cells lacking UDP-N-acetylglucosamine 2-epimerase/N-acetylmannosamine kinase. *Biol. Chem.* **2001***, 382*, 291-297.

190. Samuel, J.; Tanner, M. E. Mechanistic aspects of enzymatic carbohydrate epimerization. *Nat. Prod. Rep.* **2002***, 19*, 261-277.

191. Luchansky, S. J.; Yarema, K. J.; Takahashi, S.; Bertozzi, C. R. GlcNAc 2-epimerase can serve a catabolic role in sialic acid metabolism. *J. Biol. Chem.* **2003***, 278*, 8035-8042.

192. Oetke, C.; Hinderlich, S.; Brossmer, R.; Reutter, W.; Pawlita, M.; Keppler, O. T. Evidence for efficient uptake and incorporation of sialic acid by eukaryotic cells. *Eur. J. Biochem.* **2001***, 268*, 4553-4561.

193. Puck, T. T.; Cieciura, S. J.; Robinson, A. Genetics of somatic mammalian cells. III. Long-term cultivation of euploid cells from human and animal subjects. *J. Exp. Med.* **1958***, 108*, 945-956.

194. Lewis, N. E.; Liu, X.; Li, Y.; Nagarajan, H.; Yerganian, G.; O'Brien, E.; Bordbar, A.; Roth, A. M.; Rosenbloom, J.; Bian, C.; Xie, M.; Chen, W.; Li, N.; Baycin-Hizal, D.; Latif, H.; Forster, J.; Betenbaugh, M. J.; Famili, I.; Xu, X.; Wang, J.; Palsson, B. O. Genomic landscapes of Chinese hamster ovary cell lines as revealed by the Cricetulus griseus draft genome. *Nat. Biotechnol.* **2013***, 31*, 759-765.

195. Labun, K.; Montague, T. G.; Gagnon, J. A.; Thyme, S. B.; Valen, E. CHOPCHOP v2: a web tool for the next generation of CRISPR genome engineering. *Nucleic Acids Res.* **2016***, 44*, 272.

196. Ronda, C.; Pedersen, L. E.; Hansen, H. G.; Kallehauge, T. B.; Betenbaugh, M. J.; Nielsen, A. T.; Kildegaard, H. F. Accelerating genome editing in CHO cells using CRISPR Cas9 and CRISPy, a web-based target finding tool. *Biotechnol. Bioeng.* **2014***, 111*, 1604-1616.

197. Doench, J. G.; Hartenian, E.; Graham, D. B.; Tothova, Z.; Hegde, M.; Smith, I.; Sullender, M.; Ebert, B. L.; Xavier, R. J.; Root, D. E. Rational design of highly active sgRNAs for CRISPR-Cas9-mediated gene inactivation. *Nat. Biotechnol.* **2014***, 32*, 1262-1267.

198. Doench, J. G.; Fusi, N.; Sullender, M.; Hegde, M.; Vaimberg, E. W.; Donovan, K. F.; Smith, I.; Tothova, Z.; Wilen, C.; Orchard, R.; Virgin, H. W.; Listgarten, J.; Root, D. E. Optimized sgRNA design to maximize activity and minimize off-target effects of CRISPR-Cas9. *Nat. Biotechnol.* **2016***, 34*, 184-191.

199. Xu, H.; Xiao, T.; Chen, C. H.; Li, W.; Meyer, C. A.; Wu, Q.; Wu, D.; Cong, L.; Zhang, F.; Liu, J. S.; Brown, M.; Liu, X. S. Sequence determinants of improved CRISPR sgRNA design. *Genome Res.* **2015***, 25*, 1147-1157.

200. Zhang, J. P.; Li, X. L.; Neises, A.; Chen, W.; Hu, L. P.; Ji, G. Z.; Yu, J. Y.; Xu, J.; Yuan, W. P.; Cheng, T.; Zhang, X. B. Different effects of sgRNA length on CRISPR-mediated gene knockout efficiency. *Sci. Rep.* **2016**, *6*, 28566.

201. Grav, L. M.; la Cour Karottki, K. J.; Lee, J. S.; Kildegaard, H. F. Application of CRISPR/Cas9 genome editing to improve recombinant protein production in CHO cells. *Methods Mol. Biol.* **2017**, *1603*, 101-118.

202. Wang, Q.; Chung, C. Y.; Rosenberg, J. N.; Yu, G.; Betenbaugh, M. J. Application of the CRISPR/Cas9 gene editing method for modulating antibody fucosylation in CHO cells. *Methods Mol. Biol.* **2018**, *1850*, 237-257.

203. Smith, P. K.; Krohn, R. I.; Hermanson, G. T.; Mallia, A. K.; Gartner, F. H.; Provenzano, M. D.; Fujimoto, E. K.; Goeke, N. M.; Olson, B. J.; Klenk, D. C. Measurement of protein using bicinchoninic acid. *Anal. Biochem.* **1985**, *150*, 76-85.

204. Jourdian, G. W.; Dean, L.; Roseman, S. The sialic acids. XI. A periodate-resorcinol method for the quantitative estimation of free sialic acids and their glycosides. *J. Biol. Chem.* **1971**, *246*, 430-435.

205. Chalfie, M.; Tu, Y.; Euskirchen, G.; Ward, W. W.; Prasher, D. C. Green fluorescent protein as a marker for gene expression. *Science* **1994**, *263*, 802-805.

206. Bardor, M.; Nguyen, D. H.; Diaz, S.; Varki, A. Mechanism of uptake and incorporation of the non-human sialic acid N-glycolylneuraminic acid into human cells. *J. Biol. Chem.* **2005**, *280*, 4228-4237.

207. Alberch, L.; Yarema, K. J. In *Chapter 3 - Bioconjugation reactions in living cells: development, advances, and applications of glycan-specific technologies;* Karp, J. M., Zhao, W., Eds.; Micro- and Nanoengineering of the Cell Surface; William Andrew Publishing: Oxford, 2014; pp 43-62.

208. Horava, S. D.; Peppas, N. A. Recent advances in hemophilia B therapy. *Drug Deliv. Transl. Res.* **2017**, *7*, 359-371.

209. Zimmerman, B.; Valentino, L. A. Hemophilia: in review. *Pediatr. Rev.* **2013**, *34*, 94; quiz 295.

210. Eldar-Lissai, A.; Hou, Q.; Krishnan, S. The changing costs of caring for hemophilia patients in the U.S.: Insurers' and Patients' Perspectives. *Blood* **2014**, *124*, 199.

211. Peters, R. T.; Low, S. C.; Kamphaus, G. D.; Dumont, J. A.; Amari, J. V.; Lu, Q.; Zarbis-Papastoitsis, G.; Reidy, T. J.; Merricks, E. P.; Nichols, T. C.; Bitonti, A. J. Prolonged activity of factor IX as a monomeric Fc fusion protein. *Blood* **2010**, *115*, 2057.

212. Lyseng-Williamson, K. A. Coagulation Factor IX (Recombinant), Albumin Fusion Protein (Albutrepenonacog Alfa; Idelvion (R)): A review of its use in haemophilia B. *Drugs* **2017**, *77*, 97-106.

213. Metzner, H. J.; Weimer, T.; Kronthaler, U.; Lang, W.; Schulte, S. Genetic fusion to albumin improves the pharmacokinetic properties of factor IX. *Thromb. Haemost.* **2009**, *102*, 634-644.

214. Metzner, H. J.; Pipe, S. W.; Weimer, T.; Schulte, S. Extending the pharmacokinetic half-life of coagulation factors by fusion to recombinant albumin. *Thromb. Haemost.* **2013***, 110*, 931-939.

215. Nolte, M. W.; Nichols, T. C.; Mueller-Cohrs, J.; Merricks, E. P.; Pragst, I.; Zollner, S.; Dickneite, G. Improved kinetics of rIX-FP, a recombinant fusion protein linking factor IX with albumin, in cynomolgus monkeys and hemophilia B dogs. *J. Thromb. Haemost.* **2012***, 10*, 1591-1599.

216. Santagostino, E.; Negrier, C.; Klamroth, R.; Tiede, A.; Pabinger-Fasching, I.; Voigt, C.; Jacobs, I.; Morfini, M. Safety and pharmacokinetics of a novel recombinant fusion protein linking coagulation factor IX with albumin (rIX-FP) in hemophilia B patients. *Blood* **2012***, 120*, 2405-2411.

217. Ostergaard, H.; Bjelke, J. R.; Hansen, L.; Petersen, L. C.; Pedersen, A. A.; Elm, T.; Moller, F.; Hermit, M. B.; Holm, P. K.; Krogh, T. N.; Petersen, J. M.; Ezban, M.; Sorensen, B. B.; Andersen, M. D.; Agerso, H.; Ahmadian, H.; Balling, K. W.; Christiansen, M. L.; Knobe, K.; Nichols, T. C.; Bjorn, S. E.; Tranholm, M. Prolonged half-life and preserved enzymatic properties of factor IX selectively PEGylated on native N-glycans in the activation peptide. *Blood* **2011***, 118*, 2333-2341.

218. Begbie, M. E.; Mamdani, A.; Gataiance, S.; Eltringham-Smith, L. J.; Bhakta, V.; Hortelano, G.; Sheffield, W. P. An important role for the activation peptide domain in controlling factor IX levels in the blood of haemophilia B mice. *Thromb. Haemost.* **2005***, 94*, 1138-1147.

219. Chang, J. Y.; Brock, J.; Griffith, M. J.; Monroe, D. *Glycosylation of the activation peptide of FIX determines plasma half-life;* 2007; Vol. 5, pp M.

220. Griffith, M. J.; Monroe, D.; van Cott, K. E.; Walker, A.; Waugh, S.; Kumar, A.; Drohan, W. N. *N-Glycan sialylation is important for in vivo recovery of recombinant Factor IX;* 2007; Vol. 5, pp M.

221. Bolt, G.; Bjelke, J. R.; Hermit, M. B.; Hansen, L.; Karpf, D. M.; Kristensen, C. Hyperglycosylation prolongs the circulation of coagulation factor IX. *J. Thromb. Haemost.* **2012***, 10*, 2397-2398.

222. Brooks, A. R.; Sim, D.; Gritzan, U.; Patel, C.; Blasko, E.; Feldman, R. I.; Tang, L.; Ho, E.; Zhao, X. Y.; Apeler, H.; Murphy, J. E. Glycoengineered factor IX variants with improved pharmacokinetics and subcutaneous efficacy. *J. Thromb. Haemost.* **2013***, 11*, 1699-1706.

223. Nasri, M.; Karimi, A.; Allahbakhshian Farsani, M. Production, purification and titration of a lentivirus-based vector for gene delivery purposes. *Cytotechnology* **2014***, 66*, 1031-1038.

224. Liebman, H. A.; Limentani, S. A.; Furie, B. C.; Furie, B. Immunoaffinity purification of factor IX (Christmas factor) by using conformation-specific antibodies directed against the factor IX-metal complex. *Proc. Natl. Acad. Sci. U. S. A.* **1985***, 82*, 3879-3883.

225. Lindsay, M.; Gil, G. C.; Cadiz, A.; Velander, W. H.; Zhang, C.; Van Cott, K. E. Purification of recombinant DNA-derived factor IX produced in transgenic pig milk and fractionation of active and inactive subpopulations. *J. Chromatogr. A* **2004***, 1026*, 149-157.

226. Kaufman, R. J.; Wasley, L. C.; Furie, B. C.; Furie, B.; Shoemaker, C. B. Expression, purification, and characterization of recombinant γ-carboxylated factor IX synthesized in Chinese hamster ovary cells. *J. Biol. Chem.* **1986***, 261*, 9622-9628.

Curriculum Vitae

EDUCATION

Johns Hopkins University
Master of Science and Engineering in Biomedical Engineering May 2019
Focus area: Regenerative & Immune Engineering
GPA: 3.833/4.000
Relevant coursework: cell engineering, tissue engineering, biomedical applications of glycoengineering, polymer design and bioconjugation, systems bioengineering, chemical biology II, cell & tissue engineering lab, research laboratory safety
Thesis: "Using Metabolic and Genetic Engineering to Develop Novel Cell Platforms for the Production of Recombinant Glycoproteins with Enhanced Pharmacokinetic Properties"

The University of Wisconsin Madison
Bachelor of Science May 2017
Dual major: Biochemistry, Economics (Mathematical Emphasis); Certificate: Global Health
GPA: 3.813/4.000

RESEARCH EXPERIENCE

Masters Research | Johns Hopkins University Aug. 2017 – Present
Primary Investigator: Dr. Kevin Yarema, Department of Biomedical Engineering
- Augment the pharmacokinetic and pharmacodynamic properties of glycoproteins using genetic engineering and metabolic glycoengineering
- Budget $650,000 in grant funding to procure raw materials and manage the lab's supply chain

Research Assistant | The University of Wisconsin Madison Dec. 2015 – Aug. 2017
Primary Investigator: Dr. Aurelie Rakotondrafara, Department of Plant Pathology
- Examined the RNA sequences required for *Triticum mosaic virus* protein expression by generating and cloning novel viral mutants for translational efficiency analysis
- Managed research lab for senior scientist and graduate students by procuring supplies, completing biweekly purchasing orders, maintaining laboratory equipment, sustaining plant tissue culture, preparing various media and buffers

---

TEACHING EXPERIENCE

Cell and Tissue Engineering Lab Teaching Assistant: Sep. 2018 – Present
Johns Hopkins University | Department of Biomedical Engineering
- Guide undergraduate and graduate students through numerous lab modules covering mammalian cell culture, glycoengineering, hydrogel vascularization, gene delivery, and microfluidics
- Develop and implement a new semester-long CRISPR-Cas lab project for graduate students

Volunteer Tutor: Sep. 2015 – May 2017
The University of Wisconsin Madison | Greater University Tutoring Service
- Helped educate undergraduate students by responding to inquires in chemistry and economics

---

PROFESSIONAL EXPERIENCE

Manufacturing and Chemistry Intern: Aug. 2016 – May 2017
BioTechnique LLC (PSC Biotech) | Madison, WI

- Created SOP and User Requirement Specifications for biomanufacturing equipment and raw materials
- Collaborated to complete contract biomanufacturing formulations and fills of various pharmaceutical products
- Utilized dynamic light scattering and nanoparticle tracking analysis validate biopharmaceutical homogeneity and size distribution
- Employed a total organic carbon analyzer to assess the cleanliness of biomanufacturing equipment

Cleanroom Maintenance Specialist: May 2015 – Sep. 2016
Waisman Biomanufacturing | Madison, WI

- Implemented cGMP practices and documentation while completing weekly, monthly, and changeover cleanings in Biosafety Level I and II cleanrooms
- Monitored and maintained compressed gas cylinders (O_2, N_2, CO_2) and conducted autoclave integrity tests ("Leak", DART)

HONORS & AWARDS

- Flounder Biomedical Engineering Fellowship – Johns Hopkins - 2018
- Juli Plant Grainger scholarship in economics – UW Madison - 2017
- The University of Wisconsin Madison Award for Summer Study – 2016
- William F. Renk study abroad scholarship **–** UW Madison – 2016
- Dean's List, eight semesters – The University of Wisconsin Madison – 2013-2017

PUBLICATIONS

Agatemor, C.; **Buettner M. J.**; Ariss R.; Muthiah K.; Saeui C. T.; Yarema K. J. Exploiting metabolic glycoengineering to advance healthcare. *Nature Reviews Chemistry*. **2019 (in review)**

Buettner, M. J.; Shah, S. R.; Saeui, C. T.; Ariss, R. S.; Yarema, K. J. Improving immunotherapy through glycodesign. *Frontiers in Immunology*. **2018**

Jaramillo-Mesa, H.; Gannon, M.; Holschbach, E.; Zhang. J.; Roberts, R.; **Buettner, M. J.**; Rakotondrafara, A. Triticum mosaic virus IRES relies on a picornavirus-like YX-AUG motif to designate the preferred translation initiation site and to likely target the 18S rRNA. *American Society for Microbiology: Journal of Virology*. **2018**

ABSTRACTS & PRESENTATIONS

Saeui, C. S.; Cho, K.; Dharmarha, V.; Shah, S. R.; Gowda, P.; Park, M.; Austin, M.; Clarke, A.; Cai, E.; **Buettner, M. J.;** Ariss, R. S.; Zhang, H; Yarema, K. J. Cell line-, protein-, and glycosite-specific control of flux-based sialylation in human breast cancer cells. *Glycobiology Interest Group Area-wide Poster Session*. **2018**

Conflict of interest Statement: The author declares that the research was conducted in the absence of any commercial or financial relationships that could be construed as a potential conflict of interest.

Disclaimer: Portions of this thesis were adapted from previously published work listed below:

Buettner, M. J.; Shah, S. R.; Saeui, C. T.; Ariss, R. S.; Yarema, K. J. Improving immunotherapy through glycodesign. *Frontiers in Immunology*. 2018

Agatemor, C.; Buettner M. J.; Ariss R.; Muthiah K.; Saeui C. T.; Yarema K. J. Exploiting metabolic glycoengineering to advance healthcare. *Nature Reviews Chemistry*. 2019 (in review)